Summer 2024

Hydrogen Sulfide as a Strong Ligand Affecting Trace Metal Cycling in the Pacific and Southern Oceans

Nicole R. Buckley
Old Dominion University

HYDROGEN SULFIDE AS A STRONG LIGAND AFFECTING TRACE METAL CYCLING IN THE PACIFIC AND SOUTHERN OCEANS

by

Nicole R. Buckley
B.S. May 2018, University of Wisconsin – Milwaukee
M.S. May 2021, Old Dominion University

A Dissertation Submitted to the Faculty of
Old Dominion University in Partial Fulfillment of the
Requirements for the Degree of

DOCTOR OF PHILOSOPHY

OCEANOGRAPHY

OLD DOMINION UNIVERSITY
August 2024

Approved by:

Gregory A. Cutter (Director)

Peter N. Sedwick (Member)

George W. Luther III (Member)

ABSTRACT

HYDROGEN SULFIDE AS A STRONG LIGAND AFFECTING TRACE METAL CYCLING IN THE PACIFIC AND SOUTHERN OCEANS

Nicole R. Buckley
Old Dominion University, 2024
Director: Dr. Gregory A. Cutter

Historically, hydrogen sulfide was considered unimportant in the open ocean since it has primarily been associated with anoxic environments. Yet, in the late 1980s it was suggested that this sulfur gas is also being produced in the oxic, surface ocean through the hydrolysis of carbonyl sulfide (OCS). Since then, several studies have demonstrated that hydrogen sulfide is indeed found in oxic seawater at pico- to nanomolar concentrations due not only to carbonyl sulfide hydrolysis, but also assimilatory sulfate reduction by phytoplankton. Hydrogen sulfide's importance in seawater is largely due to its high metal-ligand stability constants allowing it to affect the cycling of certain trace metals. Although 40 years have passed since the discovery of hydrogen sulfide in the oxic open ocean, our understanding of the speciation of dissolved and particulate metal-sulfides is still limited. Therefore, additional work is necessary to further our understanding of the processes affecting hydrogen sulfide speciation in the Pacific and Southern Oceans, and the impact that hydrogen sulfide has on the biogeochemical cycling of certain transition metals like cadmium and zinc.

To explore hydrogen sulfide's role in metal cycling in the Pacific Ocean and processes affecting its abundance in the Southern Ocean, novel measurements of sulfide alongside transition metals were used to investigate the dissolved cadmium and zinc sinks observed in oxygen minimum zones (OMZs) in previous studies, and a budget was constructed for the upper water column to quantify the extent of hydrogen sulfide complexation with key trace metals. My findings

suggest that: (1) the removal of dissolved cadmium and zinc via metal-sulfide precipitation varies regionally within low-oxygen environments and instead plays a larger role in the loss of dissolved cadmium in the oxygenated subsurface, (2) aqueous metal-sulfide complexes dominate the speciation of dissolved sulfide in the open Pacific Ocean, (3) using metal specific oxidation rates, phytoplankton production estimates can balance the sulfide budgets on the coastal Alaskan Shelf, and (4) in the Southern Ocean, processes affecting hydrogen sulfide concentrations in the upper water column are largely controlled by the temperature dependence on the rate of OCS hydrolysis and the species-dependent nature of phytoplankton production.

This dissertation is dedicated to my husband and my family who always supported my pursuit as a scientist, with special thanks to my grandfather, Bradford, who always said he wanted one of us grandkids to write a book – well here it is.

ACKNOWLEDGMENTS

The work presented here and my growth as a scientist would not have been possible without the help and support of many individuals. I thank Dr. Gregory Cutter for his patience while serving as my mentor and advisor. Without his assistance, support, and encouragement, this dissertation would have been a dream. To my committee members, Dr. Peter Sedwick and Dr. George Luther, I am grateful for offering their expertise and their insightful comments when I was stuck in the weeds. I am also grateful for the support received from Dr. Peter Pommerenk who aided me in the early stages of building my Monte-Carlo simulations in R.

Special thanks go to Ekaterina Bulygina who was always there to bounce ideas off of and who was instrumental in keeping a positive outlook throughout my PhD – even on the days when everything seemed to be going wrong. To the friends I've made in my time here – Iliana Flefel for making me feel at home and always there to lend an ear, Mauricio González-Díaz for offering an external viewpoint, and Emily Frett for ensuring there was never a dull moment. I also thank the captains and crew of the *R/V Revelle*, for supporting the GEOTRACES mission in the Pacific and Southern Oceans, as well as the scientists who aided in sample collection – especially Ekaterina Bulygina, and both Phoebe Lam's and Daniel Ohnemus' pump teams.

Though my academic support was instrumental, the support from family served an equally large role in my dedication to see this through. I only made it this far with the help of my husband, Bailey, standing by my side. Thank you for listening after the long days and holding down our fort while I left for months at a time to sail the ocean. To my parents, Brian and Carisa, and my grandparents, Brad, Mary, and Cindy, who always joked I would be a forever student – you

fostered my desire to learn and provided unconditional support and encouragement throughout my academic expedition to reach this milestone.

My time and this work were funded by the National Science Foundation (grants OCE-1737342 and 2049564) awarded to G. Cutter, and through teaching opportunities in the Department of Ocean and Earth Sciences who also provided travel funding that enabled me to present subsets of this work at several conferences over the years. Thank you.

NOMENCLATURE

AAIW	Antarctic Intermediate Water
Cd	Cadmium
Chl a	Chlorophyll a
Co	Cobalt
CTD	Conductivity-temperature-depth
Cu	Copper
DCM	Deep chlorophyll maxima
ETSP	Eastern Tropical South Pacific
Fe	Iron
Hg	Mercury
HNLC	High nutrient, low chlorophyll
HS^-	Bisulfide
H_2S	Hydrogen sulfide (units: pmol L^{-1})
Mn	Manganese
nd	No data
Ni	Nickel
OCS	Carbonyl Sulfide (units: pmol L^{-1})
ODF	Oceanographic Data Facility
OMZ	Oxygen minimum zone, i.e., where the lowest dissolved oxygen concentrations are observed at a given latitude/longitude
pAVS	Particulate acid-volatile sulfide (units: pmol L^{-1} or nmol L^{-1})
Pb	Lead

pCRS	Particulate chromium reducible sulfide (units: pmol L^{-1} or nmol L^{-1})
PHREEQC	pH Redox Equilibrium (in C language)
POC	Particulate organic carbon
S^{2-}	Sulfide
SAF	Sub-Antarctic Front
sACCF	Southern Antarctic Circumpolar Current Front
SAMW	Subantarctic Mode Water
SB	Southern Boundary
STF	Sub-tropical Front
T-S	Temperature-salinity
TDS	Total dissolved sulfide (units: pmol L^{-1} or nmol L^{-1})
TS	Total sulfide (units: pmol L^{-1} or nmol L^{-1})
UCDW	Upper Circumpolar Deep Water
Zn	Zinc

TABLE OF CONTENTS

Page

LIST OF TABLES

LIST OF FIGURES

Figure Page

CHAPTER 1

GENERAL INTRODUCTION

Thanks to the international GEOTRACES program, the biogeochemical cycling of trace elements and their function in oceans has become a large focus and area of study within the oceanographic community in recent years (Anderson, 2020; Anderson et al., 2014). The chemical speciation of some of these trace elements has been examined in a large span of basins worldwide, which has in turn provided necessary information regarding the oxidation states and complexes of these trace metals that can control their bioavailability and chemical reactivity (Morel & Price, 2003). Many dissolved trace metals are largely complexed by organic ligands, mostly because inorganic ligands have weak stability constants in seawater, and therefore aren't favored for complexation (Bruland & Lohan, 2006). One inorganic ligand that can compete with organic ligands in transition metal complexation is hydrogen sulfide, due to its large stability constants for complexation with those elements (Cutter et al., 1999; Luther et al., 1996; Zhang & Millero, 1994).

Existing as both dissolved gas (H_2S_{aq}) and free ions (HS^- and S^{2-}) in oxygenated seawater, hydrogen sulfide can also react to form dissolved metal-sulfide complexes or particulate metal-sulfides (Radford-Knoery & Cutter, 1994). Earlier studies report the involvement and effect of total dissolved sulfide (TDS = free + complexed) on both the sulfur and metal cycles (Andreae et al., 1991; Cutter et al., 1999; Cutter & Krahforst, 1988; Cutter & Radford-Knoery, 1991; Kuwabara & Luther, 1993; Luther et al., 1991; Luther & Tsamakis, 1989; Radford-Knoery & Cutter, 1994; Theberge et al., 1997). The impact of sulfide complexation on various chemical cycles can be seen in the open ocean and coastal waters, where TDS can reach up to 1 nmol L^{-1}

and control a large portion of the copper speciation (Kuwabara & Luther, 1993). Additionally, in the open ocean, it has been shown that hydrogen sulfide can dominate mercury speciation, and up to 60% of the speciation of other metals like copper, nickel and zinc (Cutter et al., 1999; Theberge et al., 1997). Therefore, hydrogen sulfide should have some impact on the oceanic cycling of numerous bioactive metals.

The purpose of this dissertation research was to further examine the mechanisms that influence the distribution and speciation of hydrogen sulfide in the Pacific and Southern Oceans and the role that hydrogen sulfide plays in the biogeochemical cycling of chalcophile trace metals like cadmium and zinc. The considerable amount of dissolved and particulate sulfide and trace metal measurements from the 2018 US GEOTRACES GP15 expedition from the Alaskan shelf to Tahiti, in addition to those from the 2022–2023 US GEOTRACES GP17-OCE expedition from Tahiti to the Antarctic ice edge to Chile provided us an opportunity to further evaluate hydrogen sulfide as a strong inorganic ligand and its impact on trace metal cycling throughout the oceanic water column. Specific aspects of the biogeochemistry of hydrogen sulfide that were investigated during this work include:

1) Testing the hypothesis of Janssen and colleagues (2014; 2015) that dissolved cadmium and zinc deficits observed in the low-oxygen Northeast Pacific can be explained by precipitation with sulfides. These results are described in Chapter 2, which was previously published by the American Geophysical Union in the journal *Global Biogeochemical Cycles* (https://doi.org/10.1029/2023GB007881).
2) Constructing a mass balance for hydrogen sulfide in various regimes of the North Pacific and quantifying the extent of dissolved hydrogen sulfide complexation with key trace metals throughout the Pacific Ocean. These results are described in Chapter 3.

3) Evaluating the processes responsible for controlling the concentrations of dissolved and particulate hydrogen sulfide observed in the Southern Ocean. These results are described in Chapter 4.

Chapters 2 and 3 were written so as to be self-contained. Chapter 4 is largely qualitative and will benefit from further assessment as more data becomes available from collaborators. Chapter 5 synthesizes the major findings in previous chapters, as well as future directions that will further our understanding of the biogeochemistry of hydrogen sulfide and its influence on metal cycling. The remainder of this chapter is dedicated to a review of the processes that impact the concentration and phase speciation of hydrogen sulfide in the open ocean.

1.1 Biogeochemical cycle of hydrogen sulfide in the surface ocean

Since hydrogen sulfide (H_2S) dissolved in seawater undergoes oxidation to sulfate (e.g., by oxygen; Millero et al., 1987; Vazquez et al., 1989), it was previously believed that hydrogen sulfide was only present in measurable concentrations in anoxic ocean waters. However, Elliott et al. (1987) proposed that H_2S could be produced in surface waters by carbonyl sulfide (OCS) hydrolysis. Shortly thereafter, Cutter and Krahforst (1988) reported the first profiles of hydrogen sulfide in oxic seawater where it existed in pico- to nanomolar concentrations in the western Atlantic, and verified the prediction of OCS hydrolysis (Elliott et al., 1987) acting as a major source of dissolved sulfide to the oxic seawater. Since then, Walsh et al. (1994) demonstrated that sulfide is also produced by phytoplankton in the fully oxic water column as a by-product of photosynthesis through assimilatory sulfate reduction.

Hydrogen sulfide can exist as several chemical species in seawater: free sulfide, namely dissolved and uncomplexed ions which exist as hydrogen sulfide (H_2S_{aq}), bisulfide (HS^-), and sulfide (S^{2-}). These ions are strong ligands, which can go on to form an assortment of dissolved

metal-sulfide complexes (e.g., Luther et al., 1996; Zhang & Millero, 1994) as well as insoluble particulate metal sulfides (Cutter & Radford-Knoery, 1991; Dyrssen & Wedborg, 1989). Analytically, total dissolved sulfide (TDS) is the sum of free sulfide (H_2S_{aq} + HS^- + S^{2-}) and dissolved sulfide complexes (e.g., d ZnS, $ZnHS^+$, etc.); particulate acid volatile sulfide (pAVS) includes CdS, ZnS, etc., with total sulfide (TS) representing the sum of those two (TS = TDS + pAVS). In addition, particulate chromium-reducible sulfide (pCRS) accounts for the non-acid volatile precipitates which include FeS_2, CuS, and HgS.

The proposed biogeochemical cycle of hydrogen sulfide in oxic seawater and an underlying oxygen minimum zone is shown in Figure 1. A small amount of free sulfide is introduced into surface waters due to atmospheric exchange (Andreae et al., 1991), although it is primarily produced from the hydrolysis of OCS (Cutter & Krahforst, 1988; Elliott et al., 1987) and by phytoplankton (Cutter & Krahforst, 1988; Radford-Knoery & Cutter, 1994; Walsh et al., 1994). However, the rate of OCS hydrolysis follows first order kinetics and is heavily dependent upon the temperature, salinity, and pH of the water (Elliott et al., 1989; Radford-Knoery & Cutter, 1994), whereas the rate of production via phytoplankton is heavily dependent upon the species present (Walsh et al., 1994). Some of that free sulfide is then available to react with metals to form dissolved metal-sulfide complexes and insoluble particulate metal sulfides that can then be removed by sinking out of the water column. Free sulfide can also be removed through air-sea flux (Andreae et al., 1991). However, due to the redox sensitivity of hydrogen sulfide, an important sink would be free sulfide being oxidized to sulfate via oxygen (Millero et al., 1987; Vazquez et al., 1989), iodate (Zhang & Whitfield, 1986), peroxide (Millero et al., 1989), or light (Pos et al., 1997). Although free sulfide is readily oxidized by oxygen in surface waters, it has been shown that the rate of oxidation by iodate is faster than that of oxygen (Radford-Knoery & Cutter, 1994;

Zhang & Whitfield, 1986). However, Zhang (1999) found that the speciation of sulfide (both free and complexed) heavily influences the rate of oxidation by iodate, where the reaction rate between iodate and HS^- (predominant species at pH > 6.6) is less than that of the reaction rate between

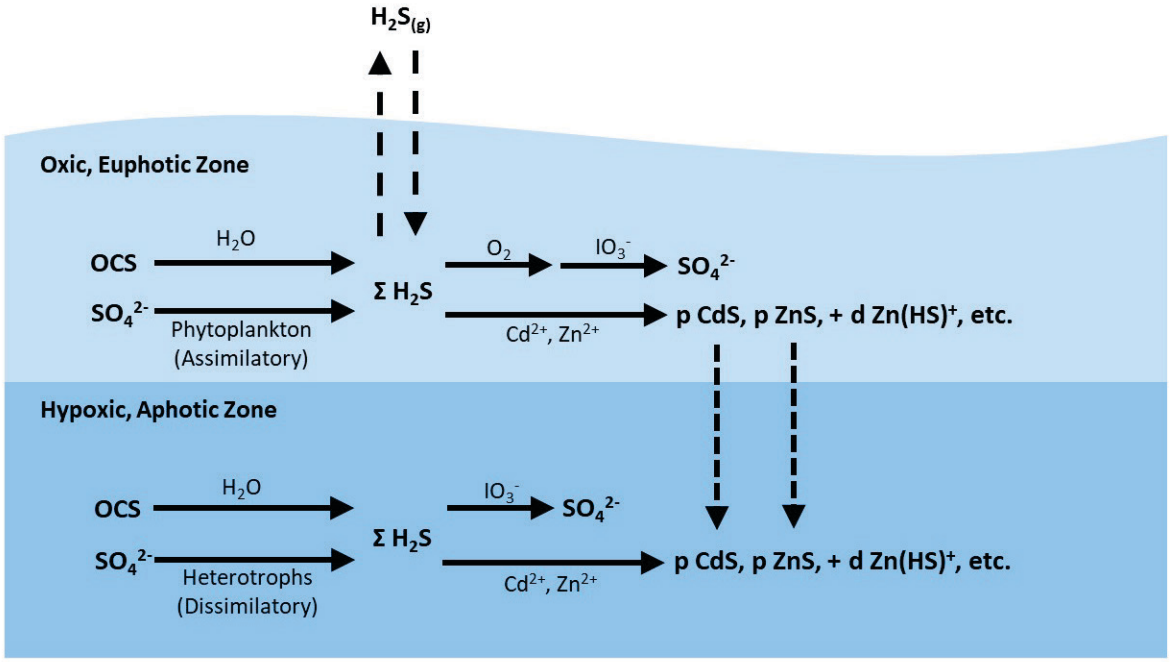

Figure 1. Proposed biogeochemical cycle of hydrogen sulfide in the surface ocean and underlying OMZ. ΣH_2S represents free, uncomplexed sulfide (H_2S_{aq} + HS^- + S^{2-}). ΣH_2S is produced via OCS hydrolysis, assimilatory sulfate reduction, dissimilatory sulfate reduction, or atmospheric interaction. ΣH_2S can then react with dissolved metals to form dissolved metal-sulfide complexes, particulate metal sulfides, or undergo oxidation to sulfate. These reaction pathways are shown as solid lines while dashed lines represent fluxes. Total dissolved sulfide (TDS) is presented by the sum of ΣH_2S and dissolved metal-sulfide complexes (d $Zn(HS)^+$, etc.), whereas particulate acid-volatile sulfide (pAVS) is represented by the particulate metal-sulfide complexes (p CdS, p ZnS, p NiS, etc.). However, it should be noted that some OMZs, like the eastern tropical South Pacific, have OMZs that shoal into euphotic waters, and thus sulfide could be produced by both dissimilatory and assimilatory sulfate reduction.

H_2S_{aq} and iodate. Similarly, at nanomolar levels, it was found that sulfide complexed with zinc slowed down the rate of oxidation relative to free sulfide, or other metal-sulfide complexes. The oxidation rate constants for different sulfide species in seawater are:

free sulfide > TDS > Ni complexes > Cd complexes >> Zn complexes

Zhang (1999) found that the reaction rate of Ni complexes is inversely proportional to the concentration of Ni^{+2} (between 0 and 20 μM), the oxidation rate for Cd complexes was quite low and was independent of the Cd^{+2} concentration, and that Zn complexes were essentially inert and resistant to oxidation by iodate. Though the kinetic stability for Cd-sulfide complexes compared to Ni-sulfide complexes is consistent with its thermodynamic stability (Zhang, 1999), the same cannot be said for the Zn-sulfide complexes. Nevertheless, this was not the first study to suggest that Zn complexes are the likely responsible for stabilization of sulfide in the oxic ocean (Luther et al., 1996; Vazquez et al., 1989). However, the identity and stability of such Zn-sulfide complexes remains unclear. While some studies suggest that this kinetic effect is due to the formation of $ZnS_{(aq)}$ complexes (Luther et al., 1996), other studies suggest that the more likely Zn-sulfide complex is $ZnHS^+$ (Al-Farawati & van den Berg, 1999), which has also been found to be unreactive with respect to oxidation by oxygen (Vazquez et al., 1989). Regardless, the formation of metal sulfide complexes does indeed slow the rate of sulfide oxidation by iodate, although it is metal specific. Therefore, sulfide speciation not only plays an important role in the global sulfur cycle but also influences the cycling of various trace metals.

1.2 Phytoplankton production

The correlation between TDS maxima and chlorophyll is what sparked Cutter and co-authors to examine the potential impact of phytoplankton on hydrogen sulfide production. In 1994, Walsh et al. showed that quite a few marine phytoplankton released TDS and pAVS in their lab

cultures (Table 1). They observed that the cyanobacteria *Synechococcus* produce the most total sulfide (TS) and total dissolved sulfide (TDS) per cubic centimeter cell volume, followed by the chlorophyte *Dunaliella tertiolecta* with the second largest TS production in the study. However, the coccolithophore *Emiliania huxleyi* produced the most particulate acid volatile sulfide (pAVS) in that study but was third in line for TS production. Oddly enough, the amount of TS produced by species is similar to the trend for the sensitivity of phytoplankton growth rates to copper toxicity (Brand et al., 1986), where the cyanobacteria was the most sensitive. Knowing this, Walsh et al. (1994) increased the amount of free copper and zinc in the *Synechococcus* cultures, which led to an increase in production of TDS and pAVS. This work proposed that phytoplankton produce TDS and pAVS as a control on the concentration of free metal within their environment through complexation.

Building from the work of Walsh et al. (1994), additional culture experiments were done to look at variability in rates between the top TS producer from the Walsh et al. study, *Synechococcus*, along with different phytoplankton species (Table 2; G. Cutter, personal communication). Yet again, *Synechococcus* produced the most TDS, however, another cyanobacterium, *Trichodesmium*, produced the most TS overall, but primarily in the form of pAVS. Most of the TS that the diatom, *Nitzschia*, produced was in the form of TDS at a rate in-between that of *Trichodesmium* and *Synechococcus*.

We know from Rennenberg (1989) that assimilatory sulfate reduction is the cause for the aerobic production of hydrogen sulfide in terrestrial plants, suggesting that may this be the same for marine phytoplankton. The mechanism for assimilatory sulfate reduction was examined by Rennenberg (1984, 1991) who suggested that cysteine synthesis in those terrestrial plants affects sulfate assimilation by releasing the by-product, hydrogen sulfide, as a feedback mechanism. They

Table 1. Production of total dissolved sulfide (TDS), particulate acid-volatile sulfide (pAVS), and total sulfide (TS) by marine phytoplankton in f/20 media during log phase growth (modified from Walsh et al., 1994).

Division	Species (Clone ID)	TDS	pAVS	TS
		per cell volume (nmol S cm^{-3})		
	Oceanic Species			
Cyanobacteria	*Synechococcus sp.* (DC2)	580 ± 52	45.3 ± 4	625 ± 56
Coccolithophore	*Emilania huxleyi* (BT6)	184 ± 48	72.7 ± 19	257 ± 67
Chlorophytes	*Pyramimonas obovata* (13-10PYR)	134 ± 31	56.5 ± 13	191 ± 44
Diatom	*Thalassiosira oceanica* (13-1)	26.5 ± 6	13.7 ± 3	40.2 ± 9
	Coastal Species			
Chlorophyte	*Dunaliella tertiolecta* (DUN)	529 ± 127	28.2 ± 7	557 ± 134
Dinoflagellate	*Amphidinium carterae* (AMPHI)	205 ± 55	22.0 ± 6	227 ± 61

suggest that this mechanism acts as a regulation of hydrogen sulfide concentration present within their cells. Thus, the amount of sulfide in oxic seawater could be heavily dependent upon the species present, with culture data indicating that a large majority of the total sulfide produced comes from cyanobacteria like *Synechococcus* and *Trichodesmium*. Tables 1 and 2 both show species specific trends in both field and culture data. Since US GEOTRACES GP15 and GP17-OCE cruises covered a wide variety of biotic regimes, these cruises provide a unique opportunity to evaluate the variations in dissolved and particulate sulfide concentrations with shifts in phytoplankton species abundance.

1.3 Relationship of hydrogen sulfide distribution to those of transition metals

Previous work has shown that the chemical speciation of dissolved sulfide is necessary to quantify hydrogen sulfide cycling in seawater, and while a number of studies report the stability constants for numerous dissolved metal-sulfide complexes (Al-Farawati & van den Berg, 1999; Cutter et al., 1999; Dyrssen, 1988a; Luther et al., 1996; Zhang & Millero, 1994), the results from

those studies vary greatly. The conditional stability constants for metal-sulfide complexes generally range between 5 to 14, and can thus compete with organic ligands in trace metal complexation (Bruland & Lohan, 2006). Although some studies have shown that the majority of dissolved sulfide exists as free sulfide (e.g., Cutter et al., 1999), others (Dyrssen, 1988; Elliott, 1988; Zhang, 1999) suggest that metal-sulfide complexes likely dominate dissolved sulfide speciation and serve to protect it from oxidation in the open ocean. In coastal environments, dissolved metal-sulfide complexes have been shown to dominate the speciation of metals like copper (e.g., Kuwabara & Luther, 1993). Whereas, in the open ocean, some studies demonstrate that dissolved sulfide complexes dominate the speciation of mercury (Zhang & Millero, 1994) and can account for a majority of the speciation of other metals like nickel, cadmium, zinc, and copper (Cutter et al., 1999; Theberge et al., 1997).

Ultimately, the impact that hydrogen sulfide has on the cycling of trace metals largely depends on pH, along with the concentrations of dissolved sulfide, dissolved metals, and any competing organic ligands. While some studies (Dyrssen & Wedborg, 1989) considered precipitation of metal sulfides in the open ocean was unlikely due to very low concentrations, others (Janssen et al., 2014; Janssen & Cullen, 2015) hypothesized that the observed deficits of dissolved Cd (up to 0.1 nmol L^{-1}) and Zn (up to 0.5 nmol L^{-1}) relative to macronutrients in the North Pacific Ocean could be explained by precipitation with sulfide in oxygen deficit zones (ODZs). Janssen and colleagues (2014; 2015) suggest that this metal-sulfide formation is due to dissimilatory sulfate reduction (Canfield et al., 2010; Janssen & Cullen, 2015) to sulfide within anoxic microenvironments of suspended particles. Yet, it is worth mentioning that historical pAVS data in the Atlantic show pAVS maxima being associated with the chlorophyll maximum and thus

Table 2. The production of total dissolved sulfide (TDS) and particulate acid volatile sulfide (pAVS) in continuous cultures of 3 phytoplankton species at near ambient nutrient and metal concentrations. The TDS and pAVS concentrations shown are those when the culture was near steady state and with a normalization to chlorophyll a concentration.

Division	**Species (media)**	**TDS**	**pAVS**	**TDS**	**pAVS**	**TDS**	**pAVS**
		(pM)		(pM / µg Chl a)		(pM hr^{-1})	
Cyanobacteria	*Synechococcus sp.* (f/20)	1061	1102	54	57	5.00	5.3
	Trichodesmium (200 nM Fe)	357	3258	3.6	33.3	2.3	20.8
Diatom	*Nitzschia sp.* (L/100)	281	35	57	7	3.0	0.4

suggest production by assimilatory sulfate reduction in the water column (Radford-Knoery & Cutter, 1994; Walsh et al., 1994).

This dissertation seeks to address some of the knowledge gaps influencing hydrogen sulfide's biogeochemistry in the open ocean as pointed out in this brief summary. The data used to close some of these gaps primarily comes from samples collected in the Pacific and Southern Oceans that cover a large span of contrasting regimes. Moreover, the inclusion of sulfide measurements alongside concurrent measurements of dissolved metals and ancillary parameters serves to constrain the assumptions made in previous studies, thereby enhancing our confidence in these results. The following chapter will test the hypothesis of Janssen and colleagues (2014; 2015) that dissolved cadmium and zinc deficits observed in the low-oxygen Northeast Pacific can be explained by precipitation with sulfides.

CHAPTER 2

RE-EVALUATING HYDROGEN SULFIDE AS A SINK FOR CADMIUM AND ZINC IN THE OXIC TO SUBOXIC UPPER WATER COLUMN OF THE PACIFIC OCEAN

PREFACE

The American Geophysical Union (Copyright 2024 AGU) previously published a modified version of this Chapter: Buckley, N. R., Black, E. E., Kenyon, J. A., Lanning, N. T., Sieber, M., Conway, T. M., Fitzsimmons, J. N., & Cutter, G. A. (2024). Re-Evaluating Hydrogen Sulfide as a Sink for Cadmium and Zinc in the Oxic to Suboxic Upper Water Column of the Pacific Ocean. *Global Biogeochemical Cycles*, *38*(3), e2023GB007881. Doi: 10.1029/2023GB007881.

2.1 Introduction

Dissolved trace elements such as iron, cadmium, and zinc are essential micronutrients for the growth of phytoplankton in the ocean, influencing carbon cycling and global climate (Bruland & Lohan, 2006; Morel et al., 2003). In seawater, dissolved cadmium (Cd) and zinc (Zn) have nutrient-like distributions (Boyle et al., 1976; Bruland et al., 1978) driven by phytoplankton assimilation in surface waters and accumulation in deeper waters due to remineralization and advection of nutrient-rich water masses from the Southern Ocean (Baars et al., 2014; Bruland &

Lohan, 2006; Vance et al., 2017). Therefore, one-dimensional dissolved Cd and Zn profiles resemble those of the macronutrients, phosphate (PO_4^{3-}) and silicate ($Si(OH)_4$), respectively, and thus broadly exhibit a linear relationship to one another (Bruland & Lohan, 2006). From global linear metal:nutrient relationships, anomalies from the canonical dissolved Cd:PO_4^{3-} (cadmium-to-phosphate) and Zn:Si (zinc-to-silicate) relationships can be expressed using the 'star' convention (Cd* and Zn*):

$$Cd^* = Cd_{measured} - PO_{4\,measured}^{3-} \times \frac{Cd_{deep}}{PO_{4\,deep}^{3-}} \quad (1)$$

$$Zn^* = Zn_{measured} - Si_{measured} \times \frac{Zn_{deep}}{Si_{deep}} \quad (2)$$

where $Cd_{measured}$ and $Zn_{measured}$ are the dissolved metal concentrations, $PO_{4\,measured}^{3-}$ and $Si_{measured}$ are the measured nutrient concentrations, and where the deep water metal:macronutrient ratios, $\frac{Cd_{deep}}{PO_{4\,deep}^{3-}}$ and $\frac{Zn_{deep}}{Si_{deep}}$, can be set locally or globally (Conway & John, 2014; Janssen et al., 2014). Such Cd* and Zn* anomalies thus represent local or water-mass specific deviations of these metal-nutrient relationships from the whole ocean values, where positive values indicate an apparent surplus and negative values indicates an apparent metal deficit compared to their paired macronutrients. However, it is important to note that while Cd* or Zn* are useful in indicating relative difference in the ratio of the metals to the macronutrients in certain samples or water masses, they do not provide any information on the reason or mechanism for this decoupling, nor do they explicitly support local loss or gain of the element.

Using Cd* and Zn* anomalies, the oxygen minimum zones (OMZ; dissolved $O_2 < 50$ µmol kg^{-1}) of the North Pacific (Conway & John, 2015b; Janssen et al., 2014, 2019; Janssen & Cullen, 2015) and the North and South Atlantic (Conway & John, 2014, 2015a; Guinoiseau et al., 2018, 2019; Janssen et al., 2014) have been identified as regions with lower observed dissolved Cd (dCd) and dissolved Zn (dZn) concentrations than predicted from macronutrient concentrations. It was

hypothesized (Janssen & Cullen, 2015) that this deficit could be explained by precipitation of insoluble metal sulfides produced by dissimilatory sulfate reduction within anoxic microenvironments of sinking organic particles in the OMZ (Fig. 1). This mechanism was postulated to serve as a major sink of dCd and dZn from the global ocean (Conway & John, 2015a; Guinoiseau et al., 2019; Janssen et al., 2014; Janssen & Cullen, 2015; Xie, Rehkämper, et al., 2019), but recent work suggests that the explanation for the apparent dissolved metal deficits in low oxygen environments is still being disputed (e.g., de Souza et al., 2022; Janssen et al., 2019; Sieber, Lanning, Bunnell, et al., 2023).

Initially, the sulfide precipitation hypothesis was supported by the apparent decoupling of Cd and PO_4^{3-} for OMZs globally with deviations of up to -0.3 nmol kg^{-1} dissolved Cd* (Conway & John, 2015a; Guinoiseau et al., 2019; Janssen et al., 2014; Xie, Rehkämper, et al., 2019); along with enrichment of isotopically light Cd particles found at OMZ depths in the North Pacific (Janssen et al., 2019) and North Atlantic (Conway & John, 2015a; Janssen et al., 2014) that is associated with CdS precipitation (Guinoiseau et al., 2018; Schmitt et al., 2009; Yang et al., 2015). However, evidence for zinc sulfide (ZnS) removal within OMZs is more equivocal, despite apparent dissolved Zn deficits previously documented within the North Pacific and Atlantic OMZs (Conway & John, 2014; Janssen et al., 2014; Janssen & Cullen, 2015). Instead, recent studies have focused on alternative explanations for relative dCd and dZn depletion in OMZs since several observations do not support the sulfide precipitation mechanism as a globally important phenomenon (e.g., Janssen et al., 2019; Ohnemus et al., 2016; Roshan & DeVries, 2021; Vance et al., 2019). These findings call into question previous interpretations such as light Cd in particles as evidence for Cd-sulfide removal (Janssen et al., 2019). It is important to note that most studies to date have not evaluated whether sufficient sulfide exists in the North Pacific OMZ to support

the proposed metal-sulfide precipitation. In fact, only the ratios of insoluble pAVS to total particulate trace metals have been examined in the eastern tropical South Pacific (ETSP; Ohnemus et al., 2016), as well as benthic fluxes of dissolved iron and cadmium coupled with hydrogen sulfide concentrations from the Peruvian shelf (Plass et al., 2020; Schlosser et al., 2018; Xie, Rehkämper, et al., 2019).

Although sulfide is more commonly associated with low oxygen environments, produced via dissimilatory sulfate reduction (Canfield et al., 2010), sulfide is also produced in the fully oxic water column (Fig. 1) via carbonyl sulfide (OCS) hydrolysis (Elliott et al., 1987) or by assimilatory sulfate reduction within phytoplankton (Walsh et al., 1994). This latter process likely dominates sulfide production in surface waters (Radford-Knoery & Cutter, 1994), but the net sulfide production depends on the biological species present and the concentration of dissolved free metals (Walsh et al., 1994). Consequently, any dissolved, uncomplexed sulfide produced by either of these mechanisms is available to react with metals to form dissolved metal-sulfide complexes or may undergo oxidation to sulfate (Jia-Zhong & Whitfield, 1986; Millero et al., 1987; Pos et al., 1997). Dissolved sulfide can also directly precipitate to form insoluble particulate metal monosulfides (e.g., CdS, ZnS, FeS, NiS) known as particulate acid volatile sulfides (pAVS; Radford-Knoery & Cutter, 1994). This pAVS term would be the particulate CdS and ZnS postulated to be in OMZs where dissolved metal deficits have been observed. However, the exact speciation of pAVS is unknown, although from a purely chemical argument regarding Cd vs Zn removal by sulfide precipitation, the more polarizable nature and larger ionic radius of the Cd^{2+}

ion ("soft" acid) would have a higher affinity for "soft" sulfide ligands than the less polarizable ("harder") Zn^{2+} ion (Pearson, 1963).

Considered together, arguments supporting a global significance of metal precipitation within OMZs have become increasingly tenuous in light of recent studies, limiting any potential impact from CdS and ZnS precipitation to the local or regional scale. Moreover, the recent re-assessment by de Souza et al. (2022) identifies a signal of Cd loss within the oxycline of the shallow subsurface that is not confined to oxygen-deficient waters but ubiquitous throughout the tropics. Here, we present sulfide measurements alongside dissolved Cd and Zn concentrations in the upper water column of the North Pacific and the ETSP from US GEOTRACES GP15 and GP16 transects. The goal of this study is to evaluate whether enough sulfide exists to account for the dissolved metal deficits observed in the North Pacific OMZ as proposed by Janssen and co-authors (Janssen et al., 2014; Janssen & Cullen, 2015), as well as explore the relationship between sulfides and dissolved metals throughout the oxic to suboxic water column of the Pacific and parts of the North Atlantic Ocean.

2.2 Methods

2.2.1 Sampling site

The US GEOTRACES GP15 Pacific Meridional Transect (hereafter referred to as GP15) was sampled between 56°N to 20°S along 152°W from 18 September to 24 November 2018, on board R/V *Roger Revelle*. Transect profiles of dissolved oxygen (Fig. 2b) and total dissolved sulfide (TDS; Fig. 2d) are shown for sixteen stations, and small size fraction (0.8 – 51 μm) pAVS for thirteen stations (Fig. 2c). For a closer examination of the coupling between Cd, Zn, and sulfide in the N. Pacific, four GP15 stations were used (Fig. 3), Station 10 (42°N, 152°W), 12 (37°N, 152°W), 14 (32°N, 152°W), and 16 (27°N, 152°W).

The US GEOTRACES GP16 East Pacific Zonal Transect (hereafter referred to as GP16) was sampled between 77.4°W to 152°W along ~12°S from 25 October to 20 December 2013, on board R/V *Thomas G. Thompson*. Transect profiles of dissolved oxygen (Fig. 4b) and small size fraction (0.8 – 51 μm) pAVS (Fig. 4c) are shown for nine stations on the GP16 cruise. To examine the coupling more closely between Cd, Zn, and particulate sulfide in the ETSP, two stations were used (Fig. 5), Station 5 (12°S, 78.2°W) and 9 (12°S, 89°W).

2.2.2 Seawater sample collection

GP15 and GP16 water samples were collected using the US GEOTRACES trace metal sampling system (Cutter & Bruland, 2012) with 24-12 L GO FLO bottles mounted on a trace metal clean carousel with CTD, oxygen, fluorometer, and transmissometer sensors. Trace metal clean sampling procedures were followed (Cutter et al., 2017) and bottles were pressurized with 6 psi air (GP15) or nitrogen (GP16). 1.5 L of seawater from each depth was pressure filtered directly through 0.2 μm AcroPak Supor capsules and into 4 L polyethylene cubitainers for dissolved sulfide analyses (Radford-Knoery & Cutter, 1993). The cubitainers were then stored in a refrigerator and analyzed at sea within 8 hours. Seawater for dissolved Cd and Zn concentration analyses was filtered from the same GO FLO bottles into acid-cleaned 250 mL (Texas A&M University, TAMU) and 2 L (University of South Florida, USF) acid-cleaned Nalgene low density polyethylene (LDPE) bottles. Filtered seawater samples were acidified shipboard to 0.024 M HCl (TAMU), or back in the lab to 0.012 M HCl (USF), using ultrapure HCl, and left for at least 6 months prior to analysis.

2.2.3 Particulate sample collection

Particulate sulfide samples were collected by Phoebe Lam's sampling team using modified McLane in-situ pumps with two mini-MULVFS filter holders (Bishop et al., 2012) each plumbed with their own flowmeter (Lee et al., 2018). One of the holders contained a 51 μm polyester mesh prefilter and particles collected on a 0.8 μm polyethersulfone Supor membrane filter (0.8 – 51 μm

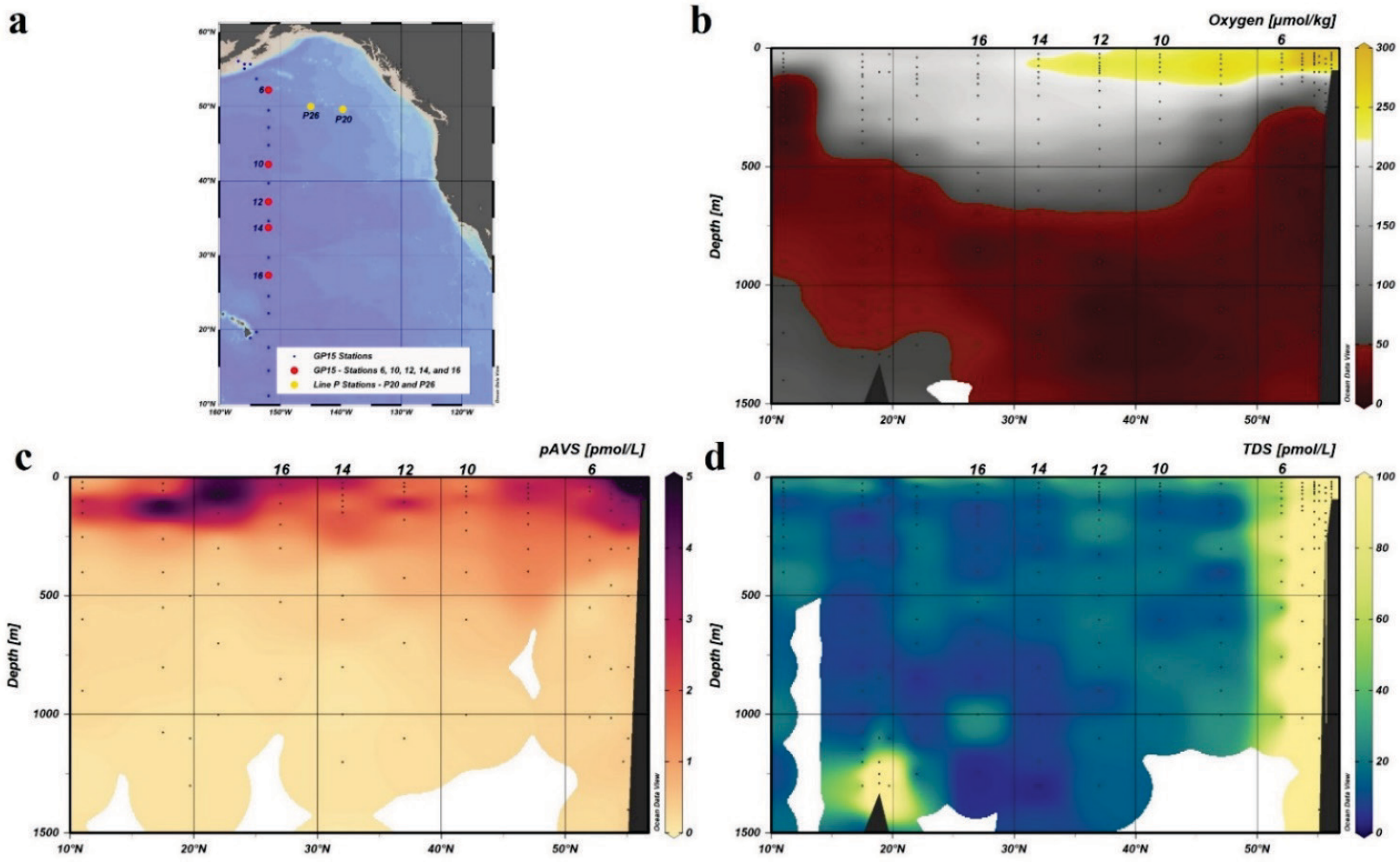

Figure 2. Sampling locations on the 2018 US GEOTRACES GP15 transect where Stations 6 (52°N, 152°W), 10 (42°N, 152°W), 12 (37°N, 152°W), 14 (32°N, 152°W), and 16 (27°N, 152°W) are shown as red dots in panel **a**. Janssen et al. (2014, 2015) stations P20 (49.6°N, 139.7°W) and P26 (50°N, 145°W) are shown as yellow dots. Contoured transect profiles of dissolved oxygen (panel **b**), particulate acid-volatile sulfide (pAVS; panel **c**), and total dissolved sulfide (TDS; panel **d**) concentrations are shown with original data points shown as black

size fraction). The other filter holder contained the same prefilter but collected particles on a Whatman QMA quartz fiber filter (1 – 51 μm size fraction; Bishop et al., 2012). Excess seawater in the filter holders was removed using a vacuum pump within an hour of pump recovery. The Supor filters were then subsectioned in the onboard trace metal clean lab by P. Lam's pump team and one-eighth of the filter subsamples placed in cryovials that were subsequently stored frozen at -80°C until analysis for pAVS. The whole Supor filters had between 100 and 1,100 L filtered through them, with an average of 400 L and thus an average effective volume of 50 L for the Supor subsample (12.5% of each filter). For particulate ^{234}Th samples, particles from the pre-filter were rinsed onto silver filters using 0.1 μm filtered seawater. Both the silver filter and 25 mm QMA subsample filter were analyzed on Risø Laboratories anti-coincidence beta counters. The entire QMA filters had between 300 and 1,540 L filtered through them, with an average filtration volume of 1,100 L and therefore an average effective volume of 43 L for a 25 mm QMA subsample (3.9% of each filter). It should be emphasized that the particulate concentrations in the study were calculated from the actual filter volumes for each sample, and not the average.

It is important to note that even though the small sized fraction (SSF; < 51 μm) pAVS analyses were performed on a subsample of the Supor (0.8 – 51 μm) filter, and SSF ^{234}Th analyses were conducted on a subsample of the QMA (1 – 51 μm) filters, it is assumed that these filters are sampling a similar population of particles (Bishop et al., 2012). Therefore, pAVS results obtained from Supor filters can be related to ^{234}Th analyses acquired from the QMA filters, as was done by Black et al. (2019). Large sized fraction (LSF; > 51 μm) particulate ^{234}Th activities were obtained from the Supor prefilter and used to estimate the unmeasured LSF pAVS flux (see discussion in Sections 3.2 and 3.3).

2.2.4 Determination of dissolved and particulate sulfide

Dissolved sulfide samples (only measured at-sea on GP15) were acidified to a pH of 1.6 with phosphoric acid and then gas stripped, cryogenically trapped, and quantified with gas chromatography/flame photometric detection using the method of Radford-Knoery and Cutter (1993). This quantifies total dissolved sulfide (TDS) as free sulfide (hydrogen sulfide ions) plus metal-sulfide complexes, with a 0.2 pmol S L^{-1} detection limit and precision of 13.7% RSD from duplicate and triplicate analyses. In addition to TDS, free sulfide was measured on all surface samples and some vertical profiles (e.g., GP15 Station 8 (47°N, 152°W)), where free sulfide was below detection limits for all samples. It should be noted that free sulfide detection limits vary depending on the pH, temperature, and salinity of the solution. Using values from Station 8 (47°N, 152°W) as an example, detection of free sulfide was limited to 3 pmol L^{-1} with a pH of 7.92, a salinity of 32.3, and at 15°C. This suggests that TDS was dominated by metal-complexed sulfide rather than uncomplexed sulfide along the entire GP15 transect.

Particulate acid volatile sulfide (pAVS) for the small size fraction (0.8 – 51 μm) was determined at sea for both GP15 and GP16 samples using the Radford-Knoery and Cutter (1993) procedure. This method entails placing the frozen Supor filter into a gas stripping vessel with deionized water, acidifying to 1 M HCl, and then the gas is stripped, cryogenically trapped, and quantified using gas chromatography/flame photometric detection. This method has a detection limit of 0.2 pmol S, which corresponds to relative detection limit of 0.004 pmol L^{-1} pAVS with average filtered volume of 50 L. Particulate AVS samples were analyzed mostly in single analyses, however, previous studies report pAVS precision near 10% RSD (Cutter & Kluckhohn, 1999; Cutter & Radford-Knoery, 1991).

2.2.5 Determination of dissolved Zn and Cd

Dissolved Zn and Cd concentrations were independently measured back on shore at TAMU by isotope dilution via pico-SEAFAST (Elemental Scientific) and inductively coupled plasma mass spectrometry (ICP-MS), and at USF using a batch extraction method and isotope dilution analysis by MC-ICP-MS. The methods of analysis at each institution have been described in detail previously (Conway et al., 2013; Jensen et al., 2020) with uncertainty on concentrations estimated as 2% (both institutions). Excellent agreement was found between the two labs (see Sieber, Lanning, Bian, et al., 2023; Sieber, Lanning, Bunnell, et al., 2023, Supporting Information). Dissolved metal concentrations from both institutions were averaged for each bottle depth for all samples except for surface Cd depths, where the 4 L samples of USF provided better accuracy than the 250 mL samples used by TAMU, and when one institution had an obvious outlier (excluded from average). More details of methods used on GP15, and an intercomparison of the full GP15 section for Cd and Zn concentrations between three institutions can be found in Sieber et al. (Sieber, Lanning, Bian, et al., 2023; Sieber, Lanning, Bunnell, et al., 2023); the GP15 dZn and dCd data used here are a subset of the full sections reported in those publications.

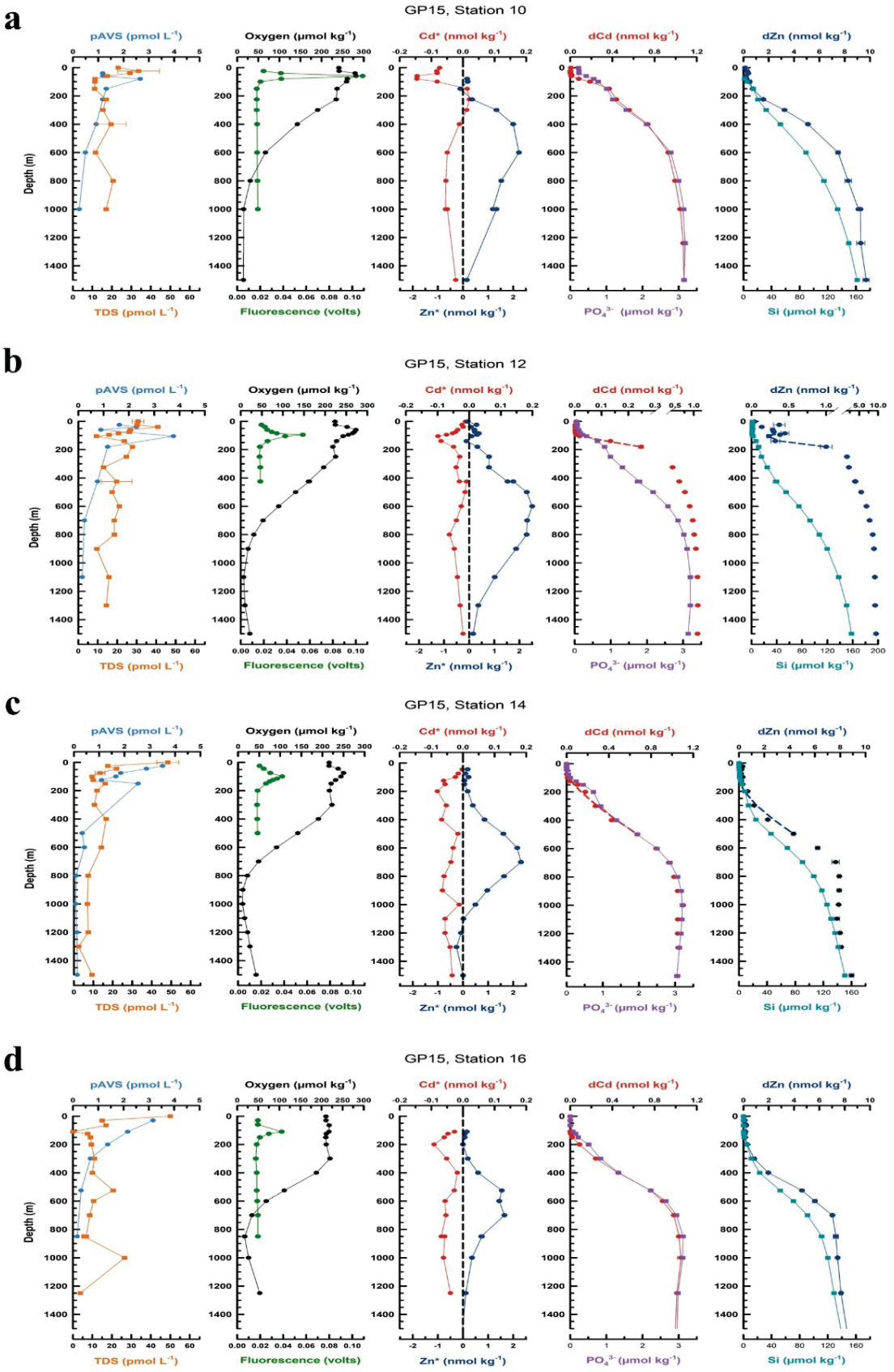

Figure 3. Vertical profiles of particulate acid-volatile sulfide (pAVS), total dissolved sulfide (TDS), dissolved

Figure 3 continued. oxygen, fluorescence, derived Cd*, derived Zn*, dissolved Cd (dCd), phosphate (PO_4^{3-}), dissolved Zn (dZn), and silicate (Si) concentrations collected on the 2018 US GEOTRACES GP15 transect in the North Pacific with Station 10 (42.0°N, 152.0°W) shown in panel **a**, Station 12 (37.0°N, 152°W) in panel **b**, Station 14 (32.0°N, 152.0°W) in panel **c**, and Station 16 (27°N, 152.0°W) in panel **d**. Error bars on TDS data indicate one standard deviation above and below the mean on samples that were analyzed in triplicate.

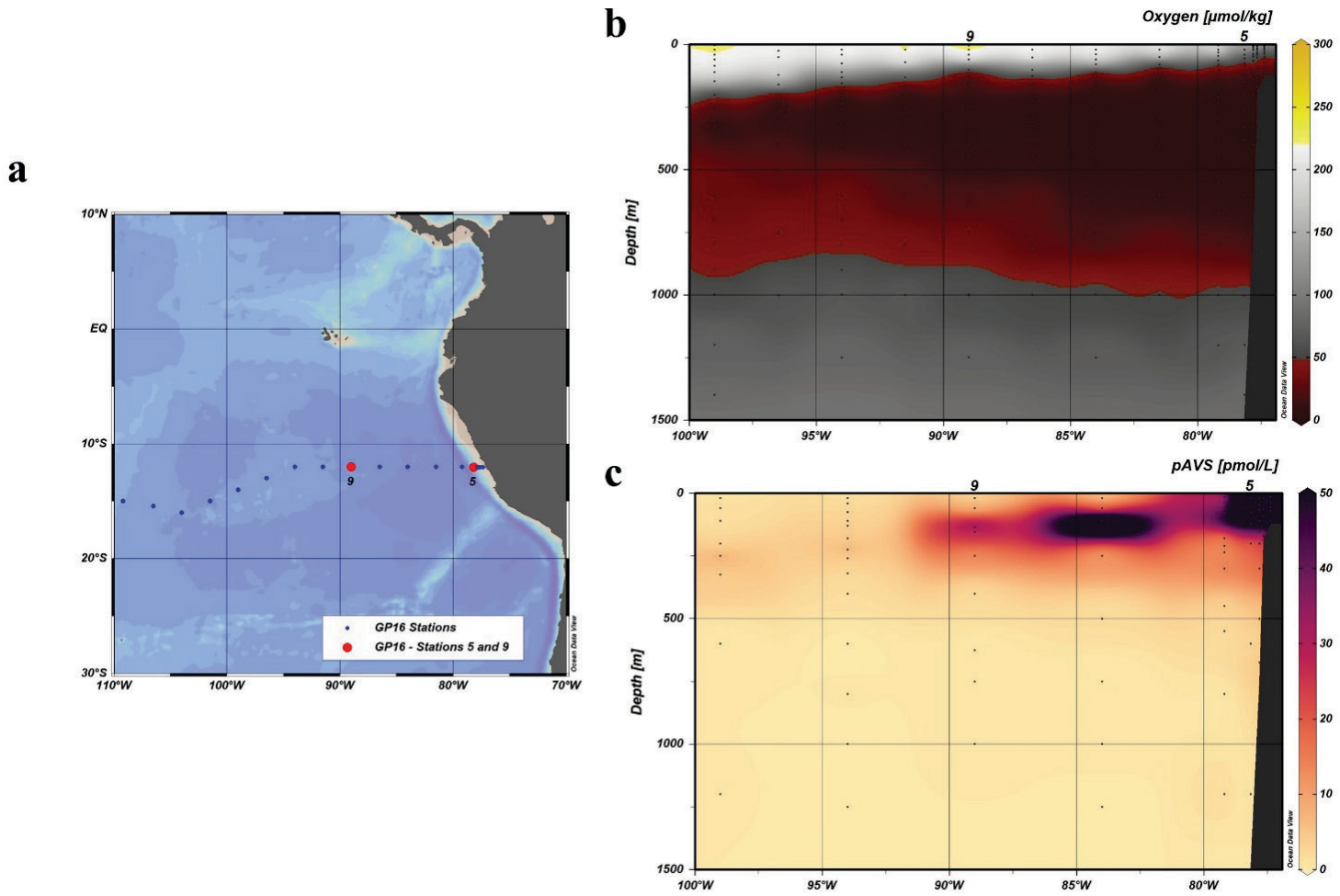

Figure 4. Sampling locations on the 2013 US GEOTRACES GP16 where Stations 5 (12.0°S, 78.2°W) and 9 (12.0°S, 89°W) are shown as red dots in panel **a**. Contoured transect profiles of dissolved oxygen (panel **b**) and pAVS (panel **c**) concentrations are shown with original data points shown as black dots. Particulate acid-volatile sulfide (pAVS) data are from Ohnemus et al. (2016) and occasionally exceeded 50 pmol L^{-1} closer to the South American coast.

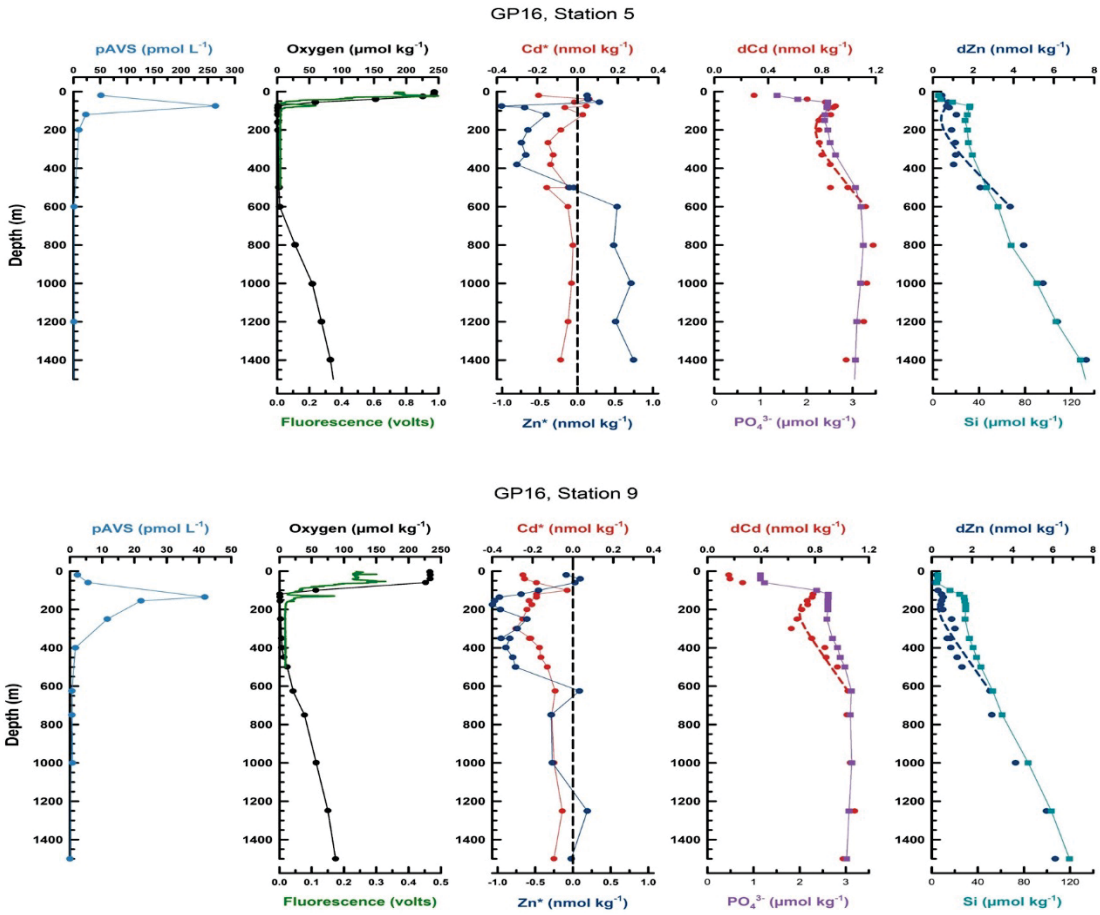

Figure 5. Vertical profiles of particulate acid-volatile sulfide (pAVS), dissolved oxygen, fluorescence, derived Cd*, derived Zn*, dissolved Cd (dCd), phosphate (PO_4^{3-}), dissolved Zn (dZn), and silicate (Si) concentrations collected on the 2013 US GEOTRACES GP16 transect in the Eastern Tropical South Pacific with Station 5 (12.0°S, 89.0°W) shown on top and Station 9 (12.0°S, 78.2°W) on the bottom. pAVS data are from Ohnemus et al. (2016) and dissolved Cd and Zn data are from John et al. (2018).

2.2.6 Calculation of dissolved Zn* and Cd*

Cd* and Zn* were calculated using equations 1 and 2 following Janssen et al. (2014), Conway and John (2014), and Janssen and Cullen (2015). The $\frac{Cd_{deep}}{PO_{4\,deep}^{3-}}$ represents the average deep water ratio of 0.35 mmol mol^{-1} taken from Janssen et al. (2014), and the $\frac{Zn_{deep}}{Si_{deep}}$ represents the average deep water ratio of 0.059 mmol mol^{-1} taken from Janssen and Cullen (2015). Studies in the North and South Pacific (Janssen et al., 2014; Sieber et al., 2019) in combination with GP15 data show that the deep Cd: PO_4^{3-} ratio is 0.35 mmol mol^{-1} throughout the deep Pacific (Sieber, Lanning, Bunnell, et al., 2023). This is similar to the globally-relevant deep Zn:Si ratio (0.064 mmol mol^{-1}) and Cd: PO_4^{3-} ratio (0.33 mmol mol^{-1}) suggested by Vance et al. (2017) and de Souza et al. (2022) respectively, but here we chose to use 0.059 mmol mol^{-1} and 0.35 mmol mol^{-1} to be most comparable to existing Pacific Zn and Cd studies, applying the same deep ocean reference ratios to both Pacific study regions in this paper for consistency. To assess the propagated uncertainty of Cd* and Zn*, we used the reported 1SD uncertainties in PO_4^{3-} (± 0.02 µmol kg^{-1}) and Si (± 0.7 µmol kg^{-1}) based on replicate measurements of their respective reference materials (Cutter, Casciotti, et al., 2018), in combination with the 1SD uncertainties of Cd (± 0.01 nmol kg^{-1}) and Zn (± 0.1 nmol kg^{-1}) based on their inter-laboratory reproducibility (see Sieber, Lanning, Bian, et al., 2023; Sieber, Lanning, Bunnell, et al., 2023, Supporting Information). Together, these yield a conservative estimate of the maximum propagated uncertainty (1SD) of ± 0.015 nmol kg^{-1} for Cd* and ± 0.14 nmol kg^{-1} for Zn* for the GP15 samples.

2.2.7 One-dimensional advection/diffusion modeling

Removal fluxes of dCd and dZn in subsurface waters were calculated using a simple one-dimensional advection/diffusion model originally developed for the deep sea and allowing non-conservative removal to be calculated (Craig, 1969), but later adapted to compute removal rates in the upper ocean (Cutter, 1991; Cutter, Moffett, et al., 2018). This model assumes mixing of two end member water masses with no horizontal inputs, so it can only be applied where there is a linear T-S range (Fig. 6). For this reason, it should be noted that it was only possible to apply the model to two stations in the oxic subsurface waters on GP15, and two stations in the oxycline on GP16.

In the oxygenated North Pacific for GP15, the modeling efforts used two stations. The linear T-S range for Station 12 was from 85 – 180 m and the dissolved Cd fluxes were computed over this depth range (Fig. 7, top). In contrast, the linear T-S was from 75 – 500 m at Station 14 and the dCd losses were computed over this range (Fig. 7, bottom). However, the large gap in pAVS data from 150 – 500 m forced us to reduce the dissolved Cd losses to only between 75 – 150 m. For advection/diffusion calculations, ^{7}Be-based-vertical eddy diffusion coefficients, K_z, and upwelling rates (Moriyasu, Bolster, et al., 2023) at each station were used to compute a rate of production/consumption, J, that was assumed to be constant over the specified depth range. The J term was then multiplied by the depth interval to yield removal fluxes for dCd at both stations. Particulate AVS fluxes were calculated over the same depth ranges as dissolved Cd using the ^{238}U-^{234}Th disequilibrium method (Buesseler et al., 1992) as applied to sinking particle fluxes, which combines measurements of ^{234}Th activities and pAVS concentrations on small particles (<51 μm).

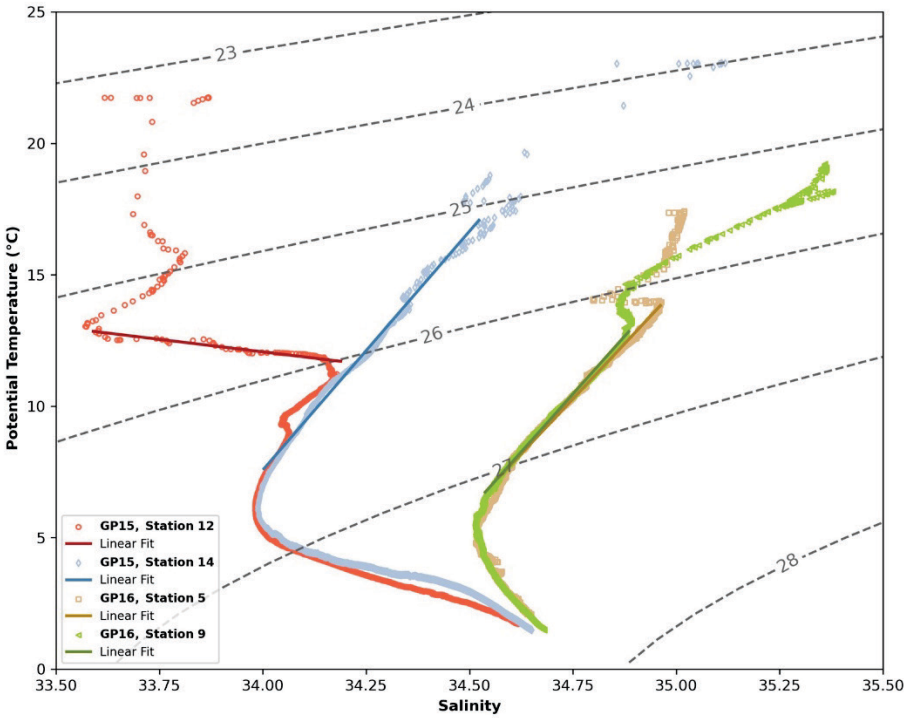

Figure 6. Temperature-salinity (T-S) diagram with density isolines of four stations from GP15 and GP16 where 1-D advection-diffusion modeling was applied. The open, red circles represent Station 12 (37°N, 152°W) from GP15 where a linear fit (r^2 = 0.9027) shown as a red line was applied over the modeled range (85 – 180 m). The open, blue diamonds represent Station 14 (32°N, 152°W) from GP15 where a linear fit (r^2 = 0.9904) shown as a blue line was applied over the modeled range (75 – 500 m). The open, brown squares represent Station 5 (12.0°S, 78.2°W) from GP16 where a linear fit (r^2 = 0.9937) shown as a brown line was applied over the modeled range (75 – 600 m). The open, green triangles represent Station 9 (12.0°S, 89°W) from GP16 where a linear fit (r^2 = 0.9954) shown as a green line was applied over the modeled range (135 – 625 m).

Two stations from the oxycline in the ETSP for GP16 were also examined, where the linear T-S range at Station 5 went from 75 – 600 m and at Station 9 from 135 – 625 m. However, the dissolved Cd and Zn fluxes were only computed for the range of 75 – 200 m at Station 5 (Fig. 8, top) and 135 – 200 m at Station 9 (Fig. 8, bottom) to match the pAVS flux calculations, since ^{234}Th fluxes were limited to the upper 200 m (Black et al., 2018). For GP16 advection/diffusion

calculations, ^{7}Be-based-vertical eddy diffusion coefficients, K_z, and upwelling rates from Kadko (2017) at each station were used to compute a rate of production/consumption, J, that was held constant over the specified depth range as was done for the GP15 data set.

Although pAVS include CdS and ZnS precipitates, other metal sulfide precipitates are included in the pAVS fraction such as FeS, NiS, PbS, etc. However, the precipitates PbS, CdS, and ZnS are thermodynamically favored due to lower solubility product constants and are more likely to precipitate at lower sulfide concentrations (e.g., Goates et al., 1952); they are also favored due to faster water exchange reaction kinetics (Morse & Luther, 1999). Though, due to relevant Pb, Cd, and Zn concentrations in the Pacific, it seems reasonable that CdS and ZnS precipitates are likely to make up the majority of pAVS. Therefore, this study assumes that the apparent removal is the maximum possible removal if all pAVS were bound only to Cd and Zn (for GP16) and only to Cd (for GP15; see discussion in Sections 2.3.1 and 2.3.3).

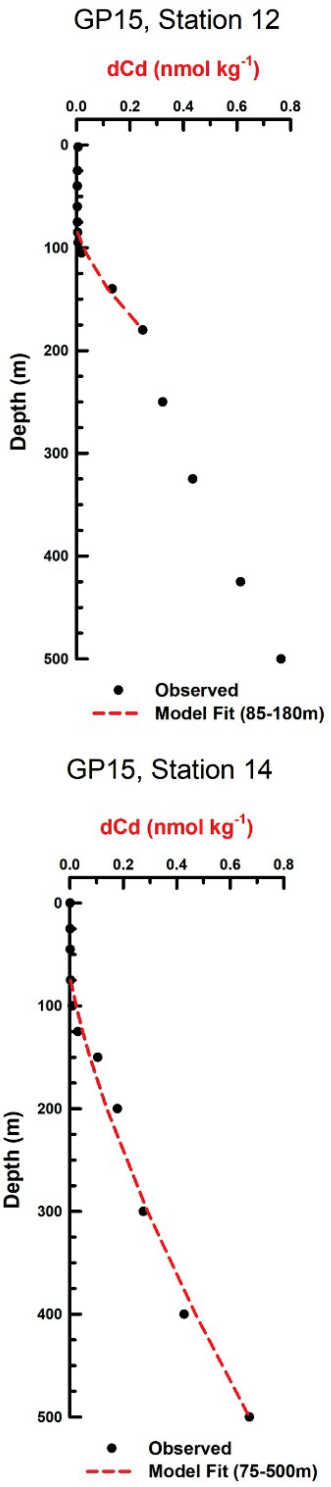

Figure 7. 1-D vertical advection/diffusion model was applied to observed dissolved Cd (dCd) at GP15 Station 12 (37.0°N, 152°W, top, $r^2 = 0.9842$) and Station 14 (32.0°N, 152.0°W, bottom, $r^2 = 0.9871$) to estimate the losses of dCd to deeper waters over the modeled range. The dashed line indicates the fit of the model to the observed dCd concentrations which was used to calculate a rate of production/consumption of dissolved Cd.

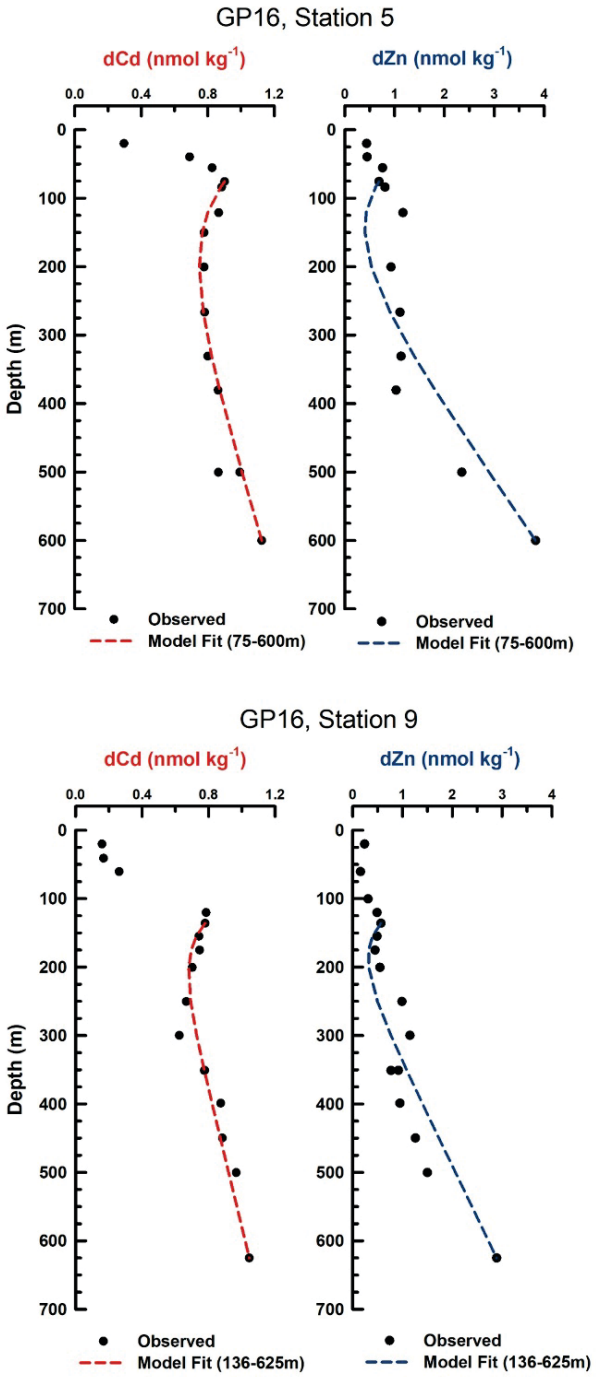

Figure 8. 1-D vertical advection/diffusion model was applied to observed dissolved Cd (dCd) and dissolved Zn (dZn) at GP16 Station 5 (12.0°S, 89.0°W, top, Cd: $r^2 = 0.7608$, Zn: $r^2 = 0.7852$) and Station 9 (12.0°S, 78.2°W, bottom, Cd: $r^2 = 0.8809$, Zn: $r^2 = 0.7280$) to estimate the losses of dCd and dZn to deeper waters over the modeled range. The dashed line indicates the fit of the model to the observed dCd and dZn concentrations which was used to calculate a rate of production/consumption for each dissolved metal.

2.2.8 Determination of ^{234}Th

Total ^{234}Th samples were collected by K. Buesseler's team at all stations along the GEOTRACES GP15 (2 L samples) and GP16 (4 L samples) transects in addition to regular underway surface sampling. Total ^{234}Th analyses was done in accordance with the method developed in Buesseler et al. (2001), and further detailed in Clevenger et al. (2021). ^{234}Th is co-precipitated with Mn-oxide and collected onto a 25 mm quartz microfiber (QMA) filter and measured on Risø Laboratories anti-coincidence beta counters. A ^{230}Th yield monitor was used to determine the recovery of thorium through the chemical extraction steps. Full ^{234}Th results from GP16 are reported in Black et al. (2018). ^{238}U activities were calculated using the salinity relationship described in Owens et al. (2011):

$$^{238}U(\pm 0.047) = (0.0786 \pm 0.00446) * salinity - (0.315 \pm 0.158) \qquad (3)$$

Recent work by Xie et al. (2020) has brought into question whether the global ^{238}U-salinity relationship always holds in coastal Peruvian OMZ waters, and their results indicated that using the relationship could lead to an average underestimation of ^{234}Th fluxes of 20% at locations in the vicinity of GP16 Station 5. However, in contrast to the coastal conditions observed during the austral spring-summer 2013 GP16 campaign, Xie et al. (2020) occupied the coastal waters under El Nino-Southern Oscillation (ENSO) conditions in austral autumn-winter conditions in 2017 (i.e., weak alongshore winds, very low upwelling rates). The authors posited that the ENSO could be a driver for uranium mobilization from shelf sediments, and it is not known whether their reported deviations from the ^{238}U-salinity relationship could be persistent or present during neutral of La Nina years. We continue to use the ^{238}U-salinity relationship here, but we note the need for further study into ENSO-driven, temporal variations in the Peruvian OMZ. The activity of ^{234}Th in the surface ocean is described by the following equation:

$$\frac{\partial^{234}\mathrm{Th}}{\partial t} = \lambda_{\mathrm{Th}}(^{238}\mathrm{U} - ^{234}\mathrm{Th}) - \mathrm{P}_{\mathrm{Th_z}} + \mathrm{V} \quad (4)$$

which reflects the balance between production and loss of ^{234}Th from decay, sinking flux, and transport. ^{234}Th is the total ^{234}Th activity (dpm L^{-1}), ^{238}U is the ^{238}U activity derived from salinity, λ_{Th} is the decay constant (0.0288 d^{-1}), P is the net removal of ^{234}Th on sinking particles (dpm L^{-1} d^{-1}), and V is the sum of advective and diffusive ^{234}Th fluxes (dpm L^{-1} d^{-1}).

The disequilibrium created between ^{234}Th and ^{238}U in the surface ocean occurs when thorium attaches to sinking particles. This integrated deficit can be used to determine ^{234}Th export fluxes. In order to take the $\mathrm{P}_{\mathrm{Th_z}}$ term from equation (4) and apply it to a given element or compound [E] (AVS), the following equation is needed:

$$\mathrm{P}_{\mathrm{E_z}} = \frac{[\mathrm{E}]}{^{234}\mathrm{Th}} \mathrm{P}_{\mathrm{Th_z}} \quad (5)$$

where ^{234}Th is the activity of ^{234}Th on sinking particles, and $\mathrm{P}_{\mathrm{E_z}}$ is the particulate AVS flux at depth z. While it is often assumed that the E_{LSF}/Th_{LSF} (large sized fraction particulates, >51 μm) measured at depth z is representative of sinking particles (reviewed in Buesseler et al. (2006)), it should be noted that the small size particle ratios have been shown to be similar to large particle ratios (Hayes et al., 2018). Therefore, small sized fraction (SSF) pAVS potentially contribute the same or more towards total pAVS removal compared to larger sized fraction (LSF) pAVS.

2.3 Results and Discussion

2.3.1 Northeast Pacific OMZ

Janssen and co-authors (Janssen et al., 2014; Janssen & Cullen, 2015) suggested sulfide precipitation removes dCd and dZn from OMZ depths of stations on Line P (Fig. 2a) in the NE Pacific. This effect was manifested as a reported deficiency of up to 0.5 nmol kg^{-1} of dZn and 0.1 nmol kg^{-1} of dCd on Line P (Janssen et al., 2014; Janssen & Cullen, 2015) based on reported Zn*

and Cd* anomalies. Despite US GEOTRACES GP15 stations being approximately 1,000 km west of Line P (Fig. 2a), they share similarly low dissolved oxygen concentrations of <50 μmol kg^{-1} over a 1,000 m depth range between 30°N and 55°N, with concentrations as low as 10 μmol kg^{-1} at about 1,100 m (Fig. 2b). Yet on the GP15 section, we found similar maximum apparent deficits of up to 0.1 nmol kg^{-1} dCd, but little evidence of dZn loss (Fig. 3) at OMZ depths, based on the calculated Zn* and Cd* anomalies. In fact, Zn* was generally positive at the depths where we would expect to see the effects of sulfide precipitation, suggesting no significant role for sulfide-removal of Zn. This is consistent with the Zn* anomalies reported in Vance et al. (2019), which attributed the observed decoupling to differing length scales of dissolution of Zn and Si in the region, rather than *in situ* ZnS precipitation. Sieber, Lanning, Bian, et al., (2023) drew similar conclusions for Zn across the North Pacific, showing that Zn and Si are decoupled for several reasons, including preferential uptake and regeneration, water mass signatures, and reversible scavenging. Therefore, it is assumed that the positive anomalies seen in Zn* (Fig. 3) are associated with regeneration of organic matter with an elevated Zn/Si ratio. Below this, Zn* values return to near 0, a function of moving below the depths where regeneration of high Zn organic matter drives elevated Zn*, and not *in situ* Zn loss (Sieber, Lanning, Bian, et al., 2023) as ZnS precipitates.

Nonetheless, GP15 profiles exhibited slight Cd* depletions (~ -0.1 nmol kg^{-1}) within the OMZ (>400 m) at several stations (featured in Figure 3), similar to Janssen et al. (2014) on Line P and Conway and John (2015b) at the SAFe Station (30°N, 140°W; approximately 1,200 km east of GP15 Station 14). Even if metal sulfide loss is limited to Cd (and not Zn) in the North Pacific OMZ, the concentrations of pAVS required to support such metal removal were not observed along our GP15 section: pAVS was <1 pmol L^{-1} throughout the OMZ (Figures 2c and 3) and total dissolved sulfide (TDS; dissolved free and complexed sulfide) typically exhibited a near surface

maximum of 50 pmol L^{-1} that decreases with depth to negligible concentrations in the OMZ (Figures 2d and 3). Overall, the observed picomolar values of TDS and pAVS are stoichiometrically too low to match the 0.1 nanomolar deficit of dCd observed in the OMZ along GP15, and the dZn and dCd deficits previously reported on Line P (Janssen et al., 2014; Janssen & Cullen, 2015), signifying that any observed negative metal* anomalies cannot be fully explained by metal-sulfide precipitation in this region. However, one remaining question is whether particulate CdS could have sunk to deeper waters on the timescale of days to weeks (Coale & Bruland, 1985), preventing us from observing the particulate sulfides in the water column. If we assume that particulate AVS fluxes exhibited similar flux attenuation as that of carbon in the North Pacific (Buesseler et al., 2008; Martin et al., 1987), fluxes at OMZ depths (approx. 500 m) likely decreased at least 75% from the fluxes reported in the subsurface at 100 m (see Section 2.3.3). Under this assumption, there could have been approximately 25 pmol kg^{-1} pAVS in the OMZ (apparent deficit of dCd (0.1 nmol kg^{-1}) x flux estimate at 500 m (25%)) at Stations 12 and 14 on GP15. This 25 pmol kg^{-1} value is still 4 times too low compared to the maximum 0.1 nmol kg^{-1} dissolved Cd deficits to explain the apparent dissolved metal deficits in the GP15 dataset. Therefore, it is probable that sulfide precipitation only serves as a secondary mechanism that contributes to a portion of the dissolved Cd deficit observed in the NE Pacific OMZ, rather than the whole.

While the data examined here represent the OMZ of the NE Pacific, it should be noted that the OMZ of GP15 is deeper than the OMZ on Line P (Janssen et al., 2014; Janssen & Cullen, 2015). Station 6 (52°N, 152°W) from GP15 exhibits an oxygen depth profile (Fig. 2b) more similar to Line P Stations P20 and P26 (Fig. 2a). Though limited, the observed pAVS values reported in the Station 6 OMZ are also too small (0.52 ± 0.49 pmol pAVS L^{-1}, n = 4) to explain the apparent

dissolved Cd deficits observed on Line P and GP15, even when allowing for losses by particle sinking. These data suggest that, at least in the North Pacific along GP15, dissimilatory sulfate reduction in the OMZ does not produce sufficient sulfide to explain observed dCd deficits.

Instead of sulfide precipitation, recent studies invoke a water mass circulation artifact where the apparent dissolved metal deficits observed in N. Pacific OMZs are likely a preformed signal from the Southern Ocean (de Souza et al., 2022; Middag et al., 2018, 2019; Sieber et al., 2019; Xie, Galer, et al., 2019). In this respect, Roshan and DeVries (2021) found that low-latitude oceans have lower $Cd:PO_4^{3-}$ export ratios relative to the Southern Ocean, which acts to deplete Cd relative to phosphate in the low-latitude thermoclines. Similarly, Liu et al. (2022) also found that up to 0.5 nmol kg^{-1} Cd depletion is due to change in surface $Cd: PO_4^{3-}$ export ratios between samples within and outside the Angola Basin OMZ, instead of Cd-sulfide precipitation. More recently, Sieber, Lanning, Bunnell, et al. (2023) have argued that regeneration throughout the Pacific with a lower $Cd:PO_4^{3-}$ than the global mean may explain apparent negative Cd* signals in this region, as such signals are not limited to low oxygen waters but rather span the whole eastern North Pacific, coinciding with the PO_4^{3-} maximum. While these studies do not rule out the precipitation of CdS and ZnS occurring in low oxygen regions, they imply that the formation of sulfide precipitates is unlikely to be the primary controlling mechanism for apparent dissolved Cd and Zn deficits observed within the NE Pacific OMZ. However, it is worth noting that the focus of this study is on small particles (<51 μm) and cannot definitively speak to the accumulation of CdS within anoxic microenvironments of large (>51 μm) sinking particles within hypoxic layers (Bianchi et al., 2018; Janssen & Cullen, 2015).

2.3.2 Eastern Tropical South Pacific OMZ

Comparison to a more intense OMZ, like that in the ETSP, can provide further insights into the metal-sulfide precipitation mechanism in different ocean regions. The coastal waters off Peru, with high rates of productivity and particle export due to upwelling (Chavez et al., 2008), host an intense OMZ. Unlike the North Pacific OMZ, the oxygen concentrations in the ETSP reach low oxygen concentrations (<50 μmol kg^{-1}) at very shallow depths (< 250 m) (Fig. 4b). Previous studies (Xie, Rehkämper, et al., 2019) observed a decoupling between Cd and phosphate within oxygen-deficit waters, whereas John et al. (2018) found no evidence of large-scale Cd* depletion in the ETSP OMZ where oxygen has much lower concentrations than the other OMZs mentioned above and thus more dissimilatory sulfate reduction and metal sulfide formation might be expected (Janssen et al., 2019; John et al., 2018; Ohnemus et al., 2016). Particulate AVS data in the ETSP OMZ have been examined previously by Ohnemus et al. (2016) who concluded that the ≤1:1 mol:mol ratio of Cd-to-AVS particles in the OMZ was insufficient to support CdS precipitation as a means to enrich Cd in sinking particles. Instead, they hypothesized (Ohnemus et al., 2016) that heterotrophs within OMZs may exhibit uniquely high Cd and Zn demands that drive metal removal from the dissolved phase relative to nutrients. Despite this prior evaluation, the US GEOTRACES GP16 section in the ETSP (Fig. 4a) provides an opportunity to re-examine the pAVS data (Ohnemus et al., 2016) paired with published data for dCd and dZn (John et al., 2018) and particle flux rates using ^{234}Th-based sinking rates (Black et al., 2018) above and within an OMZ. These thorium data were not yet available for the Ohnemus et al. (2016) study.

Apparent dCd and dZn deficits were calculated as part of our reanalysis of GP16 results using the same 'star' convention (see Section 2.2.6) to compare to the NE Pacific. However, we need to consider that equatorial Antarctic Intermediate Water (eqAAIW) supplies Cd and Zn to

these waters with preformed southern-sourced Cd* (-0.1 nmol kg^{-1} (Sieber et al., 2019)) and Zn* signals (-0.5 nmol kg^{-1} (John et al., 2018)). After accounting for the preformed eqAAIW signal, GP16 stations exhibit apparent local deficits of dCd up to 0.2 nmol kg^{-1} and 0.7 nmol kg^{-1} dZn in the OMZ at Stations 5 and 9 according to Cd* and Zn* values (Fig. 5). In contrast to the North Pacific OMZ, shallow OMZ depths in the ETSP display large peaks in pAVS (Ohnemus et al., 2016) (Figs. 4c and 5) with Station 5 showing a pAVS maximum of 264 pmol L^{-1} at the base of the oxycline (Fig. 5, top). Station 9 also exhibited a pAVS maximum at the base of the oxycline, although it only reached 42 pmol L^{-1} pAVS (Fig. 5, bottom).

To quantify the deficits of dCd and dZn on the GP16 transect and compare them to pAVS fluxes, required removal fluxes of dCd and dZn were calculated using the simple one-dimensional advection/diffusion model described in Section 2.2.7 and used by Cutter, Moffett, et al. (2018) for the same stations on GP16. The calculated Zn and Cd removal rates (Table 1) were more than an order of magnitude higher in the ETSP (GP16) than in the NE Pacific (GP15). To compare these dissolved metal losses, particulate AVS fluxes were calculated over the same depth ranges using ^{238}U-^{234}Th disequilibrium (see Section 2.2.8) as applied to sinking particle fluxes. From this, the more coastal Station 5 saw a pAVS net removal rate of 1,268 nmol S m^{-2} d^{-1} between 75 – 200 m in the small sized fraction (SSF), while Station 9 had SSF pAVS net removal of 49 nmol S m^{-2} d^{-1} (Table 1) between 135 – 200 m. As such, Station 5 had a more than sufficient pAVS flux to account for the apparent removal of both dCd and dZn in the shallow, upper OMZ, while at Station 9 pAVS could account for 16% of the apparent dissolved removal of dCd and dZn (Table 1) as small CdS and ZnS precipitates. However, it is important to note that these estimates of dCd and dZn removal as pAVS only account for the measured small sized fraction (SSF) that is being exported to deeper waters. Therefore, our estimated SSF pAVS flux represents a conservative

minimum, since they do not include the more commonly considered sinking (e.g., Lam et al., 2018; Lee et al., 2018) LSF particles (not measured). Considering that pAVS is likely primarily composed of CdS (and possibly ZnS) precipitates, it is assumed that the particle distribution of pAVS resembles the pattern of distribution seen for particulate Cd (Lee et al., 2018). To address this caveat, LSF pAVS fluxes were estimated at both stations using particulate Cd concentrations (LSF and SSF; obtained from P. Lam, personal communication) alongside the LSF ^{234}Th activities. Although all of the dCd and dZn losses observed at Station 5 could be explained by the SSF pAVS, apparent removal at Station 9 was more limited. If LSF pAVS removal is considered, dCd and dZn removal via precipitation with sulfide potentially removes an additional 1.6 nmol S m^{-2} d^{-1} at Station 9 (Table 1), accounting for a 1% increase in removal of dissolved Cd and Zn as pAVS in the oxycline. These estimates suggest that the measured SSF pAVS likely makes up a larger proportion of the total pAVS (SSF + LSF) flux, and thus plays a larger role a larger role in the removal of dCd and dZn as metal-sulfide precipitates in the shallow, upper OMZ waters, than LSF pAVS.

Table 3. Removal rates of dissolved Cd and dissolved Zn (if apparent deficits in Cd* and Zn* were found) at Stations 12 and 14 on GP15, and Stations 5 and 9 on GP16. Removal rates of particulate acid-volatile sulfide (pAVS) are reported for those 4 stations. It should be noted that for GP15 and GP16, only SSF pAVS was measured, and thus, those values alone are conservative estimates as they do not factor in the sinking, large particles (unmeasured). LSF pAVS fluxes were estimated using particulate Cd (LSF and SSF obtained from P. Lam) alongside LSF ^{234}Th activities.

Cruise	**Station**	**Lat.** (°N)	**Long.** (°W)	**Depth Range** (m)	**Cd J term** (nmol L^{-1} d^{-1})	**Cd Flux** (nmol m^{-2} d^{-1})	**Zn J term** (nmol L^{-1} d^{-1})	**Zn Flux** (nmol m^{-2} d^{-1})	**Measured SSF pAVS Flux** (nmol m^{-2} d^{-1})	**Estimated LSF pAVS Flux** (nmol m^{-2} d^{-1})
GP15	12	37.0	152.0	85-180	$-1.4 \pm 0.4 \times 10^{-4}$	13 ± 4			4	1.7
GP15	14	32.0	152.0	75-150	$-2.5 \pm 0.2 \times 10^{-5}$	2 ± 0.2			4.5	3.4
GP16	5	-12.0	78.2	75-200	$-4.9 \pm 0.4 \times 10^{-4}$	61 ± 5	$-3.8 \pm 0.4 \times 10^{-3}$	475 ± 50	1268	609
GP16	9	-12.0	89.0	135-200	$-6.3 \pm 0.3 \times 10^{-4}$	41 ± 2	$-4.2 \pm 0.3 \times 10^{-3}$	273 ± 20	49	1.6

These GP16 results support the hypothesis that metal removal via precipitation with sulfide is possible but it is important to point out that the OMZ off Peru is unusual. While dissimilatory sulfate reduction has been documented in OMZ waters (Callbeck et al., 2021; Canfield et al., 2010; Schlosser et al., 2018), here the pAVS maxima coincide with the secondary fluorescence maxima (Fig. 5) (Ohnemus et al., 2016) where photosynthetic bacteria are present (Goericke et al., 2000; Lavin et al., 2010). Thus it is likely that some fraction of TDS (not measured on GP16) and pAVS are associated with assimilatory sulfate reduction during photosynthesis at these depths (Walsh et al., 1994). As a result, both assimilatory sulfate reduction (Ohnemus et al., 2016; Walsh et al., 1994) and dissimilatory sulfate reduction (Canfield et al., 2010) may contribute to the observed dCd and dZn deficits in the ETSP, potentially explaining the contrasting patterns observed in different OMZs.

2.3.3 Northeast Pacific Oxic Subsurface

In contrast to the low concentrations at OMZ depths in the Northeast Pacific, both pAVS and TDS concentrations are highest in the upper 200 m of the water column (Figures 2 and 3), where oxygen is abundant (>200 μmol kg^{-1}). Unlike GP16, no evidence of dZn loss was found in the Northeast Pacific on GP15 as indicated by Zn* (Fig. 3). However, apparent dCd deficits up to 0.1 nmol kg^{-1} were reported at Stations 12, 14, and 16, and up to 0.15 nmol kg^{-1} at Station 10 from GP15 (Fig. 3) in the oxygenated subsurface. These same waters are where Sieber, Lanning, Bunnell, et al. (2023) reported a heavier dissolved isotope signal ($\delta^{114}Cd$), which would be consistent with CdS precipitation that preferentially incorporates light Cd isotopes into the particulate phase. Significantly, this is also where pAVS maxima coincide with the local Cd*

minima in the GP15 profiles (Figure 3), and therefore sinking pAVS could potentially lead to removal of dCd in oxic waters.

To quantify the deficits of dCd on the GP15 transect and compare them to pAVS fluxes, we used the same computations as those used for the GP16 dataset (Sections 2.2.7 and 2.3.2). The estimated removal rate of dCd at Station 12 (Cd flux is 13 ± 4 nmol m^{-2} d^{-1}; Table 1) was 6.5 times larger than those calculated at Station 14 (Cd flux is 2 ± 0.2 nmol m^{-2} d^{-1}; Table 1). These dissolved Cd deficits could be due to sulfide precipitation or adsorptive loss. Like GP16, ^{234}Th data (Black et al., 2018) were used to calculate pAVS removal fluxes on GP15, where Station 12 saw a SSF pAVS net removal rate of 4 nmol S m^{-2} d^{-1} between 85 – 180 m, while Station 14 had SSF pAVS net removal of 4.5 nmol S m^{-2} d^{-1} (Table 1) between 75 – 150 m. Therefore, CdS precipitation as small pAVS could potentially explain up to 31% of subsurface dCd deficits at Station 12 and all dCd deficits at Station 14 (Table 1), assuming that all SSF pAVS were bound only to Cd. However, it is likely that some fraction of pAVS is bound to other metals such as Zn and Pb (see Section 2.2.7). These other metal-sulfide precipitates might account for a portion of the "excess" SSF pAVS removal calculated at Station 14 (2.5 nmol S m^{-2} d^{-1} in excess) compared to dCd deficit. Also, like GP16, these removal estimates are likely underestimates of the total possible removal as pAVS, since only the SSF pAVS were measured on GP15. Considering that pAVS is likely predominately composed of CdS precipitates, it is presumed that most of pAVS resides in the SSF, rather than the LSF. After estimating LSF pAVS fluxes using particulate Cd concentrations (LSF and SSF; obtained from P. Lam, personal communication) and LSF ^{234}Th activities, results suggest that the contribution of LSF pAVS to the apparent removal of dCd in the oxic subsurface is less than that of the measured SSF pAVS (Table 1). While all dCd losses at Station 14 can be explained by small CdS particles, large sinking particles might also contribute to the removal of dCd

observed at Station 12. Dissolved Cd removal via precipitation as large CdS potentially removes an additional 1.7 nmol S m^{-2} d^{-1} at Station 12 (Table 1). Therefore, small and large pAVS could account for up to 44% of the estimated dCd losses observed in the oxic, upper water column at Station 12.

These flux estimates suggest that CdS formation in near surface waters are more likely to explain the dissolved Cd deficits in the NE Pacific rather than in the OMZ where this process was originally proposed (Janssen et al., 2014; Janssen & Cullen, 2015). Markedly, in these near surface waters is where we generally see the largest dissolved Cd deficits as indicated by Cd*, alongside pAVS and fluorescence maxima – similar to GP16 results at Stations 5 and 9. In these oxic surface waters, sulfide is produced from assimilatory sulfate reduction (Walsh et al., 1994), instead of the dissimilatory sulfate reduction proposed for OMZs (Canfield et al., 2010).

2.4 Conclusions

Overall, we combined sulfide and dissolved metal measurements to test the hypothesis of Janssen and co-authors (Janssen et al., 2014; Janssen & Cullen, 2015) that dissimilatory sulfate reduction within anoxic microenvironments of sinking organic particles facilitates dCd and dZn loss via metal-sulfide precipitation in OMZs. Within the NE Pacific OMZ, picomolar pAVS and TDS concentrations were too low to account for the apparent nanomolar deficits in dCd. Thus, CdS precipitation cannot be the primary mechanism responsible for the apparent deficits of dCd in the NE Pacific OMZ, as pointed out by others (de Souza et al., 2022; Janssen et al., 2019; Middag et al., 2018, 2019; Sieber et al., 2019; Xie, Galer, et al., 2019). Instead, the decoupling of Cd from PO_4^{3-} (and Zn from Si) are likely a consequence of the physical circulation, variable

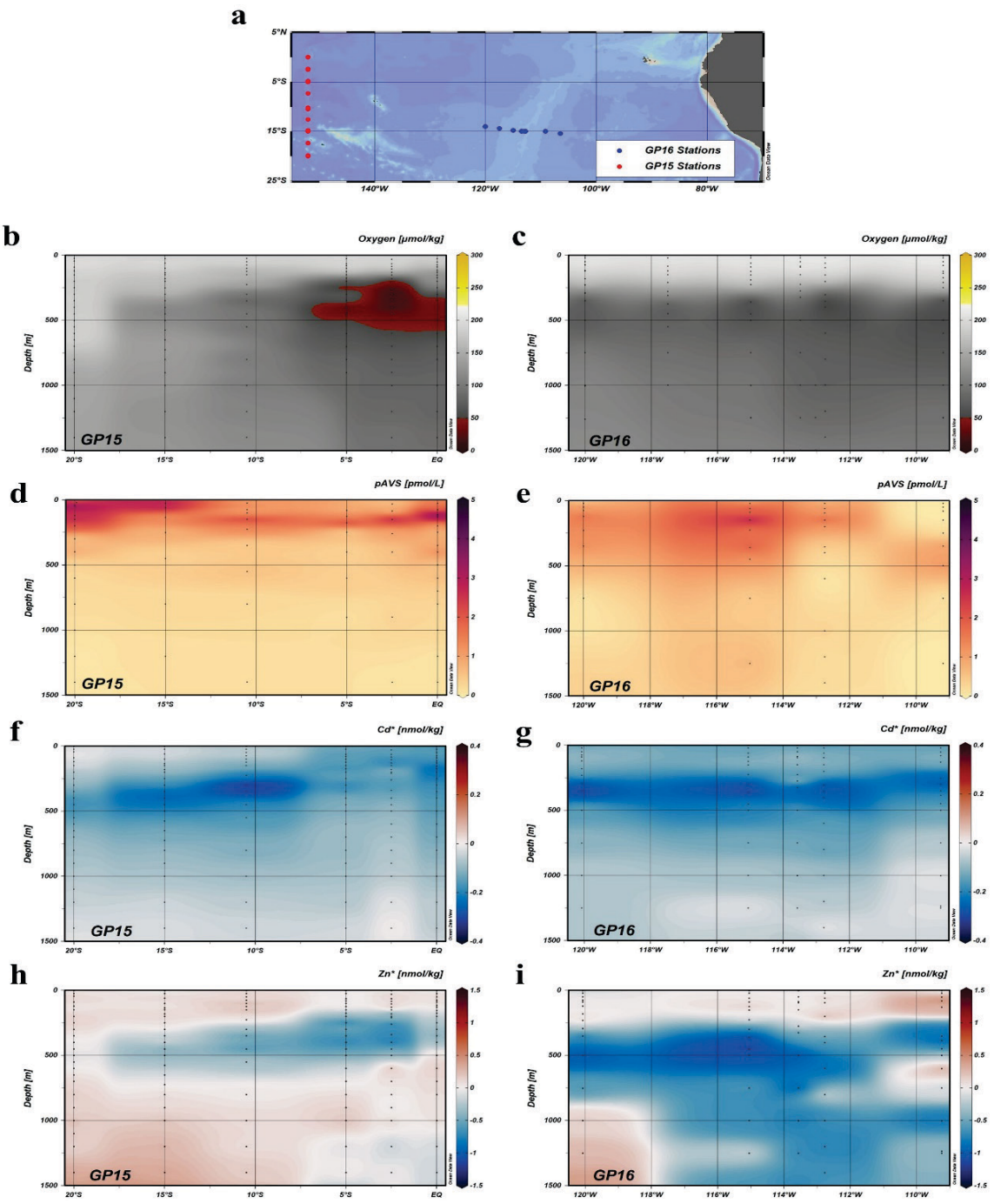

Figure 9. Sampling locations in the oxygenated, open Pacific Ocean (panel **a**) where blue dots are stations west of 109°W on the 2013 US GEOTRACES GP16 and red dots are sampling locations south of the equator on the 2018 US GEOTRACES GP15. Contoured transect profiles of dissolved oxygen (panel **b**), pAVS (panel **d**), derived Cd* (panel **f**), and derived Zn* (panel **h**) concentrations from those GP15 sampling locations are shown for the upper 1500 m with original data points shown as black dots. Contoured transect profiles of dissolved oxygen (panel **c**),

Figure 9 continued. pAVS (panel **e**), derived Cd* (panel **g**), and derived Zn* (panel **i**) concentrations from those GP16 sampling locations are shown for the upper 1500 m with original data points shown as black dots. Zn* and Cd* profiles for GP15 were reported in Sieber, Lanning, Bian, et al., (2023) and Sieber, Lanning, Bunnell, et al., (2023), respectively. A subset of those data were replotted in panels **f** and **h**. Zn* and Cd* profiles for GP16 (panels **g** and **i**) were plotted from data reported in John et al. (2018).

stoichiometry of biological uptake, and/or different regeneration length scales of micro- and macronutrients (de Souza et al., 2022; Middag et al., 2018, 2019; Sieber et al., 2019; Sieber, Lanning, Bian, et al., 2023; Sieber, Lanning, Bunnell, et al., 2023; Vance et al., 2019; Weber et al., 2018; Xie, Galer, et al., 2019).

We speculate that the observed metal deficits in the more intense OMZ in the ETSP can be explained by a combination of both assimilatory and dissimilatory sulfate reduction producing sulfide (Fig. 1), due to the shoaling of the oxycline into shallower waters and the euphotic zone. Together, Stations 5 and 9 from GP16 support the hypothesis that metal-sulfide precipitation can account for at least a portion of dCd and dZn metal deficits in the water column, not only within OMZs but also from shallow oxygenated ocean layers. Even so, we cannot speculate on whether this unique combination of assimilatory and dissimilatory processes is present in other ocean OMZs.

However, the GP15 dataset and associated flux estimates support a revised metal-sulfide removal process that occurs in near surface waters where the greatest apparent dissolved Cd deficits appear along with pAVS and fluorescence maxima (Fig. 3 and Table 1). The areal extent of this revised hypothesis is supported by the dCd anomalies observed in oxygenated waters globally (Baars et al., 2014; Conway & John, 2015a, 2015b; de Souza et al., 2022; Janssen et al., 2014; Sieber, Lanning, Bunnell, et al., 2023) in the upper 300 m. Further support is found in the oxygenated central Pacific (GP15 and GP16), where the largest dissolved Cd and Zn deficits typically occurred in the upper 500 m, where pAVS concentrations are also greatest (Fig. 9). Although limited, additional sulfide data from the oxygenated N. Atlantic (Cutter & Radford-Knoery, 1991) and central Pacific (Radford-Knoery, 1993) display elevated total pAVS (> 0.4 μm) concentrations in the upper 200 m (Fig. 10), suggesting that Cd precipitation as sulfides might play

a global role in the removal of dissolved Cd in the oxic subsurface. We suggest that in this revised removal scenario metals like Cd (and perhaps Zn) are partly removed from the water column by phytoplankton production of free sulfide (Fig. 1), via assimilatory sulfate reduction as a by-product of photosynthesis (Walsh et al., 1994). Taken together, our results suggest that removal of dCd and dZn in low oxygen environments via precipitation with sulfides likely varies regionally. In contrast, the negative anomalies in dCd, and the pAVS abundance in the oxic, upper 200 m may be an important sink in upper ocean removal on a global scale, and support a revised process for metal-sulfide precipitation in surface waters.

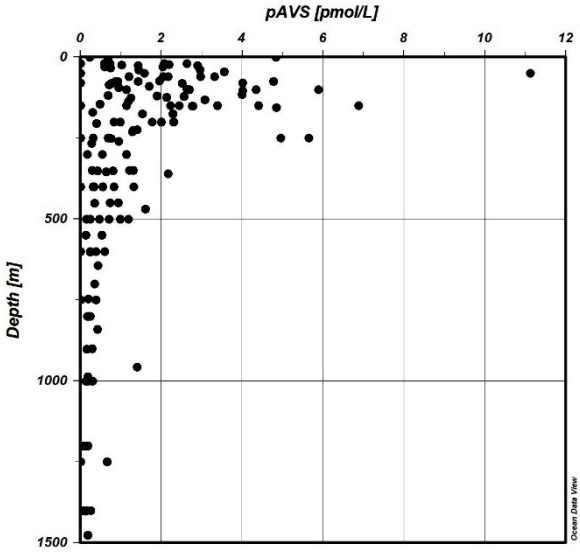

Figure 10. Particulate acid volatile sulfide (pAVS) data from the upper 1500 m of the oxygenated Pacific Ocean on GP15 and GP16 (from all stations shown in panel a of Fig. 10), three stations (5°S, 138.3°W; 0°N, 140°W; 15°N, 152.5°W) occupied in the central equatorial Pacific Ocean during August 1991, and two profiles from the BATS (31.8°N, 64.2°W) station in the North Atlantic Ocean during April 1989 and March 1995 where concentrations occasionally exceed 5 pmol L^{-1}. The pAVS data from BATS in April 1989 was replotted from data reported in Cutter & Radford-Knoery (1991). Particulate AVS data from GP15 and GP16 represent only the small sized fraction (0.8 – 51 μm). Whereas pAVS data from BATS (1989 and 1995) and from the central equatorial Pacific in 1991 were obtained using a 0.4 μm filter and thus include both the small and large size particles as there was no prefilter.

In summary, these picomolar concentrations of dissolved and particulate sulfide in the surface waters have implications for the removal of dissolved metals as sinking particles in both oxic and anoxic regimes. While we suggest that the pAVS are predominantly composed of cadmium and zinc sulfides, due to their stability, the strong interactions between metal and sulfides are not limited to the particulate phase. Additional studies are necessary to evaluate the impact of dissolved metal-sulfide complexes on the biogeochemical cycling of sulfide and certain trace metals. The following chapter will assess the speciation of dissolved sulfide in the surface waters of several regimes throughout the North Pacific and produce a mass-balance budget to determine the rate of production expected by phytoplankton that would be necessary to balance the other, better-constrained sources and sinks of dissolved sulfide from the surface layer.

CHAPTER 3

PRODUCTION AND FATE OF HYDROGEN SULFIDE IN THE EUPHOTIC ZONE OF THE NORTH PACIFIC

3.1 Introduction

The study of trace metals in the marine environment has grown over the years due to their influence on the growth of certain phytoplankton species and the concern over potential toxicity to some organisms (Brand et al., 1986). Yet, the bioavailability of these metals and their cycling is largely influenced not only by the concentration of the metal, but also by their complexation with ligands. While many studies have largely focused on complexation by organic ligands (Bruland & Lohan, 2006), some inorganic ligands like hydrogen sulfide have extremely high stability constants for metal-sulfide complexes (e.g., Dyrssen, 1985, 1988a) and should also be considered when evaluating processes affecting the cycling of some trace metals. However, the cycling of hydrogen sulfide in surface waters is a poorly constrained part of the global sulfur cycle.

As a diprotic acid, hydrogen sulfide dissociates in seawater to form an equilibrium with bisulfide and sulfide ions. At seawater pH, bisulfide is the dominant ion (Millero, 1986), but both of these ions can go on to interact with metals to form soluble dissolved complexes and insoluble particles (Radford-Knoery & Cutter, 1993). To differentiate between the forms of dissolved sulfide in seawater, the same terminology as introduced in Chapter 1 is also used here. Total dissolved sulfide (TDS) is the sum of both free sulfide (uncomplexed ions + dissolved gas) and any dissolved metal sulfide complexes. Dissolved sulfide can be produced in surface waters through the hydrolysis of OCS, or by phytoplankton as a by-product of photosynthesis (Cutter & Krahforst,

1988; Elliott et al., 1987; Walsh et al., 1994). Of these two pathways, OCS hydrolysis is better constrained, but is heavily dependent on the pH and temperature of the seawater (Elliott et al., 1989; Radford-Knoery & Cutter, 1994). There is less confidence in the rate of sulfide production by phytoplankton, since its production is heavily dependent upon the species present (Walsh et al., 1994). And while atmospheric exchange of H_2S gas can serve as a source or a sink in the ocean depending on the region (Andreae et al., 1991), its impact on the mass balance in other regions is thought to be negligible (Radford-Knoery & Cutter, 1994; Zhang, 1999). Removal by oxidation of dissolved sulfide to sulfate has been better constrained over the years thanks to the work of Millero et al. (1987) for oxidation with oxygen, and Zhang (1999) for oxidation with iodate, but the loss of dissolved sulfide from the surface through sinking particles requires additional data to constrain. The overall balance between these sources and sinks determines the concentration and distribution of TDS in the ocean.

Although it is well known that free sulfide forms strong complexes with "B-type" metals (Stumm & Morgan, 1981), little is actually known about the complexation of sulfide with trace metals in the surface ocean. That is in part due to the uncertainty in the conditional stability constants of metal-sulfide complexes (Elliott & Rowland, 1990), further compounded by the large number of metal-sulfide complexes proposed to exist in marine ecosystems (Rickard & Luther, 2006). Previous studies (Luther et al., 1996, 1996; Rozan et al., 2003) have shown that the metals Mn, Fe, Co, and Ni will generally form bisulfide (MHS^+) complexes that are kinetically labile to dissociation, yet metals like Cu, Zn, and Pb have been shown to form mononuclear (MS) complexes that are kinetically inert to dissociation, and therefore are less reactive than free or metal-bisulfide complexes. Work examining the effect of metals on the rate of oxidation of sulfide support these claims where oxidation by oxygen (Millero et al., 1987; Vazquez et al., 1989) or

iodate (Zhang, 1999) in seawater demonstrate that Zn-sulfide complexes are essentially inert, thus protecting dissolved sulfide from oxidation. In comparison, free, uncomplexed sulfide demonstrates the highest rates of oxidation by iodate compared to metal-sulfide complexes. Metal sulfide complexes with Cd and Ni are kinetically stable but are more susceptible to oxidation than Zn-sulfide complexes, but less so than free sulfide (Zhang, 1999). Thus, the exact complexation of dissolved sulfide will largely influence the stability of TDS, and therefore play a major role in determining the distribution of hydrogen sulfide in the surface ocean.

While several studies have used thermodynamic equilibrium models to predict the speciation of hydrogen sulfide in aquatic environments, there is little consistency between these models regarding the species included and the stability constants assigned to those complexes. Some studies have shown that more than 70% of dissolved sulfide is uncomplexed in the upper 500 m of the water column (Cutter et al., 1999; Zhang & Millero, 1994), while others have suggested that more than 98% of TDS must be complexed with metals like copper or mercury (Al-Farawati & van den Berg, 1999; Dyrssen, 1988b; Dyrssen & Wedborg, 1989; Elliott & Rowland, 1990; Luther et al., 1996; Radford-Knoery & Cutter, 1994). Therefore, calculating the speciation of dissolved sulfide may be inaccurate due to the large uncertainty associated with the published stability constants for these metal-sulfide complexes, whether or not competing ligands were included, and the metal concentrations incorporated into the model.

In an attempt to constrain the speciation of dissolved sulfide in the Pacific Ocean and produce a budget for hydrogen sulfide in surface waters, measurements of free sulfide were used to serve as a constraint on model complexation predictions for the biogeochemistry of dissolved sulfide in several regimes. Rates of production and removal of sulfide were then estimated to construct a mass balance for three stations, ranging from the highly productive coastal waters in

the Gulf of Alaska, to the oligotrophic sub-tropics. Since phytoplankton production is the least constrained input in the surface ocean, all other sources and sinks were determined in order to estimate the rate of production by phytoplankton that would be necessary to balance the hydrogen sulfide budget. These estimates were then compared to the existing, albeit limited, phytoplankton production rates from previously published (Walsh et al., 1994; Zhang, 1999) and unpublished (Table 2) work.

3.2 Methods

3.2.1 Sampling Sites

Samples were obtained during the US GEOTRACES GP15 Pacific Meridional Transect on board R/V *Roger Revelle*, that followed 152°W between 56°N and 20°S from 18 September to 24 November 2018. Vertical profiles of free sulfide necessary to constrain the model were only generated at select coastal stations and at "super" stations. Similarly, the iodate concentrations necessary to constrain the removal of oxidation were only measured at select "demi" and super stations. Therefore, mass balances for hydrogen sulfide were constructed for three stations that were chosen, due to the resolution of the sulfide data collected, and the overlap with the ancillary data necessary to perform these calculations. Station locations are shown in Figure 11, where Station 3 is representative of an HNLC region on the Alaskan slope, while Station 14 is representative of the North Pacific subtropical gyre, and Station 23 represents an upwelling regime just north of the Equator.

3.2.2 Sample Collection

TDS and free sulfide water samples were collected using the US GEOTRACES trace metal sampling system (Cutter & Bruland, 2012) with twenty-four 12 L GO FLO bottles mounted on a

trace metal clean carousel with CTD, oxygen, fluorometer, and transmissometer sensors. Trace metal clean sampling procedures were followed (Cutter et al., 2017) and bottles were pressurized with 6 psi air for filtration. Due to the large volume requirement, samples for free sulfide were only acquired at 5 super stations, and from the surface towfish (Cutter et al., 2017) where at least 3 L of unfiltered seawater was transferred to 4 L polyethylene cubitainers. Exact volumes were monitored and recorded using an Omega Micro-Flow meter. The cubitainers were then stored in a refrigerator and analyzed at sea within 2 hours. For TDS, cubitainers were rinsed 3 times with the sample before filling hermetically with approximately 1.5 L of seawater from each depth which was pressure filtered directly through 0.2 µm AcroPak Supor capsules and into 4 L polyethylene cubitainers for dissolved sulfide analyses (Radford-Knoery & Cutter, 1993) and then stored in a refrigerator and analyzed at sea within 8 hours.

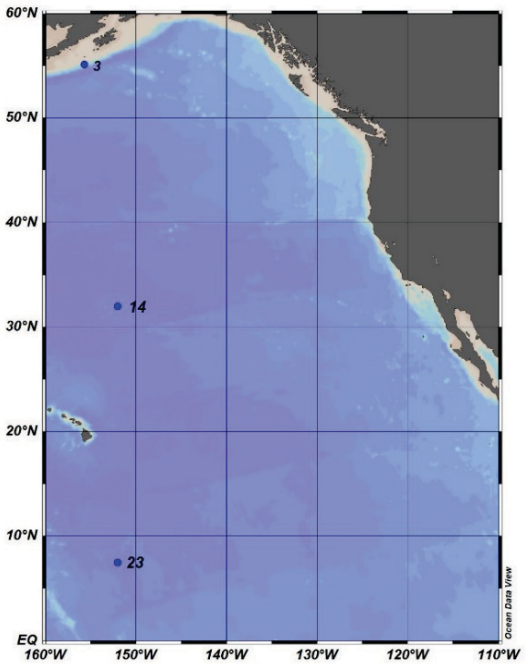

Figure 11. Select stations from GP15 where the speciation of dissolved sulfide and the rates of production and removal were calculated in the North Pacific Ocean.

pH samples were subsampled from the surface towfish and from 12 L GO FLO bottles mounted on a trace metal-clean carousel. 60 mL polypropylene syringes were fitted with polycarbonate 3-ways valves to remove air bubbles and prevent exchange of CO_2 prior to analysis. The syringes were then kept at room temperature in the dark until placed in a circulating bath at 25°C for a minimum of 20 minutes to bring the samples close to analysis temperature. The samples were analyzed at sea within 3 hours of collection using the method of Carter et al. (2013).

3.2.3 Determination of Dissolved and Particulate Sulfide

At sea, dissolved sulfide samples were quantified using the method of Radford-Knoery and Cutter (1993). Samples were acidified with phosphoric acid, stripped with helium, and the evolved H_2S gas was cryogenically trapped and quantified using a gas chromatograph coupled with a flame photometric detector. This method quantifies TDS as free ions and metal-sulfide complexes with detection limits of 0.2 pmol L^{-1} for TDS and 1.3 pmol L^{-1} for OCS for 300 mL samples. Dissolved sulfide water samples were mostly analyzed in duplicate, occasionally triplicate when time permitted. To ensure accuracy, the H_2S and OCS gases were calibrated using permeation tubes whose permeation rates have been gravimetrically measured every 6 months. By trapping and measuring known amounts of permeated H_2S and OCS over a range of times, linear calibration curves for each gas were assembled daily and applied to the samples.

Particulate acid volatile sulfide (pAVS) for the small size fraction (0.8 – 51 μm) was determined at sea using the procedure outlined by Radford-Knoery and Cutter (1993). The frozen Supor filter was placed into a gas stripping vessel with deionized water, acidified to 1 M HCl, and then the gas stripped, cryogenically trapped, and quantified using gas chromatography/flame photometric detection. This method has particle detection limit of 0.2 pmol S, which corresponds

to relative detection limit of 0.004 pmol L^{-1} pAVS with average filtered volume of 50 L. Particulate AVS samples were analyzed mostly in single analyses, however, previous studies report pAVS precision near 10% RSD (Cutter & Kluckhohn, 1999; Cutter & Radford-Knoery, 1991).

3.2.4 Determination of Free Sulfide

Free sulfide was quantified at sea using the method of Radford-Knoery & Cutter (1993). A known helium headspace was introduced into the cubitainer and allowed to equilibrate with shaking. An aliquot of the headspace was subsampled and then injected and cryogenically trapped before quantified as H_2S using a gas chromatograph coupled with a flame photometric detector. For this method, it is crucial that the volume of the seawater sample and the gas headspace introduced are known, along with Henry's law constant, the temperature, salinity, and pH to determine the concentration of free sulfide. Known seawater volumes were obtained from a calibrated Micro-Flo digital flowmeter that was plumbed between the towfish/GO FLO bottles and the cubitainer. Temperature, salinity, and pH values were obtained for all samples from individual GO FLO bottles. At all stations, free sulfide was below detection limits for all samples, suggesting that TDS was primarily metal-complexed along the entire transect, rather than existing as dissolved gas or uncomplexed sulfide.

3.2.5 Determination of pH

Samples were analyzed primarily in single analyses using an automated Ocean Optics UV-VIS spectrophotometric system that was modified from Carter et al. (2013) with pure m-cresol purple (mCP) indicator dye. The salinity-temperature dependent pH equation from Clayton and Byrne (Clayton & Byrne, 1993) was applied.

Once at analysis temperature (25°C), each syringe was attached to one of the ports on an automated syringe pump that delivered sample and dye to a 10 cm cell with an inner volume of 10 mL. The cell is placed in a thermostated-holder that is temperature controlled by water continuously pumped from a circulating water bath, so the sample remains at 25±0.1°C during analysis. Automated measurement and data processing were controlled from a program written in LabVIEW.

The samples were analyzed at sea within 3 hours of collection and the automated measurement sequence was initiated in LabVIEW and required a total processing time of 5 minutes per sample. Due to the interference of the dye on pH, dye corrections were later applied using the method of Clayton and Byrne (1993), with intercalibration samples provided by Andrew Dickson's lab at University of California, San Diego (UCSD). Two reference materials (B162 and B164) from Andrew Dickson's lab at UCSD were used to evaluate the accuracy of our shipboard pH results. pH values of 7.9143 ± 0.0065 and 7.5532 ± 0.0030 were recorded, in comparison the reported values for these reference materials were 7.9100±0.0005 and 7.5407±0.0010, respectively (Bockman and Dickson, unpublished). This translates to a 99.95% agreement for B162 and a 99.83% agreement for B164.

3.2.6 Modeling and choice of conditional metal-sulfide stability constants

To predict the chemical equilibrium speciation of dissolved sulfide with respect to trace metal complexation in the Pacific Ocean, the speciation of TDS was calculated using the computer programs R and PHREEQC. Inputs into the program were the concentrations of TDS, concentrations of major ions in seawater (as calculated from salinity; Millero, 1996), measured pH, temperature, oxygen, and trace metal concentrations. However, the choice of metal-sulfide

complexes incorporated into the model and their associated stability constants were dependent on two criteria: the availability of dissolved metal concentrations from this cruise, and whether or not that the dissolved metal-sulfide complex would have been quantified with our current method. Dissolved metal concentrations for Cd, Co, Fe, Mn, Ni, Pb, and Zn were incorporated into the model, where at most, three dissolved metal-sulfide complexes (MS, MHS, and $M(HS)_2$) were defined for each metal (where applicable). While some studies suggest that other metal-sulfide complexes exist, few have been confirmed in the natural environment or exist at sulfide concentrations relevant to this study (Daskalakis & Helz, 1993; Morse & Luther, 1999; Ste-Marie et al., 1964; Wang & Tessier, 1999). Therefore, no additional metal-sulfide complexes or clusters were included in this model, other than those reported in Table 4. Additionally, since the method for measuring TDS is limited to acid volatile metals (e.g., cadmium, zinc, nickel, etc.), copper-sulfide and mercury-sulfide complexes were not quantified in this method. Yet is important to note that several studies suggest sulfide speciation is dominated by Cu- and Hg-sulfide complexes (Al-Farawati & van den Berg, 1999; Dyrssen, 1988b; Dyrssen & Wedborg, 1989; Elliott & Rowland, 1990; Luther et al., 1996) and therefore could serve an important role that is overlooked in this study. However, organic ligands were incorporated to allow for competition between inorganic sulfide and organic ligands. Since concentrations of organic ligands and their conditional stability constants were not available from this cruise, values from nearby Pacific Ocean datasets were used (Table 5; see further discussion in Section 3.3.1).

To address the large variability in stability constants for metal-sulfide complexes published in literature, the PHREEQC package was coupled with R to setup and run multiple Monte Carlo simulations. This interface made it possible to generate random log K values that were normally distributed over the specified published range (see Table 4) to calculate the speciation of a sample

under 50 different simulations at once. Measurements of free, uncomplexed sulfide served as a constraint on the model to verify the accuracy of the calculated speciation. Since free sulfide was below detection at all stations, it was assumed that all TDS was complexed and thus, only simulations that predicted all sulfide as complexed were considered. To minimize any bias, the stability constants of those simulations were averaged, and the respective log K values were applied to all stations and depths examined in this study, in order to calculate the chemical speciation of dissolved sulfide in those surface waters. Thermodynamic equilibrium constants for all other dissolved species were integrated into the model using the minteq.v4 data base within PHREEQC.

3.2.7 Phytoplankton Community Composition

To produce a mass balance for several GP15 stations, the rates of known production and removal were calculated. However, since sulfide production by phytoplankton is species dependent, the phytoplankton assemblage was predicted using the Phytoclass program (Hayward et al., 2023). This program is similar to CHEMTAX (Mackey et al., 1996) and relies on the ratio of pigment-to-Chl a to predict the composition of the phytoplankton community. Concentrations of 12 pigments were used to determine the expected abundance of 8 different phytoplankton classes: prasinophytes, chlorophytes, cryptophytes, diatoms, dinoflagellates, haptophytes, pelagophytes, and *Synechococcus*. Due to the requirement of Chl a in the model, the program neglects to consider several species of phytoplankton that do not produce the pigment chlorophyll a. *Prochlorococcus*, another cyanobacteria ubiquitous throughout the lower latitudes (Ulloa et al., 2021) is not supported as a phytoplankton group in the model since the primary pigment associated with *Prochlorococcus* is divinyl chlorophyll a. Therefore, the TDS production estimates made in

this chapter based on the phytoplankton community are likely an underestimate of the total possible sulfide production by phytoplankton due to exclusion of several phytoplankton species that might produce dissolved sulfide. While the creators of the Phtyoclass (Hayward et al., 2023) model have mentioned including *Prochlorococcus* in future versions, divinyl chlorophyll a concentrations were not analyzed for this cruise. Thus, the missing data limits the extent to which we can re-evaluate the coincidental biological and TDS data, should later model outputs include other phytoplankton groups. Another consideration of these biomass estimates is the limited depth coverage for pigment data in the upper water column. The sulfide budgets constructed in this chapter reach up to 175 m depth – yet in some cases, the pigment data only reaches up to 100 m. Therefore, the depth integrated average calculated for sulfide production by phytoplankton is not comparable to the depth integrated values applied to all other flux calculations. It is likely that the depth integrated average of phytoplankton production calculated in the top 100 m is larger than what would be calculated in the top 175 m due to an increase in light attenuation with depth – potentially serving as an overestimate in our calculations. Despite these shortcomings, coupling both the biomass estimates for several phytoplankton groups along with TDS production rates previously measured (Walsh et al., 1994; Zhang, 1999; Table 2), allowed us to validate some of the phytoplankton production fluxes estimated from the budget generated at several stations.

3.2.8 Data Sources

The data used for the mass balance calculations were from three stations in different regimes in the North Pacific Ocean: the more coastal sub-arctic Station 3 (55.1°N, 155.7°W), Station 14 (32°N, 152°W) within the northern part of the oligotrophic subtropical gyre, and Station 23 (7.5°N, 152°W) just north of the equator. At Station 3, particulate sulfide fluxes could not be

determined using the ^{238}U-^{234}Th disequilibrium method. Instead, pAVS fluxes were estimated using pAVS-to-POC ratios from this cruise coupled with POC fluxes from the upper 150 m of nearby, representative stations from Ocean Station PAPA (Buesseler et al. 2020). Iodate concentrations were obtained from Moriyasu et al. (2023). Dissolved metal concentrations necessary to predict the speciation of dissolved sulfide at the 3 stations came from several sources (Table 6). Dissolved Cd (Sieber, Lanning, Bunnell, et al., 2023), Fe, and Zn (Sieber, Lanning, Bian, et al., 2023) are a merged dataset from the labs of T. Conway (University of South Florida, USF), J. Fitzsimmons (Texas A&M University, TAMU), and S. John (University of Southern California, USF). Dissolved Co (Chmiel et al., 2022) was obtained from M. Saito (Woods Hole Oceanographic Institute, WHOI). Dissolved Mn, Ni, and Pb were obtained from A. Shiller (University of Southern Mississippi, USM; unpublished). Data used in this chapter can be accessed from the Biological & Chemical Oceanography Data Management Office (BCO-DMO) under project 695926 “US GEOTRACES Pacific Meridional Transect (GP15)”.

Table 4. Conditional stability constants (log K_{cond}) used for the calculations with the corresponding references serving as the range of possible stability constants fed into the Monte Carlo simulations in R.

Metal	Species	log K_{cond}	Reference
Cd^{2+}	CdS[a]	8.72	Tsang et al. (2006)
	$CdHS^+$	8.1	Ste-Marie et al. (1964), Zhang and Millero (1994), Al-Farawati and van den Berg (1999)
	$Cd(HS)_2$	14.85	Ste-Marie et al. (1964), Zhang and Millero (1994), Al-Farawati and van den Berg (1999)
Co^{2+}	$CoHS^+$	5.57	Zhang and Millero (1994), Luther et al. (1996), Al-Farawati and van den Berg (1999)
	$Co(HS)_2$	10.2	Al-Farawati and van den Berg (1999)
Fe^{2+}	$FeHS^+$	5.29	Zhang and Millero (1994), Luther et al. (1996), Al-Farawati and van den Berg (1999)
Mn^{2+}	$MnHS^+$	5.02	Luther et al. (1996), Al-Farawati and van den Berg (1999)
	$Mn(HS)_2$	9.9	Al-Farawati and van den Berg (1999)
Ni^{2+}	$NiHS^+$	5.42	Zhang and Millero (1994), Luther et al. (1996), Al-Farawati and van den Berg (1999)
	$Ni(HS)_2$	10.79	Al-Farawati and van den Berg (1999)
Pb^{2+}	PbS[a]	8.25	Rozan et al. (2003)
	$PbHS^+$	8.37	Luther et al. (1996), Al-Farawati and van den Berg (1999), Rozan et al. (2003)
	$Pb(HS)_2$	15.21	Luther et al. (1996), Al-Farawati and van den Berg (1999), Rozan et al. (2003)
Zn^{2+}	ZnS[a]	6.85	Luther et al. (1996)
	$ZnHS^+$	6.25	Zhang and Millero (1994), Luther et al. (1996), Al-Farawati and van den Berg (1999)
	$Zn(HS)_2$	12.17	Dyrssen (1991), Zhang and Millero (1994), Al-Farawati and van den Berg (1999)

[a] MS species were corrected for metal side reactions but not sulfide side reactions

Table 5. Conditional stability constants and ligand concentrations for the competing metal-organic ligands used for the speciation calculations.

Metal	Ligand Concentration [nmol L^{-1}]	log K'_{M-L}	Reference
Cd	0.1	12.04	Burland (1992)
Co	0.22	15.82	Ellwood and van den Berg (2001) Saito and Moffett (2001)
Fe	L_1 = 0.37	12.46	Rue and Bruland (1995)
	L_2 = 1.5	11.64	Buck et al. (2012) Moore et al. (2021)
Ni	2	14.74	van den Berg and Nimmo (1987) Boiteau et al. (2016)
Pb	0.35	9.7	Capodaglio et al. (1990)
Zn	1.5	10.71	Burland (1989) Coale and Bruland (1990)

Where L is the competing organic ligand.

Table 6. Dissolved metal concentrations of metals included in the speciation calculations. Dissolved Cd, Fe, and Zn are a merged dataset from the labs of T. Conway (USF), J. Fitzsimmons (TAMU), and S. John (USC). Dissolved Co was obtained from M. Saito (WHOI). Dissolved Mn, Ni, and Pb were obtained from A. Shiller (USM).

				Dissolved Metal Concentrations [nmol kg^{-1}]						
Station	**Lat.** [°N]	**Long.** [°W]	**Depth** [m]	**Cd**	**Co**	**Fe**	**Mn**	**Ni**	**Pb**	**Zn**
3	55.1	155.7	0	0.20	0.028	0.45	2.12	4.06	0.02	0.72
			30	0.38	0.098	0.57	1.42	4.68	0.03	1.45
			60	0.57	0.095	0.33	1.28	5.05	0.03	2.03
			100	0.80	0.100	0.35	0.93	5.81	0.03	4.48
			175	1.14	0.093	0.77	1.19	6.88	0.04	9.39
14	32	152	0	0.01	0.000	0.10	0.75	2.30	0.04	0.03
			25	0.01	0.000	0.12	0.75	2.26	0.04	0.24
			45	0.01	0.018	0.08	0.63	2.58	0.05	0.21
			75	0.01	0.021	0.08	0.65	2.45	0.05	0.17
			100	0.01	0.007	0.07	0.63	2.48	0.05	0.39
			125	0.03	0.021	0.13	0.60	2.62	0.05	0.25
			150	0.11	0.069	0.12	0.44	2.86	0.06	0.33
23	7.5	152	0	0.01	0.017	0.12	1.54	2.17	0.01	0.03
			25	0.01	0.003	0.34	1.61	2.14	0.02	0.11
			60	0.01	0.041	0.18	1.18	2.21	0.02	0.09
			80	0.01	0.053	0.25	0.88	2.28	0.02	0.06
			100	0.09	0.076	0.09	0.61	2.76	0.03	0.15
			130	0.24	0.080	0.15	0.56	3.34	0.04	0.22
			160	0.55	0.135	0.19	0.59	4.42	0.04	0.50

3.3 Results and Discussion

3.3.1 Equilibrium Speciation of Dissolved Sulfide in the Pacific Ocean

While mass balance calculations yield some insight into the relative inputs of hydrogen sulfide via several pathways, the abundance in surface waters is largely controlled by the stabilization of dissolved sulfide through complexation with metals. Several studies have made assumptions as to what fraction of dissolved sulfide is complexed, fortunately, our confidence in this assumption is bolstered by the measurement of free sulfide, which consistently fell below detection limits along the entire transect (see Section 3.2.4). Despite those certainties, the exact speciation of TDS is unknown due to the large variability in published stability constants for metal-sulfide complexes.

Using observed pH, temperature, salinity, and concentrations of TDS and dissolved metals in solution, the speciation of TDS was predicted, using free sulfide to verify the model predictions. The speciation of TDS was calculated using PHREEQC with minteq.v4 as the primary database; however, conditional stability constants for relevant dissolved metal sulfide complexes were incorporated into the model (see Section 3.2.6 for further details). Even though the minteq.v4 database contains data relevant for certain organic ligands, this feature was not utilized since in seawater, dissolved metal is bound by relatively metal-specific and largely uncharacterized organic ligands. To address this, metal-specific organic ligand stability constants and relevant ligand concentrations were incorporated in this model (summary in Table 5). Organic ligands specifically binding dissolved cadmium exist in the North Pacific at low concentrations on the order of 0.1 nmol L^{-1} (Bruland, 1992); a conditional stability constant for Cd-specific competing organic ligands ($\log K'_{cond,CdL} = 12$) was incorporated and kept constant for all depths, but might reflect an overestimation of organically bound Cd at deeper depths due to weaker stability constants reported below 100 m. Cobalt, on the other hand, has much larger reported conditional stability

constants ($\log K'_{cond,CoL} = 15.1 - 16.1$) in the Northeast Atlantic, with low ligand concentrations on the order of 22-60 pmol L^{-1} (Ellwood & van den Berg, 2001). Since organic complexation of dissolved cobalt has not been reported for the Pacific Ocean, the low end of ligand concentrations reported in the Atlantic (0.22 pmol L^{-1}) was utilized to account for cobalt complexation by organic ligands. In the central North Pacific, dissolved iron organic ligands have been shown to consist of two classes (Buck et al., 2012; Moore et al., 2021; Rue & Bruland, 1995). The stronger ligand (L_1) has surface concentrations around 0.4 nmol L^{-1} ($\log K'_{cond,FeL_1} = 12.7 - 13.2$), while the weaker ligand (L_2) exists at concentrations roughly three times that of the strong ligand (1.5 nmol L^{-1}; $\log K'_{cond,FeL_2} = 1\,1.3 - 11.8$) and have been included in the model. Organic complexation with nickel was incorporated into the model using average oceanic ligand concentrations reported in the eastern tropical North Pacific (Boiteau et al., 2016) and coastal British (Van Den Berg & Nimmo, 1987) waters where ligand concentrations were on the order of 2 nmol L^{-1} but variable conditional stability constants ($\log K'_{cond,NiL} = 12.7 - 18.7$). It was assumed that the ligand concentrations available in the North Pacific resembled the 2 nmol L^{-1} reported previously, but due to the large range of published stability constants for organic nickel complexes, the average value (Table 5) was incorporated into this model as stated in Section 3.2.6. Conversely, lead complexation with organic ligands occurs at much lower seawater ligand concentrations of 0.2 to 0.5 nmol L^{-1} and conditional stability constants on the order of $\log K'_{cond,PbL} = 9.7$ in the eastern tropical North Pacific (Capodaglio et al., 1990). Therefore, it was assumed that our stations exhibited similar ligand concentrations applying the average of 0.35 nmol L^{-1} throughout the upper water column. In the North Pacific (Bruland, 1989; Coale & Bruland, 1990), it has been shown that the concentration of organic ligands strongly bound to zinc ($\log K'_{cond,ZnL} = 11$) are relatively uniform in the surface waters and are on the order of 1.5 nmol L^{-1}, which was assumed for all three

stations. Since the organic complexation of dissolved manganese has not been reported in seawater, only complexation with inorganic sulfide ligands was included in the model. It should be noted that metals like copper and mercury were omitted from these equilibrium calculations, since the method used to quantify TDS in this study does not account for non-acid volatile metals like copper and mercury. It is important to note that this distinction alone could have a large influence on the speciation of dissolved sulfide in surface waters due to the large conditional stability constants reported for copper and mercury sulfide complexes and the concentration of dissolved Cu reported in the Pacific Ocean. Therefore, future studies should consider including dissolved copper and mercury sulfide complexes if a method becomes available to quantify those non-acid volatile dissolved sulfide complexes.

Based on previous studies (e.g., Radford-Knoery & Cutter, 1994), it is well known that the speciation calculations are largely regulated by the stability constants utilized in the model, along with the concentration of dissolved metals. Using the dissolved metal concentrations reported in Table 6, observed TDS (Figures 14 – 16), and stability constants reported in Tables 4 and 5, the speciation of TDS was calculated for three stations in the North Pacific Ocean. The accuracy of the speciation calculations was verified using the measured free sulfide concentrations, which demonstrated that all TDS is metal-complexed, therefore only simulations where all TDS was predicted to be complexed were considered.

At all stations, the speciation of TDS was largely predicted to be dominated by metal sulfide (MS) complexes, despite the negligible concentrations of sulfide (S^{2-}) at seawater pH values, with all metal-bisulfide complexes (MHS^+ and $M(HS)_2$) effectively zero in all simulations. Although it should be noted that there is limited support for the existence of MS species in seawater (Luther et al., 1996; Rozan et al., 2003; Tsang et al., 2006) compared to MHS^+ complexes, this is

why the speciation at these stations in restricted to dissolved zinc sulfide (ZnS), cadmium sulfide (CdS), and lead sulfide (PbS) complexes. At Station 3 on the Alaskan slope (Figure 12), CdS was predicted to be the dominant dissolved metal-sulfide complex in the upper 60 m, representing roughly 55% of the TDS pool, where dissolved ZnS made up the other ~40%. Below 100 m, TDS speciation was largely dominated by ZnS and varied between 60 and 74% over the next 75 m. Dissolved PbS was consistently expected to represent less than 4% of TDS in the upper 175 m. Further south at Station 14 in the oligotrophic subtropical gyre (Figure 13), the fraction of TDS as dissolved ZnS and PbS was relatively similar throughout the upper 150 m, each accounting for around 45% of the TDS pool in the surface and dropping to approximately 20% each at 150 m with the fraction of CdS generally increasing with depth. In the equatorial Pacific at Station 23 (Figure 14), dissolved ZnS and PbS still largely controlled the TDS speciation similar to Station 14, but the vertical extent was reduced to the upper 80 m, below which TDS speciation shifted towards CdS representing 67% of all TDS observed down to 150 m. Interestingly, with dissolved zinc sulfide complexes dominating the speciation, this is consistent with the work of Zhang (1999), who argues that zinc complexes are essentially inert and serve to protect TDS from rapid oxidation by iodate, whereas dissolved cadmium sulfide complexes had the next lowest rate of oxidation by iodate. Additionally, Millero et al. (1987) has also shown that formation of MS slows the kinetics of oxidation by oxygen as well, with the formation of PbS complexes exhibiting the fastest rates of formation despite having the lowest dissolved concentrations of 20-60 pmol L^{-1}. Furthermore, some studies provide evidence of clusters and nanoparticles (retained within the dissolved fraction) existing, albeit at micromolar levels (Luther et al., 1999), but we suspect that these nanoparticles might also form at lower concentrations as these results are similar to what has been seen at higher concentrations of dissolved sulfide. Overall, these results are in contrast with those previously

published in literature (Al-Farawati & van den Berg, 1999; Cutter et al., 1999; Dyrssen, 1988b; Dyrssen & Wedborg, 1989; Elliott & Rowland, 1990; Luther et al., 1996) likely for several reasons. First, the output of the model is largely controlled by the stability constants reported for both metal-sulfide complexes which are known to vary on the order of several magnitudes, demonstrating the importance of accurate metal-sulfide stability constants.

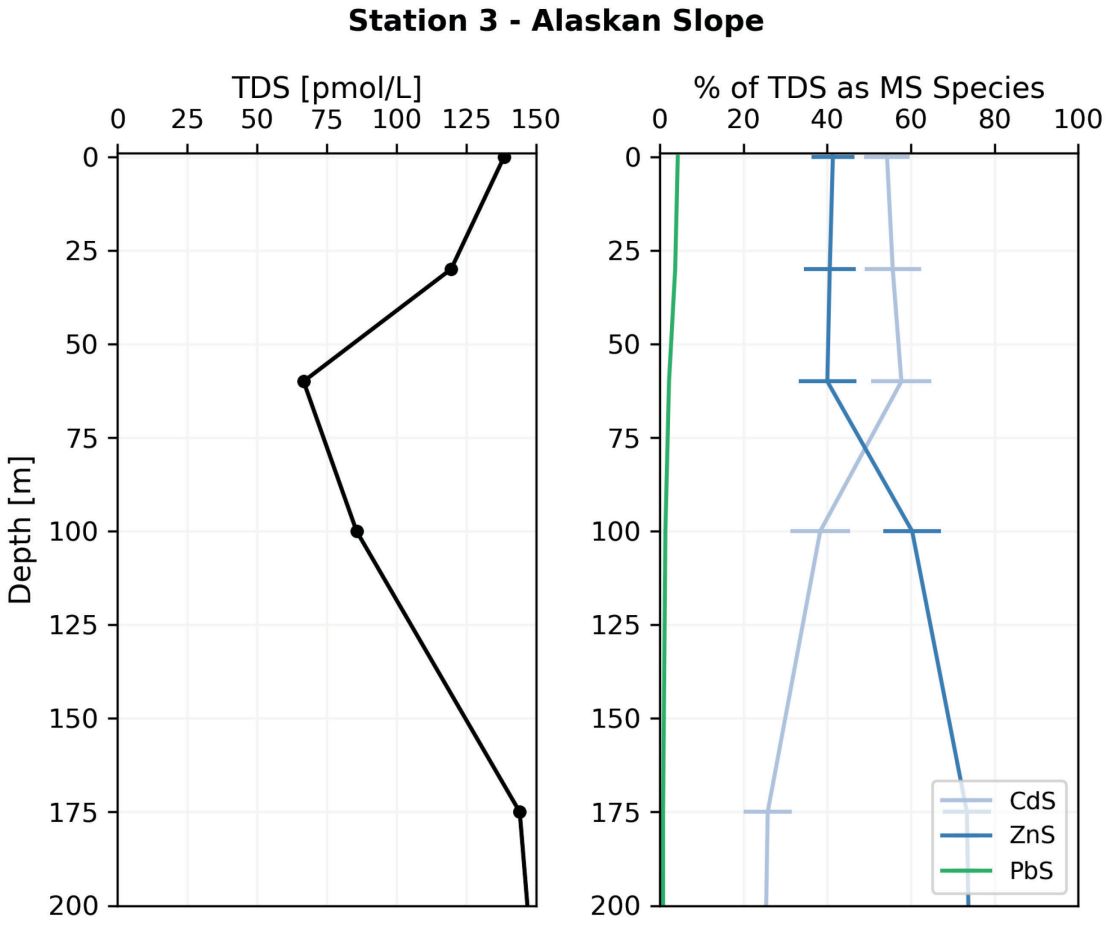

Figure 12. Vertical profiles of TDS and its predicted speciation as MS complexes in the top 200 m Station 3 in coastal Alaska (55.1°N, 155.7°W). Error bars represent the range of each fraction calculated by varying the conditional stability constant (K_{cond}) for each metal-sulfide complex from its lowest to highest values.

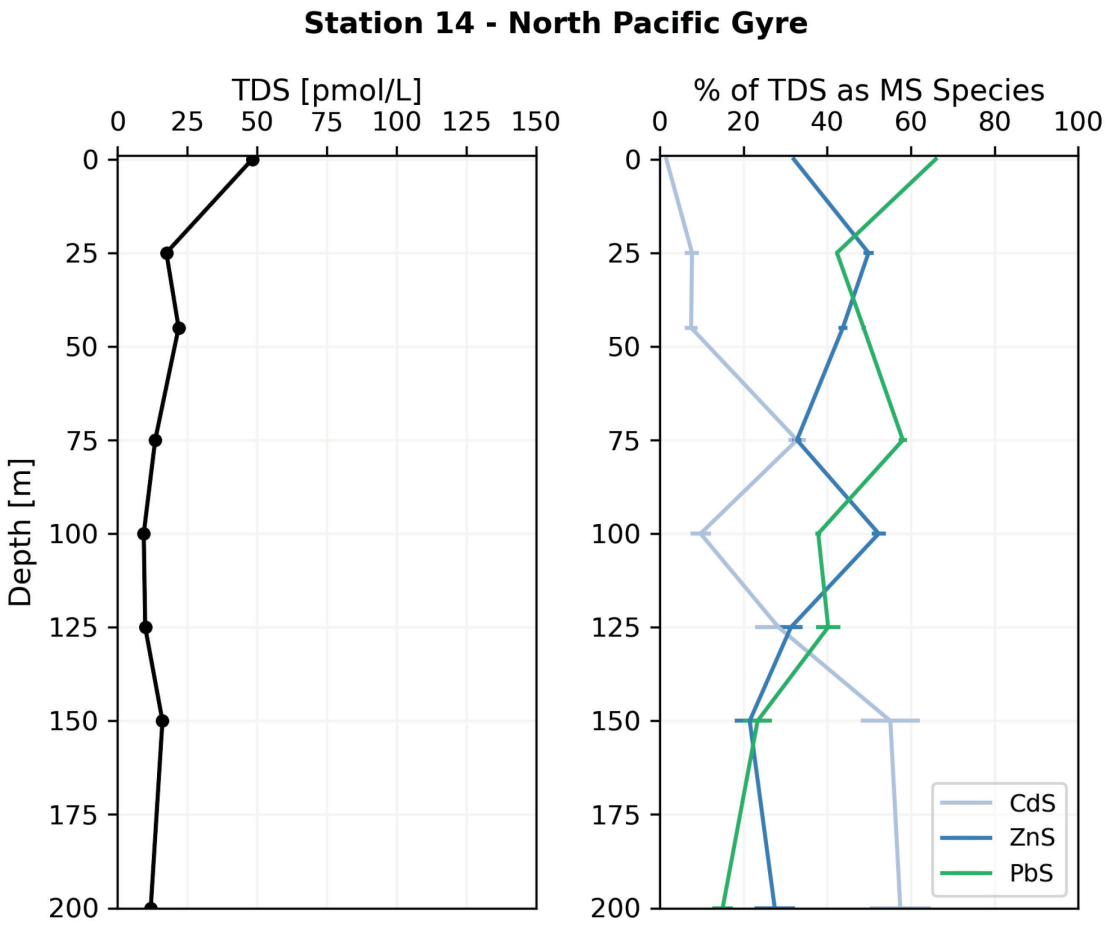

Figure 13. Vertical profiles of TDS and its predicted speciation as MS complexes in the top 200 m Station 14 in the North Pacific subtropical gyre (32°N, 152°W). Error bars represent the range of each fraction calculated by varying the conditional stability constant (K_{cond}) for each metal-sulfide complex from its lowest to highest values.

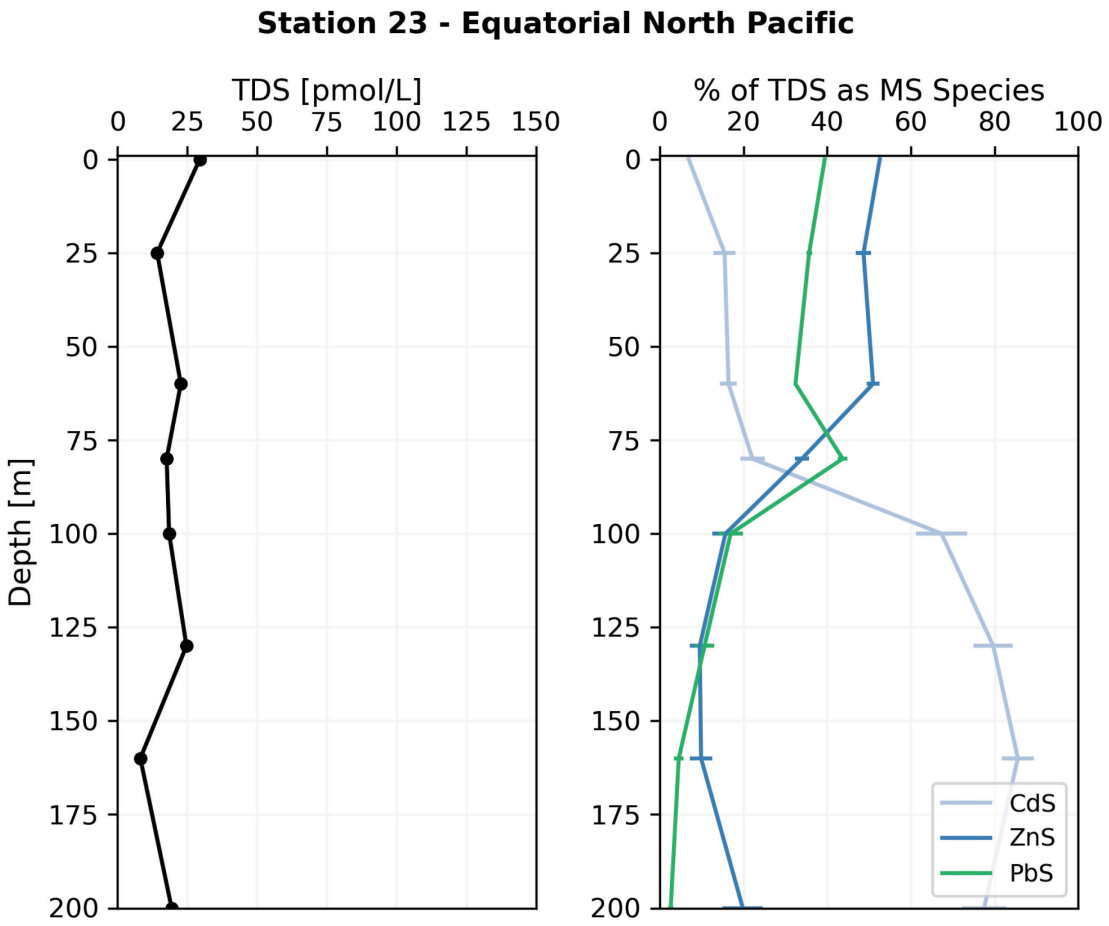

Figure 14. Vertical profiles of TDS and its predicted speciation as MS complexes in the top 200 m Station 23 in the equatorial North Pacific (7.5°N, 152°W). Error bars represent the range of each fraction calculated by varying the conditional stability constant (K_{cond}) for each metal-sulfide complex from its lowest to highest values.

Also, the inclusion or exclusion of certain metals or ligands would considerably shift the predicted complexation of sulfide in seawater, as has been demonstrated by several studies that included copper sulfide ligands (Al-Farawati & van den Berg, 1999; Dyrssen, 1988b; Dyrssen & Wedborg, 1989; Elliott & Rowland, 1990; Luther et al., 1996). While some studies suggest that copper-sulfide (Cu-S) and mercury-sulfide (Hg-S) complexes can control the speciation of TDS, these species have been excluded from these calculations because Cu-S and Hg-S complexes are not quantified by the method used to measure TDS in this study. Additionally, some studies consider complexes that might not exist at relevant seawater concentrations (such as Daskalakis & Helz, 1993; Luther et al., 1999; Morse & Luther, 1999; Ste-Marie et al., 1964; Wang & Tessier, 1999). The application of these results to the real world is heavily dependent upon the accuracy of the data (metal concentrations, sulfide stability constants, and competing organic ligands) used in the speciation calculations. However, the largest influence on speciation was apparently the inclusion and/or exclusion of specific metal-sulfide complexes. For example, regardless of the conditional stability constants applied for MHS^+ and $M(HS)_2$ species in this study, the results presented are largely controlled by the inclusion of the aqueous MS species (Figures 12-14) where uncertainty in MS species predictions rarely exceeded 7 percent.

3.3.2 Distributions of Hydrogen Sulfide in Seawater

In the Pacific Ocean along 152°W, concentrations of TDS range from 1.4 – 350 pM, and typically decrease with depth and distance from the coastal margins to the open ocean. TDS concentrations were higher closer to the Alaskan coast, where TDS on average was 157 ± 40 pM (Fig. 2d). In the open ocean, surface TDS concentrations dropped to 23 ± 14 pM in the upper 150 m of the water column. Similar to vertical profiles in other basins (Cutter & Radford-Knoery,

1991; Radford-Knoery & Cutter, 1994), both TDS and particulate sulfide had maxima at or near the surface, with a secondary subsurface maximum that was observed between 25 and 100 m, and a rapid decrease below 150 m that remained relatively constant with increasing depth (Fig. 2c and 2d). Profiles of dissolved and particulate sulfide from the US GEOTRACES GP15 cruise (Fig. 2c and 2d) share similar features as those observed in other basins (Radford-Knoery & Cutter, 1994) – albeit at much lower sulfide concentrations than reported for previous cruises in the Atlantic and Pacific. Nevertheless, the processes influencing the distribution of sulfide in the Pacific are likely similar to those observed in the Atlantic (Radford-Knoery & Cutter, 1993, 1994). Therefore, similar production and removal pathways were considered when evaluating the mass balance of hydrogen sulfide in the Pacific Ocean (Figure 1).

3.3.3 Sources and Sinks of Hydrogen Sulfide in Seawater

In order to assess the cycling of hydrogen sulfide in the surface ocean, the processes influencing its distribution must be well constrained. Figure 1 outlined the mechanisms proposed for the full water column, but for the purpose of this chapter, we are focused on the processes observed in the surface, euphotic-zone waters.

It is well known that the hydrolysis of OCS is one of the primary sources of hydrogen sulfide in the surface ocean (Elliott et al., 1987, 1989; Radford-Knoery & Cutter, 1994) where OCS is produced in surface waters through the photooxidation of dissolved organic sulfur (Ferek & Andreae, 1984). The hydrolysis of OCS (Elliott et al., 1989) follows first order kinetics and can hydrolyze into gaseous hydrogen sulfide or bisulfide, and is expressed by the following reactions:

$$OCS + H_2O \leftrightarrow H_2S_{(g)} + CO_2$$

$$OCS + OH^- \leftrightarrow SH^- + CO_2$$

where the rate is dependent upon the temperature and pH of the solution which has previously been determined by Elliott et al. (1989) and Radford-Knoery and Cutter (1994). Because OCS hydrolysis proceeds along both the acidic and alkaline pathways (Elliott et al., 1989), the rate of hydrolysis is dependent upon the sum of both pathways. Using the parameters defined by Radford-Knoery and Cutter (1994), rate constants were calculated and used to quantify the flux of dissolved sulfide produced by OCS hydrolysis in the Pacific Ocean. This input can be express as:

$$\frac{d[H_2S]_T}{dt} = k_{hyd}[OCS] \quad (6)$$

where k_{hyd} is the hydrolysis rate constant determined from observed temperature and pH, and [OCS] is the observed carbonyl sulfide concentration at each depth. Since this production is largely temperature dependent, the rate of OCS hydrolysis is greatly reduced at the higher latitudes, as shown in Figure 15 from the upper 170 m of three stations along the US GEOTRACES GP15 transect.

Unlike OCS hydrolysis rates, sulfide produced by phytoplankton is not as well constrained. Cutter and Krahforst (1988) noticed a correlation between the TDS maxima and chlorophyll at several stations in the Atlantic and suggested that other mechanisms must be in play to produce the pico- to nanomolar levels of sulfide found in the surface ocean. In 1994, Walsh et al. found evidence to support their observations and demonstrated that several marine phytoplankton released both dissolved and particulate sulfide, which they suggested served as a control over the concentration of free metal within the cells' environment through complexation. They (Walsh et al., 1994) found that cyanobacteria like *Synechococcus* produced the most total sulfide, whereas the coccolithophore *Emiliania huxleyi* and the chlorophyte *Pyramimonas obovata* produced half as much, and the diatom *Thalassiosira oceanica* produced the least of all species examined (Table 1). Notably, such trends were also observed on the GP15 Pacific meridional transect where the

surface distributions of TDS were correlated with two cyanobacterial species, *Synechococcus* and *Prochlorococcus* (Figure 16), providing additional evidence for the crucial role that phytoplankton play in supplying sulfide to the surface open ocean. And while limited culture studies and coincidental biological data make it difficult to accurately determine the relative flux of sulfide to the surface ocean by phytoplankton, the better constrained removal fluxes will allow us to estimate the production of sulfide by phytoplankton in several regions. Despite its reported stability in oxygenated seawater, it is important to remember that the redox sensitivity of hydrogen sulfide makes it susceptible to undergo oxidation to sulfate via oxygen (Millero et al., 1987) , iodate (Zhang & Whitfield, 1986; Zhang, 1999), hydrogen peroxide (Millero et al., 1989),

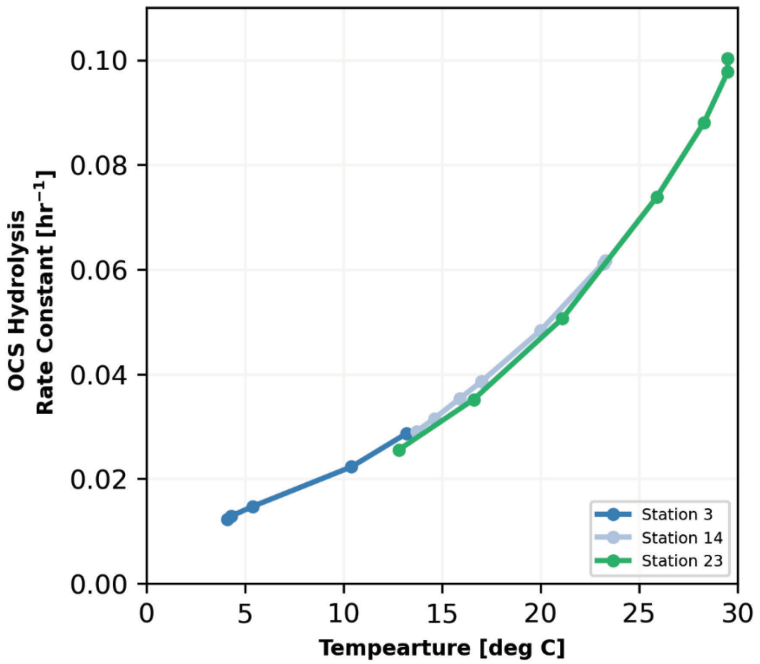

Figure 15. Carbonyl sulfide (OCS) hydrolysis rate constants calculated for the top 170 m of the three stations modeled from GP15. Since this process is temperature and pH dependent, rates were calculated from Radford-Knoery and Cutter (1994). Station 3 off the coast of Alaska is shown in dark blue, Station 14 in the subtropical gyre is shown in light blue, and Station 23 near the equator is shown in green.

or light (Pos et al., 1997), although the relative contribution to removal by each oxidant varies greatly. Surface concentrations of oxygen in the Pacific along GP15 reached 320 μmol kg^{-1}, where oxygen and TDS follow first-order kinetics. Rate constants for loss by oxidation using oxygen were calculated using the equation outlined in Millero et al. (1987), and are salinity-pH-temperature-dependent. This loss can be expressed as:

$$\frac{d[H_2S]_T}{dt} = k_{O_2}[O_2][H_2S]_T \quad (7)$$

While free sulfide is readily oxidized by oxygen in surface waters, several studies have demonstrated that oxidation by iodate is faster (Radford-Knoery & Cutter, 1994; Zhang & Whitfield, 1986; Zhang, 1999) despite iodate existing at lower concentrations in the upper ocean, between 250 – 420 nmol kg^{-1}. Even though more recent work on the rate of removal by iodate (11.1 pmol L^{-1} hr^{-1}; Zhang, 1999) reveal that the removal flux was an order of magnitude less than that calculated in earlier studies (112 pmol L^{-1} hr^{-1}; Radford-Knoery & Cutter, 1994; Zhang & Whitfield, 1986), iodate still had a larger impact on removal of dissolved sulfide from surface waters compared to oxygen. But, it is important to note that Zhang (1999) took into consideration the speciation of TDS when calculating oxidation by iodate and although the rate is metal specific, the overall rate of oxidation for metal-sulfide complexes was much less than that for free sulfide. Because free sulfide was below detection in this study, the rate constant specific to TDS was utilized in this study rather than that of free sulfide (Zhang, 1999). The loss of dissolved sulfide through oxidation by iodate can be expressed as:

$$\frac{d[H_2S]_T}{dt} = k_{IO_3^-}[H_2S]_T[IO_3^-]^{0.5} \quad (8)$$

where the rate of TDS oxidation is first-order in TDS and half-order in iodate. Peroxide can also react with TDS and serve as a sink in seawater. Although oxidation by peroxide follows second-

order kinetics (Millero et al., 1989), the peroxide low concentrations available in the surface ocean (< 60 nmol L^{-1}; Yuan & Shiller, 2004) limit the influence this process has on the mass balance of hydrogen sulfide as demonstrated by Radford-Knoery and Cutter (1994) in the Atlantic (loss rate = 0.02 pmol L^{-1} hr^{-1}). In the euphotic zone, TDS can also undergo photooxidation, with the highest rates exhibited at the surface and decreasing exponentially with depth, due to light attenuation (Pos et al., 1997). During peak daylight hours, photooxidation rates have been shown to be 3 times larger than that of oxidation by oxygen (Pos et al., 1997), but unlike oxygen, photooxidation's significance in sulfide removal is limited to surface waters.

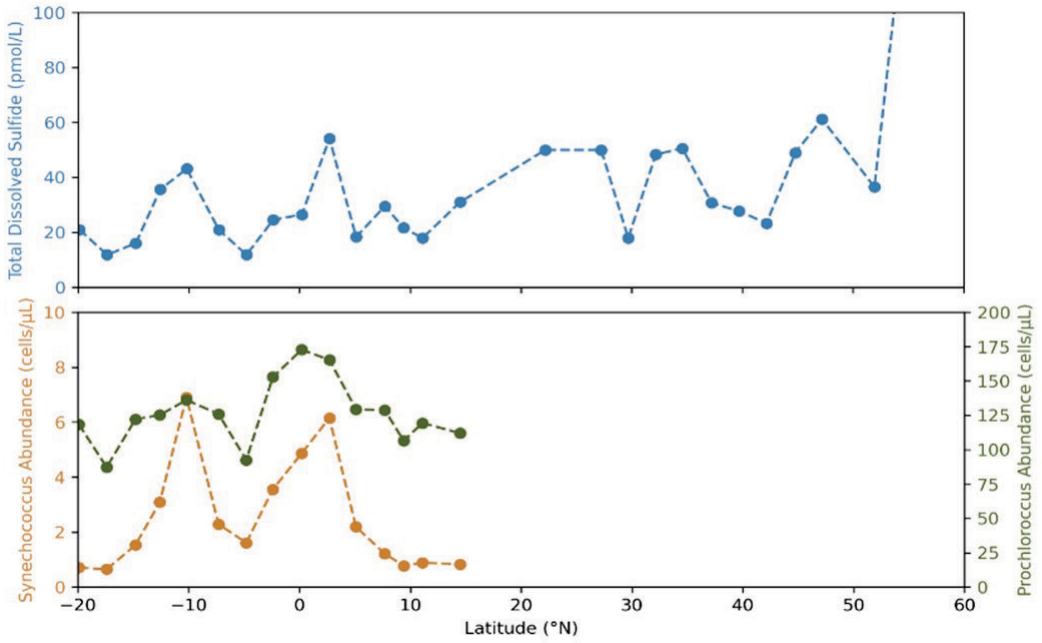

Figure 16. Surface distributions of total dissolved sulfide (TDS) throughout the GP15 cruise shown in blue in the top panel, along with abundances of *Synechococcus* (orange) and *Prochlorococcus* (green) from Leg 2 are shown in the bottom panel. Cyanobacterial abundance corresponds to increases in TDS in the surface waters. Data was collected by a SeaFlow flowcyotmeter and analyzed by the Armbrust lab (University of Washington).

Another important sink to consider is the precipitation of dissolved sulfide with metals, allowing the vertical transport of sulfide to greater depths. Similar to Chapter 2, sinking fluxes for particulate sulfide can be estimated using the ^{238}U-^{234}Th disequilibrium method. Previous mass balances constructed for hydrogen sulfide demonstrated that the contribution of sinking particulate sulfide in the Atlantic was minimal, where Radford-Knoery and Cutter (1994) estimated removal of < 0.2 pmol L^{-1} hr^{-1}, while Zhang's (1999) estimates were 3 orders of magnitude lower at 0.0002 pmol L^{-1} hr^{-1}.

To estimate the rate of phytoplankton sulfide production at three stations in the Pacific Ocean, the remaining sources and sinks outlined above were used to calculate the input and removal of dissolved sulfide in the upper water column. Fluxes were calculated at all depths within the upper 150 m, and averaged to construct a budget for hydrogen sulfide, for three different regimes across the Pacific Ocean (Figure 11): the HNLC Alaskan slope (Station 3), the North Pacific subtropical gyre (Station 13), and the northern equatorial Pacific (Station 23). Rates of OCS hydrolysis (Radford-Knoery & Cutter, 1994), along with rates of sulfide oxidation by oxygen (Millero et al., 1987) and iodate (Zhang, 1999), and loss via sinking particles were recalculated for this study using data obtained on GP15, while sulfide losses by oxidation via peroxide (Radford-Knoery & Cutter, 1994) and light (Zhang, 1999), and input through air-sea exchange (Andreae et al., 1991; Radford-Knoery & Cutter, 1994) were ignored due to the lack of coincidental measurements and the negligible influence on the mass balance calculations reported in previous studies.

3.3.4 Mass Balance of Hydrogen Sulfide in the coastal Pacific Ocean

At Station 3 (55.1°N, 155.7°W) on the Alaskan slope, input of total sulfide was quantified in the upper 175 m of the water column where five depths were sampled over this vertical span. OCS hydrolysis rate constants were calculated from Radford-Knoery and Cutter (1994) using the corresponding temperature and pH measurements (Figure 17). The production of dissolved sulfide was then calculated using equation (6) along with observed OCS concentrations (Figure 17). Temperature ranged from 13.2°C in the surface to 4.1°C at 175 m, while carbonyl sulfide varied between 30 and 65 pmol L^{-1} with the maximum at 30 m. The calculated rate of production from OCS hydrolysis ranged between 0.4 and 1.6 pmol L^{-1} hr^{-1}, with a depth-integrated average of 0.9 pmol L^{-1} hr^{-1} (Table 7). This value is less than 20 percent of the flux that was measured in the open Atlantic (Radford-Knoery & Cutter, 1994).

Removal of sulfide by dissolved oxygen was calculated using equation (7), along with observed oxygen concentrations and the temperature, salinity, and pH dependent rate constants calculated using the function determined by Millero et al. (1987). In these coastal waters, dissolved oxygen concentrations dropped to 60 µmol kg^{-1} at 175 m with concentrations as high as 320 µmol kg^{-1} resulting in an average sulfide loss of 1.17 pmol L^{-1} hr^{-1} (Table 7) over the top 175 m. Rate of oxidative loss by iodate was calculated using the rate constant equation specific to metal-sulfide complexes, equation (8) (Zhang, 1999) since all measurable TDS was below detection, suggesting that free sulfide was not present. Iodate concentrations ranged from 320 – 390 nmol L^{-1} between 30 and 175 m, although it should be noted that iodate was not measured in surface samples (Moriyasu, Bolster, et al., 2023) during this study. It was assumed that if surface samples had been measured, their surface concentrations resembled those of other Pacific studies (Ştreangă et al.,

2024), which reported surface iodate concentrations around 250 nmol L^{-1}. This resulted in a calculated depth-integrated average sulfide loss of 10.31 pmol L^{-1} hr^{-1} (Table 7).

Although previous studies suggest that sinking particles play a minor role in the removal of dissolved sulfide from the surface, sinking fluxes were calculated using the ratio of measured, small particulate AVS-to-particulate organic carbon (POC; pAVS:POC = $2.8x10^{-6}$ µmol µmol^{-1}). Since ^{234}Th fluxes were not available at the time of writing, the POC flux (3.15 mmol C m^{-2} d^{-1}; Buesseler et al., 2020) from Ocean Station PAPA, roughly 900 km south, was utilized. Using those estimates, the sinking flux of pAVS over the upper 175 m averages to 0.37 pmol L^{-1} hr^{-1} (Table 7).

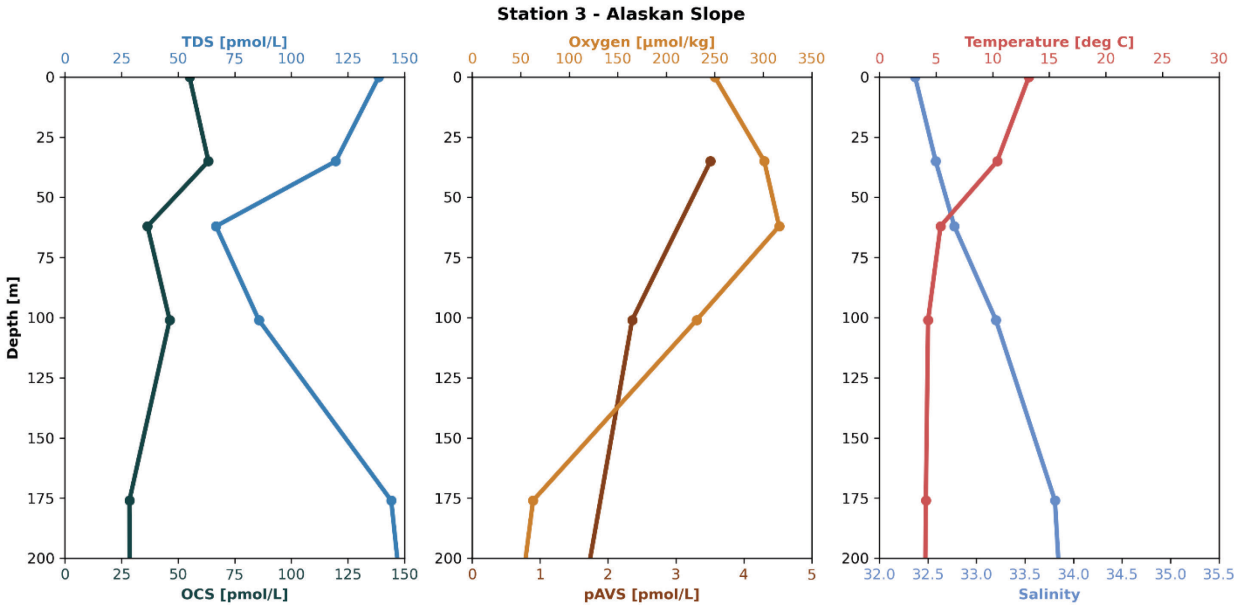

Figure 17. Vertical profiles of total dissolved sulfide (TDS), carbonyl sulfide (OCS), particulate acid volatile sulfide (pAVS), oxygen, temperature, and salinity in the top 200 m of Station 3 on the Alaskan slope (55.1°N, 155.7°W).

Compared to the budgets previously calculated for the Equatorial Pacific Ocean (Zhang, 1999), the rate of OCS hydrolysis and sulfide oxidation by oxygen are nearly identical, but the oxidative losses by iodate were ten times larger near the coast. Compared to the open Atlantic Ocean, the more coastal Pacific Ocean (Station 3) saw a large reduction in the rates of OCS hydrolysis (up to 85%) and oxidation of hydrogen sulfide by oxygen (up to 60%), whereas the losses by iodate were three times larger and unsurprisingly, the estimated flux of sinking particles more than 99% greater (Zhang, 1999). It is worth noting however that the removal by sinking particles is likely an underestimate since only the small size fraction; < 51 μm was measured, thus the inclusion of large particles (> 51 μm) would only serve to increase the total sinks for this coastal margin station.

Using the above calculations, a mass balance was generated for Station 3 on the Alaskan Slope where the difference between the known sources and sinks of hydrogen sulfide would suggest that production by phytoplankton must be on the order of 11 ± 3 pmol L^{-1} hr^{-1} (Table 7) in the coastal Pacific, in order to balance the other, better constrained fluxes. Zhang (1999) calculated the rate of production for several phytoplankton species during log phase growth from the data published by Walsh et al. (1994), with the rate of TDS production being a function of observed Chlorophyll a (Chl a) concentration. Although the rate of TDS production by phytoplankton predicted for the present budget is much higher than previous production estimates by oceanic phytoplankton (Zhang (1999); Table 2, unpublished), it is important to remember that chlorophyll a concentrations are much larger along the Alaskan shelf than the open Atlantic ocean, and therefore, greater algal TDS production might be expected. In an attempt to resolve whether this rate of TDS production by phytoplankton is a reasonable estimate, pigment data collected in the top 100 m at this station were run through the Phytoclass package (Hayward et al., 2023) to

determine the chlorophyll a biomass of several phytoplankton groups. Using rates calculated by Zhang (1999) from the data published by Walsh et al. (1994), along with the predicted biomass Chl a concentrations, the production of TDS by four species was estimated (Table 8). The depth integrated rate of production is 1.81 ± 1.43 pmol L^{-1} hr^{-1}. Moreover, TDS production estimates from continuous cultures (Table 2, unpublished) are not significantly higher than those calculated by Zhang (1999) from the culture studies performed by Walsh et al. (1994). Those studies estimate that cyanobacteria can produce between 2.3 and 5 pmol TDS L^{-1} hr^{-1}, while diatoms could produce 3 pmol TDS L^{-1} hr^{-1} (Table 2, unpublished). Although these species dependent production estimates are slightly higher than those estimated in Table 8, they are still insufficient to close the gap between phytoplankton production predicted from the budget and that estimated from culture studies. Nevertheless, it is important to note that the total class-specific TDS production only considers four different phytoplankton groups, due to limited production rate data available from cultures (Walsh et al., 1994). In point of fact, at Station 3, these classes represent between 50 and 85% of the phytoplankton groups that contribute to the total Chl a biomass. However, it is worth mentioning that if we assumed all Chl a at Station 3 was produced by a phytoplankton species like the largest known TDS producer, *Synechococcus*, then the gap between production estimated from culture studies (16.4 pmol L^{-1} hr^{-1}) and that predicted by the budget (11 ± 3 pmol L^{-1} hr^{-1}) would close. Without more reliable data on the assemblage of the phytoplankton community and associated rates of sulfide production, it becomes difficult to verify whether the influx of hydrogen sulfide to surface waters by phytoplankton predicted here is a reasonable estimate. Our results suggest that TDS production by assimilatory sulfate reduction must be much larger in the coastal environment than the rates determined previously in lab cultures (Walsh et al., 1994; Zhang, 1999; Table 2). However, it is important to note that these large production rates are largely controlled

by the phytoplankton species present, and might be more representative of a high-nutrient, low chlorophyll (HNLC) environment than the oligotrophic regions previously examined in the Atlantic and Pacific Oceans (Radford-Knoery & Cutter, 1994; Zhang, 1999). It is recommended that future studies determine the sulfide production rates by several species under relevant seawater conditions, but also that species specific biological data be collected in conjunction with the sulfide measurements to help resolve the large discrepancies in sulfide production estimates by phytoplankton versus those estimated by mass balance.

Table 7. Sources and sinks of TDS in the euphotic zone of the North Pacific Ocean. Sulfide oxidation by iodate using the TDS-specific rate constant (Zhang, 1999).

	Ranges of species concentration	Depth-averaged sulfide fluxes (pmol L^{-1} hr^{-1})		
Station		3	14	23
Coordinates		55.1°N, 155.7°W	32°N, 152°W	7.5°N, 152°W
Depth Range		0-175 m	0-150 m	0-160 m
Sources:				
Atmospheric Input		0.03	0.03	0.03
OCS hydrolysis	30 - 120 pmol/L OCS	0.90	1.90	4.29
	Total Sources:	0.93 ± 0.06	1.93 ± 0.17	4.32 ± 0.88
Sinks:				
Sulfide Oxidation	50 - 320 µmol/L O_2	1.17	0.53	0.64
	0.25 - 0.42 µmol/L IO_3^-	10.31	1.72	1.59
Particle Sinking	pAVS	0.37	0.12	0.09
	Total Sinks:	11.85 ± 3.33	2.37 ± 1.14	2.32 ± 0.83
Budget Balance:				
Phytoplankton production		***10.92 ± 3.39***	***0.44 ± 1.31***	***-2.00 ± 1.71***

Table 8. TDS production estimates by 4 different classes of phytoplankton at Station 3 on the Alaskan slope. Contribution to Chl a biomass was estimated using Phytoclass (Hayward et al., 2023) and TDS production was determined using 4 species from rates calculated by Zhang (1999) based upon the Walsh et al. (1994) study. The species included in the TDS production estimates are: *Emiliania huxleyi* (haptophyte), *Pyramimonas obovata* (chlorophyte), *Thalassiosira oceanica* (diatom), and *Synechococcus*.

	Chl a biomass of different phytoplankton classes [ng L^{-1}]				**Species Dependent TDS Production** [pmol L^{-1} hr^{-1}]				**Total TDS Production** [pmol L^{-1} hr^{-1}]
Depth [m]	Haptophytes	Chlorophytes	Diatoms	*Synechococcus*	Haptophytes	Chlorophytes	Diatoms	*Synechococcus*	
3	238.0	80.9	75.5	13.8	1.89	0.64	0.08	0.75	3.35
25	285.2	117.7	95.2	14.1	2.26	0.93	0.10	0.77	4.05
35	120.5	55.2	65.4	6.5	0.95	0.44	0.07	0.35	1.81
60	56.4	34.3	42.4	4.3	0.45	0.27	0.04	0.24	1.00
75	21.3	19.9	13.0	0.0	0.17	0.16	0.01	0.00	0.34
100	17.2	9.8	9.0	2.0	0.14	0.08	0.01	0.11	0.33
							Depth Integrated Average:		1.81 ± 1.43

3.3.5 Mass Balance of Hydrogen Sulfide in the North Pacific Oligotrophic Gyre

The mass balance in the oligotrophic North Pacific was determined using values from GP15 Station 14 (32°N, 152°W; Figure 18). Due to sample resolution, flux calculations were performed for seven depths in the upper 150 m of the water column. Individual rates for sulfide production and loss were calculated for each depth in the same way as for the coastal Station 3 (Section 3.3.4), and the depth integrated average was utilized to calculate the mass balance. OCS hydrolysis rates ranged between 1.19 and 3.08 pmol L^{-1} hr^{-1}, with a depth integrated average of 1.90 pmol L^{-1} hr^{-1}. The rate of sulfide oxidation via oxygen varies between 0.16 and 1.62 pmol L^{-1} hr^{-1}, with a depth integrated average of 0.53 pmol L^{-1} hr^{-1}. Losses by oxidation due to iodate still represent the largest removal, and range between 0.90 and 3.78 pmol L^{-1} hr^{-1} with a depth integrated average of 1.72 pmol L^{-1} hr^{-1}. Removal through sinking particles was estimated using the ^{238}U-^{234}Th disequilibrium method (Chapter 2), and pAVS losses are estimated to be 0.12 pmol L^{-1} hr^{-1}, which is comparable to the removal calculated by Radford-Knoery and Cutter (1994) in the Sargasso Sea of 0.18 pmol L^{-1} hr^{-1}. The total cumulative sulfide sink for Station 14 is 2.34 pmol L^{-1} hr^{-1}, which is half of what Zhang (1999) previously estimated for the equatorial Pacific (5.25 pmol L^{-1} hr^{-1}). To balance these losses and the addition by OCS hydrolysis, production by phytoplankton is estimated to be 0.4 ± 1.3 pmol L^{-1} hr^{-1}. A summary of these calculations is shown in Table 7. This rate of production by phytoplankton in the oligotrophic North Pacific gyre at Station 14 is comparable to the rate calculated by Zhang (1999) in the equatorial Pacific Ocean nearly 2,600 km to the south of Station 14.

Although we lack contemporaneous TDS and phytoplankton abundance data to confidently estimate production by several classes, TDS production was again estimated (Table 9) using the predicted biomass Chl a concentrations using community biomass estimates from Phytoclass

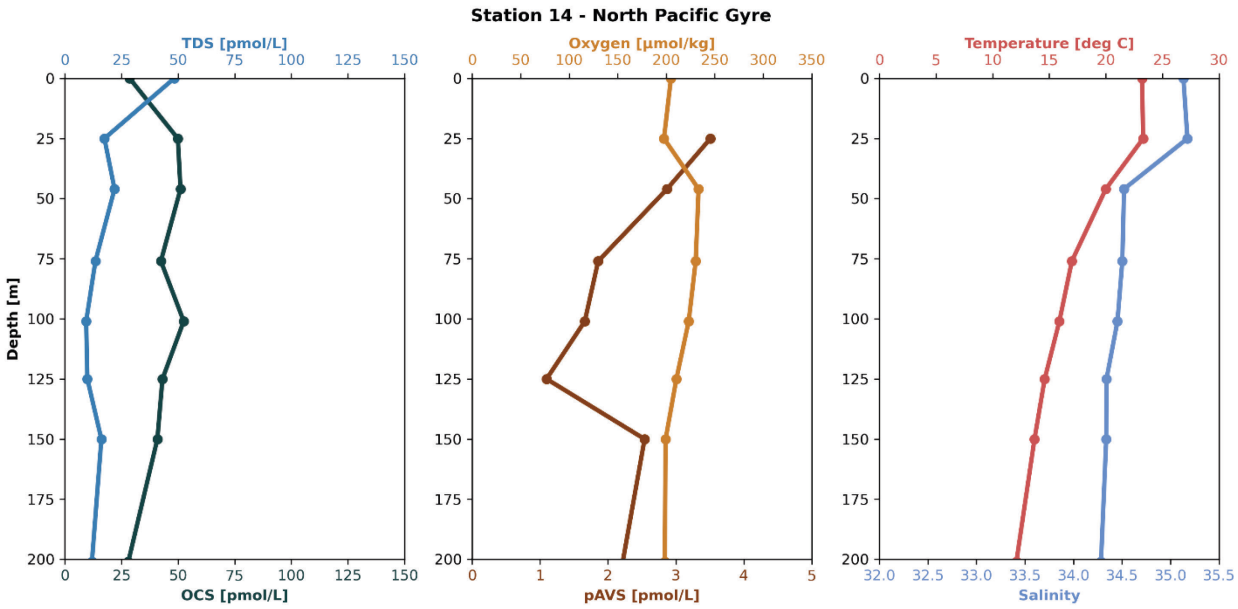

Figure 18. Vertical profiles of total dissolved sulfide (TDS), carbonyl sulfide (OCS), particulate acid volatile sulfide (pAVS), oxygen, temperature, and salinity in the top 200 m of Station 14 in the North Pacific subtropical gyre (32°N, 152°W).

(Hayward et al., 2023) coupled with the sulfide production rates calculated by Zhang (1999) from Walsh et al. (1994) for four oceanic species, as was done for Station 3. Strikingly, the depth integrated average of total TDS production in the upper 75 m at Station 14 is 4.93 ± 0.89 pmol L^{-1} hr^{-1} (Table 9), which can account for all of the phytoplankton production expected based on mass balance calculations. Based on Phytoclass estimates, these four groups (haptophytes, chlorophytes, diatoms, and *Synechococcus*) likely account for 80 to 95% of the Chl a biomass in the oligotrophic gyre of the North Pacific, and therefore sulfide production might not be largely impacted by the inclusion of other species. Overall, estimated TDS production rates by phytoplankton are in accord with the fluxes anticipated based on the mass balance between the sources and sinks of hydrogen sulfide in the surface 150 m of the North Pacific oligotrophic gyre.

Table 9. TDS production estimates by 4 different classes of phytoplankton at Station 14 in the subtropical North Pacific. Contribution to Chl a biomass was estimated using Phytoclass (Hayward et al., 2023) and TDS production was determined using 4 species from rates calculated by Zhang (1999) based upon the Walsh et al. (1994) study. The species included in the TDS production estimates are: *Emiliania huxleyi* (haptophyte), *Pyramimonas obovata* (chlorophyte), *Thalassiosira oceanica* (diatom), and *Synechococcus*.

	Chl a biomass of different phytoplankton classes [ng L^{-1}]				**Species Dependent TDS Production** [pmol L^{-1} hr^{-1}]				**Total TDS Production** [pmol L^{-1} hr^{-1}]
Depth [m]	Haptophytes	Chlorophytes	Diatoms	*Synechococcus*	Haptophytes	Chlorophytes	Diatoms	*Synechococcus*	
5	34.0	3.9	4.8	56.1	0.27	0.03	0.00	3.04	3.35
25	36.8	17.0	4.9	76.2	0.29	0.13	0.00	4.13	4.56
38	39.8	20.9	4.9	75.5	0.31	0.17	0.00	4.09	4.58
45	49.0	18.9	6.3	88.4	0.39	0.15	0.01	4.79	5.34
60	68.0	46.1	8.7	95.1	0.54	0.37	0.01	5.15	6.07
75	70.7	52.3	8.7	86.7	0.56	0.41	0.01	4.70	5.68
							Depth Integrated Average:		4.93 ± 0.89

3.3.6 Mass Balance of Hydrogen Sulfide in the Equatorial North Pacific

Similar to Station 14, the mass balance in the equatorial North Pacific was determined using data from Station 23 (7.5°N, 152°W; Figure 19). Due to sample resolution, flux calculations were performed on the top seven depths in the upper 160 m of the water column. Individual rates for sulfide production and loss were calculated for each depth in the same way as outlined previously and the depth integrated average was utilized to calculate the mass balance. Hydrogen sulfide was produced by OCS hydrolysis at a rate of 4.29 pmol L^{-1} hr^{-1}, and removed by oxidation by oxygen and iodate at depth integrated average rate of 0.64 and 1.59 pmol L^{-1} hr^{-1}, respectively (Table 7).

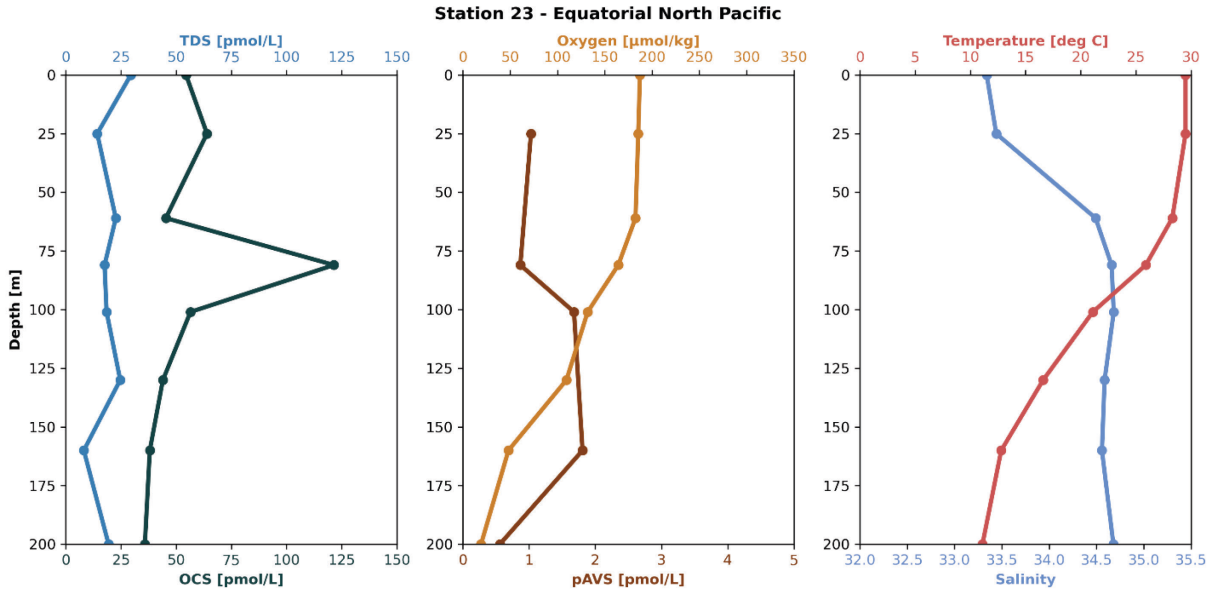

Figure 19. Vertical profiles of total dissolved sulfide (TDS), carbonyl sulfide (OCS), particulate acid volatile sulfide (pAVS), oxygen, temperature, and salinity in the top 200 m of Station 23 in the equatorial North Pacific (7.5°N, 152°W).

At the time of writing, ^{234}Th fluxes were not available for Station 23 and so, sinking pAVS fluxes were determined using the ratio of small pAVS-to-particulate ^{234}Th coupled with the ^{234}Th fluxes measured at the nearby, Station 27 (2.5°N, 152°W). From this method, loss by sinking pAVS is estimated to be around 0.09 pmol L^{-1} hr^{-1}. It should be noted that the losses by sinking particles is minimal (as demonstrated earlier in Chapter 3 and in other studies; Radford-Knoery & Cutter, 1994; Zhang, 1999) and likely has little impact on the mass balance estimates calculated here. Nevertheless, the total loss of hydrogen sulfide calculated for Station 23 is estimated to be 2.32 pmol L^{-1} hr^{-1} (Table 7) which can explain approximately 50% of the sulfide produced in the surface ocean by OCS hydrolysis. While on average, production by phytoplankton might not be necessary to balance the TDS budget in the equatorial Pacific, considering the potential errors, the budget could actually be in equilibrium.

Yet, estimating possible TDS production from available pigment data using Phytoclass, depth integrated TDS production is calculated to be on the order of 5.00 ± 1.06 pmol L^{-1} hr^{-1} in the upper 100 m (Table 10) which significantly overestimates the rate needed for the mass balance. As stated previously for Station 14, the uncertainty within these rates and the limited pigment data (extends to 100 m depth) likely contribute to the overestimation. However, it is worth noting that additional pigment data would likely only serve to increase the overestimation in the subtropics and equatorial Pacific due to the DCM generally occurring below 100 m. Additionally, the phytoplankton production estimates are based on predicted species present, not actual. The Phytoclass model suggests that *Synechococcus* makes up anywhere from 7 to 95% of the total Chl a biomass in the upper 100 m, however, this is limited by the available pigment data. It is also important to note that if a large portion of TDS production in surface waters is dominated by phytoplankton production, TDS concentrations might demonstrate diel variability (Cutter &

Krahforst, 1988), and thus the rates (Walsh et al., 1994) used to calculate the production by phytoplankton might not be representative of the production at the time of sampling or be representative of the time- and depth-averaged rate of production. Although it is worth mentioning that production from a nearby equatorial station (approx. 500 km north) had a depth integrated production by *Synechococcus* of 0.88 pmol L^{-1} hr^{-1} (Zhang, 1999) and narrows the gap between the unnecessary phytoplankton production and the other, better constrained processes. Nevertheless, like the other sources of uncertainty mentioned previously, it is important to remember that Zhang's (1999) estimates are likely an underestimate as other species are expected to contribute to TDS production in the equatorial Pacific Ocean.

3.3.7 Metal-Specific Mass Balance of Hydrogen Sulfide

Previously, sulfide losses due to oxidation by iodate were calculated using the non-metal specific TDS rate constant (Zhang, 1999). But given that the rate of sulfide oxidation by iodate varies based on the metal-sulfide complex present (Zhang, 1999), the metal-specific composition of TDS should be factored in when calculating the losses of sulfide due to oxidation by iodate. While the oxidation rate for TDS is much slower than that of free sulfide, Zhang (1999) found that Ni- and Cd-sulfide complexes exhibit a much lower rate of oxidation compared to the non-metal specific TDS rate, whereas Zn-sulfide complexes were found to be inert and resist oxidation by iodate. Therefore, knowing the chemical speciation of TDS serves to improve the sulfide budget and could reduce the dissolved sulfide losses to oxidation by iodate.

To re-evaluate the predicted mass balance in the euphotic zone of the North Pacific Ocean, the loss of dissolved sulfide through oxidation by iodate was re-calculated using the metal-specific

Table 10. TDS production estimates by 4 different classes of phytoplankton at Station 23 in the equatorial North Pacific. Contribution to Chl a biomass was estimated using Phytoclass (Hayward et al., 2023) and TDS production was determined using 4 species from rates calculated by Zhang (1999) based upon the Walsh et al. (1994) study. The species included in the TDS production estimates are: *Emiliania huxleyi* (haptophyte), *Pyramimonas obovata* (chlorophyte), *Thalassiosira oceanica* (diatom), and *Synechococcus*.

	Chl a biomass of different phytoplankton classes [ng L^{-1}]				**Species Dependent TDS Production** [pmol L^{-1} hr^{-1}]				**Total TDS Production** [pmol L^{-1} hr^{-1}]
Depth [m]	Haptophytes	Chlorophytes	Diatoms	*Synechococcus*	Haptophytes	Chlorophytes	Diatoms	*Synechococcus*	
5	32.7	21.5	3.2	83.8	0.26	0.17	0.00	4.54	4.97
25	28.6	20.7	0.0	76.2	0.23	0.16	0.00	4.13	4.52
60	93.5	50.2	4.1	86.6	0.74	0.40	0.00	4.70	5.84
70	112.9	61.4	4.2	89.8	0.89	0.49	0.00	4.87	6.25
80	132.9	109.0	8.8	64.7	1.05	0.86	0.01	3.51	5.43
100	98.4	129.0	0.0	21.6	0.78	1.02	0.00	1.17	2.97
							Depth Integrated Average:		5.00 ± 1.06

rates suggested by the TDS speciation results from Section 3.3.1, while keeping all other depth-averaged fluxes the same (Table 11). Since Zhang's (1999) work did not evaluate the effect of dissolved Pb-sulfide complexes on sulfide oxidation rates by iodate, we assumed that dissolved Pb-sulfide complexes shared the same rate of oxidation as Cd-sulfide complexes, while Zn-sulfide complexes remained inert. Results from the chemical equilibrium speciation model at Station 3 on the Alaskan slope suggest that dissolved ZnS complexes make up between 40 and 75% of TDS in the upper 200 m of the water column with dissolved CdS and PbS making up the remaining 25-to-60%. This suggests that 40-to-75% of the dissolved sulfide in the TDS pool is protected from oxidation by iodate, thereby substantially reducing the dissolved sulfide losses in the upper 175 m of the surface ocean from 10.3 pmol L^{-1} hr^{-1} to 0.6 pmol L^{-1} hr^{-1}, a 94% reduction in dissolved sulfide losses through oxidation by iodate when factoring in the specific metal complex. Station 14 and 23 also saw similar reductions in the re-calculated sulfide losses of 92% and 94% (Table 11), respectively. This reduction in dissolved sulfide losses by oxidation to sulfate would serve to diminish the gap between known production and loss terms. At Station 3 on the Alaskan shelf, TDS production by phytoplankton is re-calculated to be on the order of 1.2 ± 1.1 pmol L^{-1} hr^{-1} (Table 11) which is strikingly similar to the production estimates from pigment data (1.8 ± 1.4 pmol L^{-1} hr^{-1}; Table 8) that suggest our limited biological data might represent most of the sulfide production anticipated by phytoplankton. Whereas Stations 14 and 23 suggest that sulfide production by phytoplankton was unnecessary to close the sulfide budget in the surface ocean (Table 11). Instead, more sulfide was being produced by OCS hydrolysis than lost through oxidation to sulfate, or as sinking particles resulting in this negative balance calculated for production by phytoplankton. While that could be the case, it is important to remember that these

calculations are snapshots of the dynamic mechanisms controlling the amount of dissolved sulfide in the surface ocean and therefore overlooking the long-term rate.

3.4 Conclusions

Dissolved sulfide speciation calculations suggest that TDS is predominately composed of CdS and ZnS complexes closer to the coastal margins (Figure 12). In the open ocean, there is a shift towards ZnS and PbS complexes dominating the upper surface layer and CdS controlling the majority of TDS in the deeper euphotic zone (Figures 13 and 14). These results are strongly influenced by the dissolved metal concentrations and the inclusion of MS complexes, the exclusion of Cu-complexes, and the accuracy of the stability constants incorporated into the model. Dissolved Cd and Zn concentrations were elevated along the coastal margins and decreased towards open ocean, whereas dissolved Pb concentrations were largely unchanged between those 3 stations, demonstrating its larger influence on sulfide speciation in the open ocean as dissolved Cd and Zn pools decreased. However, these results are in contrast to those presented by several others, who predicted that Cu complexes would dominate the speciation of dissolved sulfide. It is likely that the concentration of dissolved sulfide in seawater measured in this study is an underestimate of the actual TDS concentration, due to the exclusion of non-acid volatile complexes like Cu and Hg. Preliminary results from our work suggest that by including aqueous CuS complexes, we could be underestimating the actual TDS concentration in surface seawater by 5-90%, depending on the conditional stability constant applied in the model. If a method is developed that will also quantify the non-acid volatile complexes (Cu and Hg), then future chemical speciation models should include the potential for Cu- and Hg-sulfide complexes. This would provide better insight into the extent of hydrogen sulfide's role in metal cycling and the role that

Table 11. Sources and sinks of TDS in the euphotic zone of the North Pacific Ocean. Sulfide oxidation by iodate using the metal-specific rate constants (Zhang, 1999) based on the speciation results found in Section 3.3.1.

	Ranges of species concentration	Depth-averaged sulfide fluxes (pmol L^{-1} hr^{-1})		
Station		3	14	23
Coordinates		55.1°N, 155.7°W	32°N, 152°W	7.5°N, 152°W
Depth Range		0-175 m	0-150 m	0-150 m
Sources:				
Atmospheric Input		0.03	0.03	0.03
OCS hydrolysis	30 - 120 pmol/L OCS	0.90	1.90	4.29
	Total Sources:	0.93 ± 0.06	1.93 ± 0.17	4.32 ± 0.88
Sinks:				
Sulfide Oxidation	50 - 320 µmol/L O_2	1.17	0.53	0.64
	0.25 - 0.42 µmol/L IO_3^-	0.57	0.13	0.09
Particle Sinking	pAVS	0.37	0.12	0.09
	Total Sinks:	2.11 ± 1.03	0.78 ± 0.56	0.82 ± 0.55
Budget Balance:				
Phytoplankton production		***1.18 ± 1.09***	***-1.15 ± 0.73***	***-3.50 ± 1.43***

copper-sulfide complexes have in sulfur cycling.

Sulfide budgets generated at three stations throughout the North Pacific Ocean suggest that the amount of TDS produced by phytoplankton necessary to balance TDS sources and sinks in surface waters ranges from superfluous at the equator up to 11 ± 3 pmol L^{-1} hr^{-1} along the Alaskan slope (Tables 7 and 8). In the HNLC region on the Alaskan slope, the rate calculated from predicted biomass contributions by several phytoplankton groups is insufficient to reconcile the mass balance of hydrogen sulfide within the upper 175 m, unless the rate of oxidation by iodate for specific dissolved metal-sulfide complexes is considered. However, in the oligotrophic gyre and the equatorial Pacific, TDS production by phytoplankton was not necessary to close the balance in

those surface 150 m. Additional culture studies evaluating the production rates of several phytoplankton species relevant to these regimes, along with ancillary biological data, could help resolve some of the uncertainties in the budgets.

While the results provide further insight into the details of hydrogen sulfide cycling and speciation in the North Pacific, findings may differ from those in the higher latitude South Pacific and Southern Ocean. Examination of other regions may help resolve some discrepancies between observed and calculated speciation, along with the rates of addition and removal of dissolved hydrogen sulfide in the surface layer. The following chapter focuses on the production and phase of hydrogen sulfide across several oceanographic fronts, and how budgets calculated for the surface Southern Ocean might differ compared to those calculated for North Pacific.

Chapter 4

ASSESSING THE VARIABILITY OF SULFIDE PRODUCTION THROUGH THE SOUTH PACIFIC AND SOUTHERN OCEAN

4.1 Introduction

Even though the distribution of hydrogen sulfide has been studied in several regimes in the open ocean, few studies have crossed extreme oceanographic gradients that would allow for an in-depth examination on the processes affecting the production of hydrogen sulfide in surface waters. It is well documented that the hydrolysis of another sulfur gas, carbonyl sulfide (OCS), serves as a source of hydrogen sulfide in oxic seawater (Andreae et al., 1991; Elliott et al., 1987; Figure 1). This process is largely controlled by the temperature and pH of the solution. While some suggested that the hydrolysis of OCS was sufficient to sustain the levels of dissolved sulfide observed in seawater, several others suggested that there is a biotic source contributing to its existence, based on observed diel variations in sulfide concentrations (Cutter & Krahforst, 1988). This was later supported by Walsh et al. (1994), who presented evidence that assimilatory sulfate reduction by phytoplankton is another major contributor to sulfide in the surface ocean (Figure 1), however, this contribution is heavily dependent on the species present. Between these two sources, production by phytoplankton is poorly constrained, due to limited culture studies (Walsh et al., 1994). However, prior research (Andreae, 1990; Cutter & Krahforst, 1988; Radford-Knoery & Cutter, 1994; Walsh et al., 1994) and mass balance calculations (Radford-Knoery & Cutter, 1994; Zhang, 1999; Chapter 3) indicate that phytoplankton production could account for a significant portion of sulfide present in the surface ocean.

This chapter qualitatively examines the variability of sulfide production across the contrasting regimes encountered on the 2022 US GEOTRACES GP17-OCE transect. Beginning in the oligotrophic subtropical gyre of the South Pacific where cyanophytes like *Prochlorococcus* are expected to dominate the phytoplankton community (Bonnet et al., 2008) and are thought to produce the largest amount of dissolved sulfide (Walsh et al., 1994). In contrast, the higher latitude sub-Antarctic region is largely dominated by haptophytes and diatoms, for which some species reportedly produce up to 40% and 6%, respectively, of the sulfide produced by cyanophytes (Walsh et al., 1994). Concentrations of several photosynthetic pigments from the euphotic zone along the GP17-OCE transect allowed us to assess the phytoplankton community composition across several ocean nutrient gradients, using the Phytoclass package in R (Hayward et al., 2023). This analysis provided additional support for the important role that certain phytoplankton, like cyanobacteria, play in the production of sulfide in the open ocean.

4.2 Methods

4.2.1 Sampling Site

Samples were collected during the US GEOTRACES GP17-OCE Transect on board R/V *Roger Revelle*, that departed Tahiti on 1 December 2022 and headed south to ~67°S, then headed eastward along the Antarctic ice edge during Austral summer before ending on the Chilean shelf by 25 January 2023 (Figure 20). Of the 38 stations sampled on GP17-OCE, vertical profiles of total dissolved sulfide (TDS) and small size fraction (0.8 – 51 μm) particulate acid-volatile sulfide (pAVS) were obtained for 19 and 16 stations, respectively. Based on temperature, nutrient, and salinity profiles, R/V *Roger Revelle* first crossed the Sub-Tropical Front (STF) at Station 8 (37.5°S, 149.28°W), the Sub-Antarctic Front (SAF) at Station 14 (52.31°S, 146.4°W), the Polar Front (PF)

and the southern Antarctic Circumpolar Current Front (sACCF) at Station 17 (55.89°S, 145.4°W), and the Southern Boundary (SB) at Station 19 (56.84°S, 145.11°W).

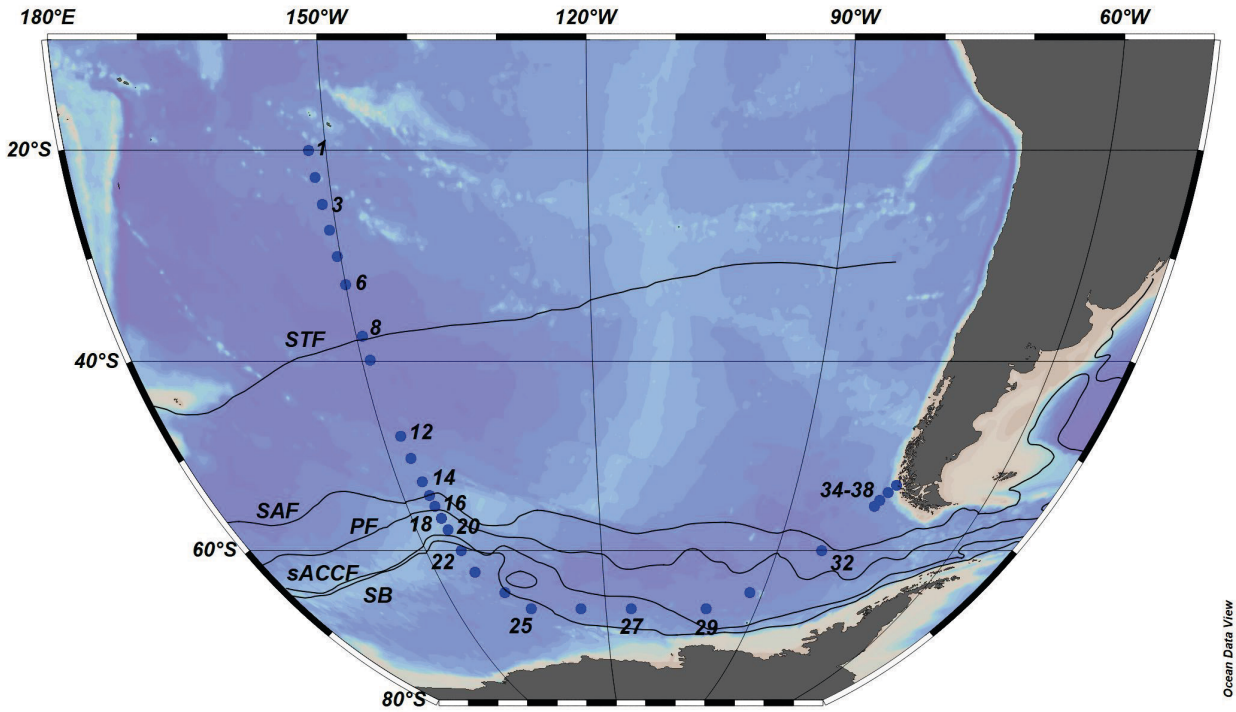

Figure 20. Full transect of GP17-OCE where dissolved sulfide was sampled. Stations numbers are labeled for stations where profiles were taken for the upper 1000 m of the water column. Station locations without labels indicate where surface towfish samples were collected. Major fronts intersected on this cruise are labeled: Sub-tropical Front (STF), Sub-Antarctic Front (SAF), Polar Front (PF), southern Antarctic Circumpolar Current Front (sACCF), and Southern Boundary (SB). Fronts used in this figure are defined by Orsi et al. (1995).

4.2.2 Sample Collection

Water samples for TDS and OCS analyses were collected using the Scripps Oceanographic Data Facility (ODF) rosette with 36-10.4 L Niskin bottles mounted with a CTD, oxygen, fluorometer, and transmissometer sensors. For TDS, the cubitainers were rinsed 3 times with the sample before filling hermetically with approximately 1.5 L of unfiltered seawater from each depth and then stored in a refrigerator and analyzed at sea within 8 hours. It should be noted that the samples were unfiltered due to time constraints with gravity filtration, compared to the pressurized GO FLO bottles used on the trace metal-clean carousel. Due to the large volume requirement, samples for free sulfide were only acquired from the surface towfish where at least 3 L of unfiltered seawater was transferred to a 4 L polyethylene cubitainer. The cubitainers were then stored in a refrigerator and analyzed at sea within 2 hours.

Pigments were sampled from the surface towfish and the shallowest 4-6 depths on the ODF rosette. Water was collected in 2 L amber bottles that were rinsed 3 times with the sample before collection. Samples were vacuum filtered onto 25 mm GF/F filters after collection and frozen at -80°C until analysis (Bidigare et al., 1989; Mantoura & Llewellyn, 1983).

Particulate sulfide samples were collected by D. Ohnemus's (Skidaway Institute of Oceanography) sampling team using modified McLane in-situ pumps with two mini-MULVFS filter holders (Bishop et al., 2012), each plumbed with their own flowmeter. One of the holders contained a 51 μm polyester mesh prefilter and particles collected on a 0.8 μm Supor polyethersulfone membrane filter (0.8 – 51 μm size fraction). The other filter holder contained the same prefilter, but collected particles on a Whatman QMA quartz fiber filter (1 – 51 μm size fraction; Bishop et al., 2012). Excess seawater in the filter holders was removed using a vacuum pump within an hour of pump recovery. The Supor filters were then subsectioned in the onboard

trace metal clean lab by D. Ohnemus's pump team and one-sixteenth of the filter subsamples placed in cryovials that were subsequently stored frozen at -80°C until analysis for pAVS. The whole Supor filters had between 20 and 1,100 L filtered through them, with an average of 310 L, thus an average effective volume of 19.4 L for the Supor filter subsample (6.25% of each filter). It should be noted that the particulate AVS concentrations in the study were calculated from the actual filtered volumes for each sample, and not the average. It is important to mention that sample coverage past Station 16 (55°S, 145.66°W) is greatly diminished due to inclement weather conditions resulting the loss of sampling equipment and/or the cancellation of the deployment.

4.2.3 Determination of Dissolved and Particulate Sulfide

At sea, dissolved sulfide samples were quantified using the method of Radford-Knoery & Cutter (1993). The gas stripping vessel was filled with the seawater sample and purged with helium. The cryogenic trap was immersed in liquid nitrogen, followed by injecting 1.5 M phosphoric acid and the gases stripped/trapped the gases before quantifying TDS and OCS using a gas chromatograph coupled with a flame photometric detector. This method quantifies TDS as free ions and metal-sulfide complexes with detection limits of 0.2 pmol/L for TDS and 1.3 pmol/ L for OCS for 300 mL samples. Dissolved sulfide water samples were mostly analyzed in duplicate, occasionally triplicate when time permitted; precision was generally within 10% RSD. To ensure accuracy the H_2S and OCS gases are calibrated using permeation tubes whose permeation rates have been gravimetrically measured every 6 months. By trapping and measuring known amounts of permeated H_2S and OCS over a range of times, linear calibration curves for each gas were assembled daily and applied to the unknown samples.

Particulate acid volatile sulfide (pAVS) for the small size fraction (0.8 – 51 μm) was determined at Old Dominion University (ODU) using the procedure outlined in Radford-Knoery and Cutter (1993). The frozen Supor filter was placed into a gas stripping vessel with deionized water, acidified to 1 M HCl, and then the gas stripped, cryogenically trapped, and quantified using gas chromatography/flame photometric detection. This method has a particle detection limit of 0.2 pmol S, which corresponds to relative detection limit of 0.01 pmol L^{-1} pAVS for an average filtered volume of 20 L. Particulate AVS samples were analyzed in duplicate, with precision near 10% RSD, similar to other studies (Cutter & Kluckhohn, 1999; Cutter & Radford-Knoery, 1991).

4.2.4 Phytoplankton Community Predictions

Composition of the phytoplankton community was assessed using the Phytoclass package by Hayward et al. (2023) in R. This approach is similar to the CHEMTAX program (Mackey et al., 1996), however, a major improvement to the program is that unlike CHEMTAX, Phytoclass does not heavily depend on the initial pigment-to-Chl a ratios to determine the composition of the phytoplankton community. The program requires two matrices to be imported into the program: 1) a matrix that contains the samples and their pigment concentrations and 2) an initial solution that contains a matrix of pigment-to-Chl a ratios associated with each phytoplankton class. Since we do not have known pigment-to-Chl a ratios for phytoplankton classes for this study, we used the program's default pigment-to-Chl a matrix as an initial starting point for the simulated annealing algorithm performed on the sample and solution matrices. Of the 19 pigment concentrations determined for each sample, only 12 were incorporated into the sample matrix, due to the current default limitations of the program. These 12 pigments were used to estimate the

expected abundance of 8 different classes: prasinophytes, chlorophytes, cryptophytes, diatoms, dinoflagellates, haptophytes, pelagophytes, and *Synechococcus*.

4.3 Results and Discussion

Due to the temperature dependency of OCS hydrolysis and the species-dependent sulfide production by phytoplankton, these two processes likely have a substantial and varying impact on the concentrations of TDS observed along the GP17-OCE transect. Also, since sulfide production by phytoplankton is poorly constrained (Radford-Knoery & Cutter, 1994; Walsh et al., 1994; Chapter 3), estimates of the composition of the phytoplankton community could help tease apart the variable concentrations of TDS and pAVS observed on the GP17-OCE transect.

The warmest temperatures (Figure 21a) and highest salinities (Figure 21b) were encountered north of the Sub-Tropical Front (STF) in the oligotrophic gyre, where nutrients were low (Figure 21c, d). However, this is also where the highest TDS concentrations were observed in surface waters (Figure 21e). TDS concentrations had subsurface maxima in the upper 100 m of the water column and decreased with depth. South of the Polar Front (PF), silicate (Figure 21c) and nitrate (Figure 21d) concentrations were elevated and influenced shifts in phytoplankton community – likely towards heavily silicified diatoms (DiTullio et al., 2003). South of the Sub-Antarctic Front (SAF) beyond Station 14, surface TDS concentrations were generally below detection limits (< 0.2 pmol L^{-1}; Figure 21e) while surface OCS concentrations were larger at the higher latitudes (Lennartz et al., 2020; Chapter 3). Though it might be assumed that these elevated levels of OCS could lead to larger concentrations of TDS, our results suggest that the rate of production is heavily reduced due to the < 5°C temperature encountered in the Southern Ocean, compared to the lower latitudes. While there is an 87% reduction in the rate constant between

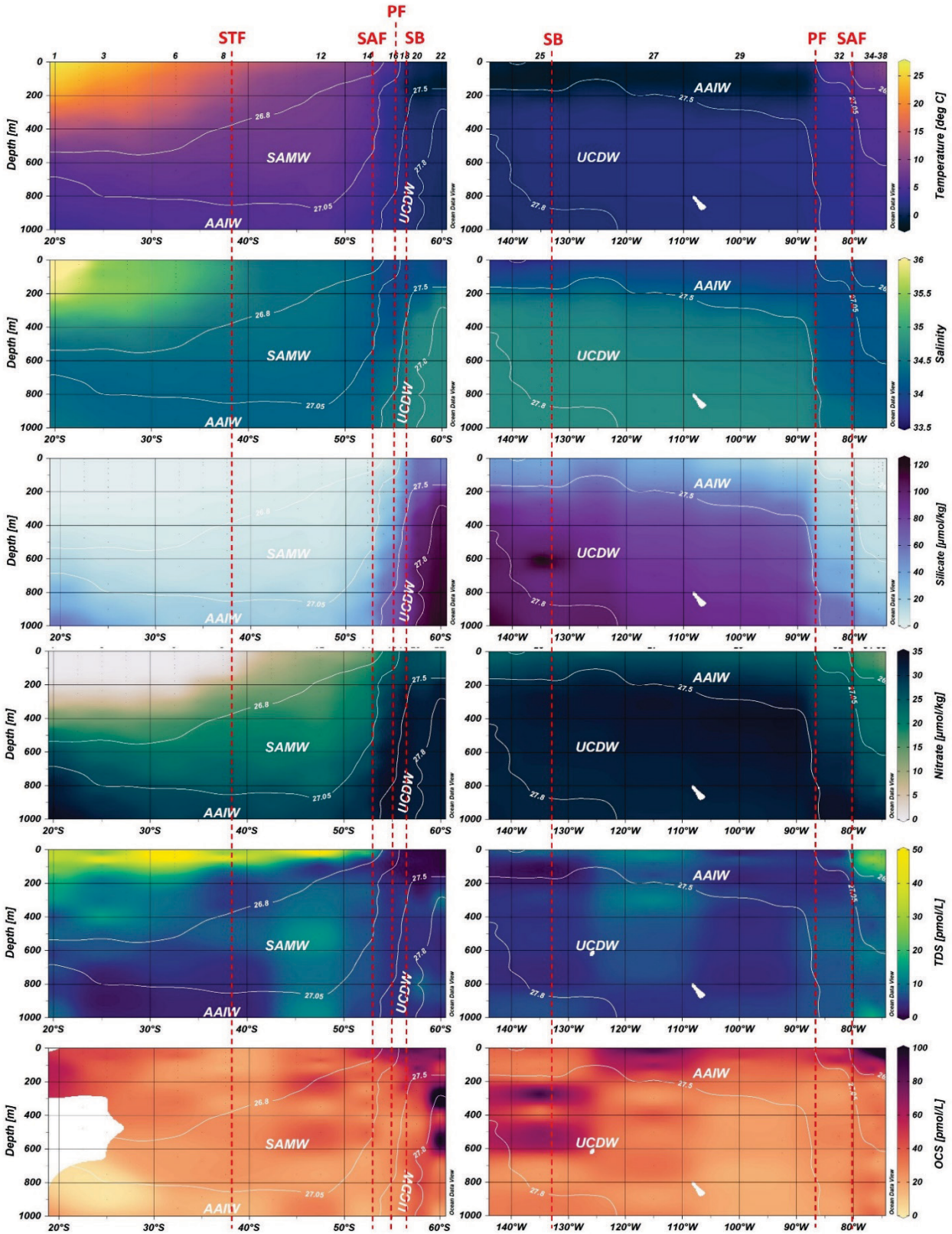

Figure 21. Transect profiles of the upper 1000 m for temperature (panel a) and salinity (panel b), along with concentrations for silicate (panel c), nitrate (panel d), total dissolved sulfide (TDS; panel e), and carbonyl sulfide

Figure 21 continued. (OCS; panel f) for the entire GP17-OCE transect. Stations numbers are indicated above the top panel. Potential density anomalies (σ, [kg/m^3]) are shown as white isolines with water masses identified (SAMW = Subantarctic Mode Water, AAIW = Antarctic Intermediate Water, and UCDW = Upper Circumpolar Deep Water). Transect was split between latitudinal and longitudinal sections where Stations 1-23 are displayed on the left (against latitude) and Stations 24-38 are displayed on the right (against longitude). Red dashed lines indicate the Sub-tropical Front (STF), the Sub-Antarctic Front (SAF), Polar Front (PF), and Southern Boundary (SB) encountered on the GP17-OCE transect.

Station 3 (25°S, 151.25°W) in the sub-tropics and Station 29 (67°S, 100°W) in the Antarctic Circumpolar Current (ACC; from 19.62×10^{-6} s^{-1} at Station 3 to 2.56×10^{-6} s^{-1} at Station 29), this translates to a 60% reduction in the production of dissolved hydrogen sulfide by OCS hydrolysis (Figure 22) even for OCS concentrations that are four times larger.

Despite this reduction in OCS hydrolysis, previous studies (Radford-Knoery & Cutter, 1994; Walsh et al., 1994; Zhang, 1999) suggest that phytoplankton might produce more sulfide than OCS hydrolysis, yet this is largely species-dependent. Silicate (Figure 21c) and nitrate (Figure 21d) concentrations were elevated along the transect south of the Polar Front (PF), and parallel shifts in phytoplankton from a *Synechococcus* (and possibly *Prochlorococcus*) dominated community towards diatoms. While all data necessary to determine the rate of dissolved sulfide produced by the hydrolysis of OCS are available from this transect, community composition data are restricted to estimates using pigment data and the Phytoclass program (Figure 23). In the oligotrophic sub-tropical South Pacific, between 20° and 40°S, low chlorophyll a concentrations are prevalent with the deep chlorophyll maxima (DCM) occurring below 100 m depth (Figure 23). The cyanobacteria, *Synechococcus*, dominate the phytoplankton assemblage with prasinophytes also existing predominately at the DCM (Figure 23a, b), as has been reported by others (Bonnet et al., 2008; DiTullio et al., 2003) and in our earlier studies (Figure 16; Chapter 3).

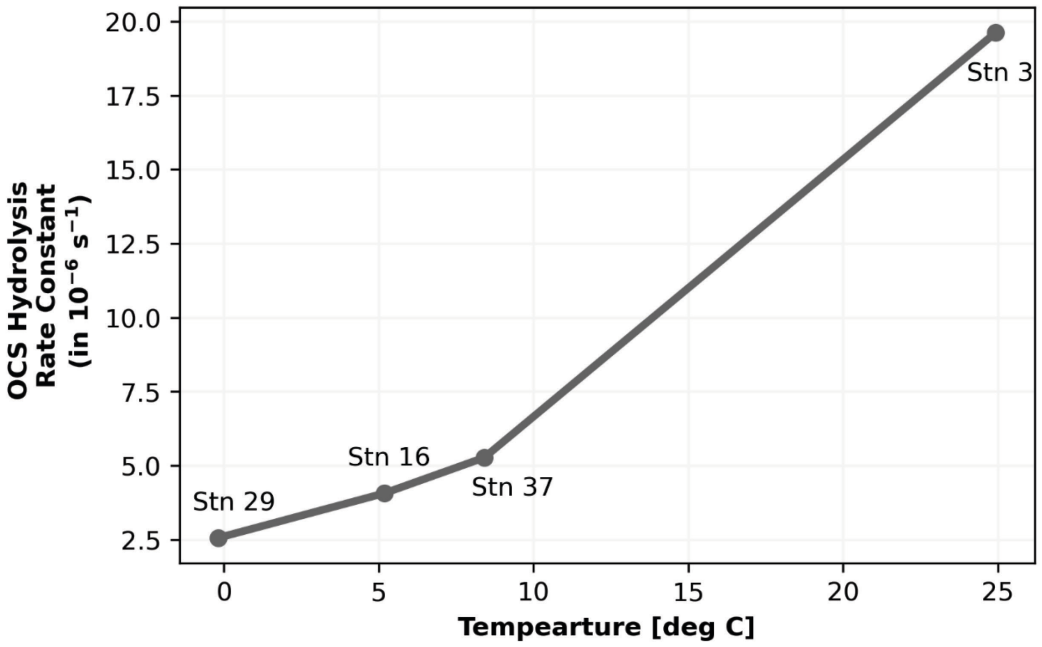

Figure 22. Carbonyl sulfide (OCS) hydrolysis rate constants at several surface stations along the GP17-OCE transect. OCS hydrolysis is temperature dependent, and the rates were calculated from Radford-Knoery and Cutter (1994). Station 3 in the sub-tropics, Station 16 in the Subantarctic, Station 29 in the Antarctic, and Station 37 off the Chilean margin.

Between the STF and SAF, *Synechococcus* and prasinophytes are still large contributors to the Chl a biomass, yet the abundance of haptophytes (Figure 22c), chlorophytes (Figure 22d), and dinoflagellates (Figure 22e) increased in this region, with haptophytes representing the majority of the phytoplankton classes present (Figure 24), similar to CHEMTAX estimations made by DiTullio et al. (2003) along 170°W. Diatoms dominated the phytoplankton assemblage in the Antarctic, and are responsible for up to 80% of total Chl a at the DCM (Figure 23f) as might be expected with elevated silicate concentrations (Figure 23c).

Regardless of the limited studies conducted on sulfide production via assimilatory sulfate reduction by marine phytoplankton, Walsh et al. (1994) demonstrated that cyanophytes were likely the largest producers of total sulfide (TDS + pAVS) with more than 90% of that as TDS. This

likely explains the larger concentrations of TDS observed in the sub-tropics (Figure 21e and 25a), where *Synechococcus* is believed to be abundant (Figures 23a and 24). However, it is important to note that while cyanophytes are known to dominate the phytoplankton classes present in the sub-tropical South Pacific (Bonnet et al., 2008; DiTullio et al., 2003), the cell counts for *Prochlorococcus* are 20 times higher than those of *Synechococcus* in the surface waters (DiTullio et al., 2003; Figure 16). This brings up an important limitation of both CHEMTAX and Phytoclass – both programs require initial estimates on the ratio of pigment-to-Chl a for each phytoplankton group considered to determine its relative contribution to total chlorophyll a biomass; therefore limiting the output from the model to only species that contain the pigment chlorophyll a. Species like *Prochlorococcus* which do not contain chlorophyll a are consequently excluded from these community predictions since they instead use pigments such divinyl chlorophyll a and b (Goericke et al., 2000). Although *Prochlorococcus* has not been utilized for any sulfide culture studies, the similarly between the abundance of both cyanophytes and TDS concentrations in the equatorial South Pacific (Figure 16) would suggest that *Prochlorococcus* might serve as a large source of sulfide to surface waters. Regrettably, of the suite of pigments analyzed, divinyl chlorophyll marker pigments were not one of them. Therefore, any potential contribution by *Prochlorococcus* is still merely speculation but should be considered in future studies.

Nevertheless, several other algal classes have been shown to produce measurable amounts of dissolved and particulate sulfide. Walsh et al. (1994) noticed that chlorophytes and haptophytes were the second and third largest total sulfide producers, yet their production was roughly 30% and 40% of the production accorded to cyanophytes. In the Subantarctic region (between the STF and SAF), haptophytes are predicted to be the largest contributor to Chl a biomass, with chlorophyte abundance also increasing. Notably, a decrease in TDS concentrations was observed

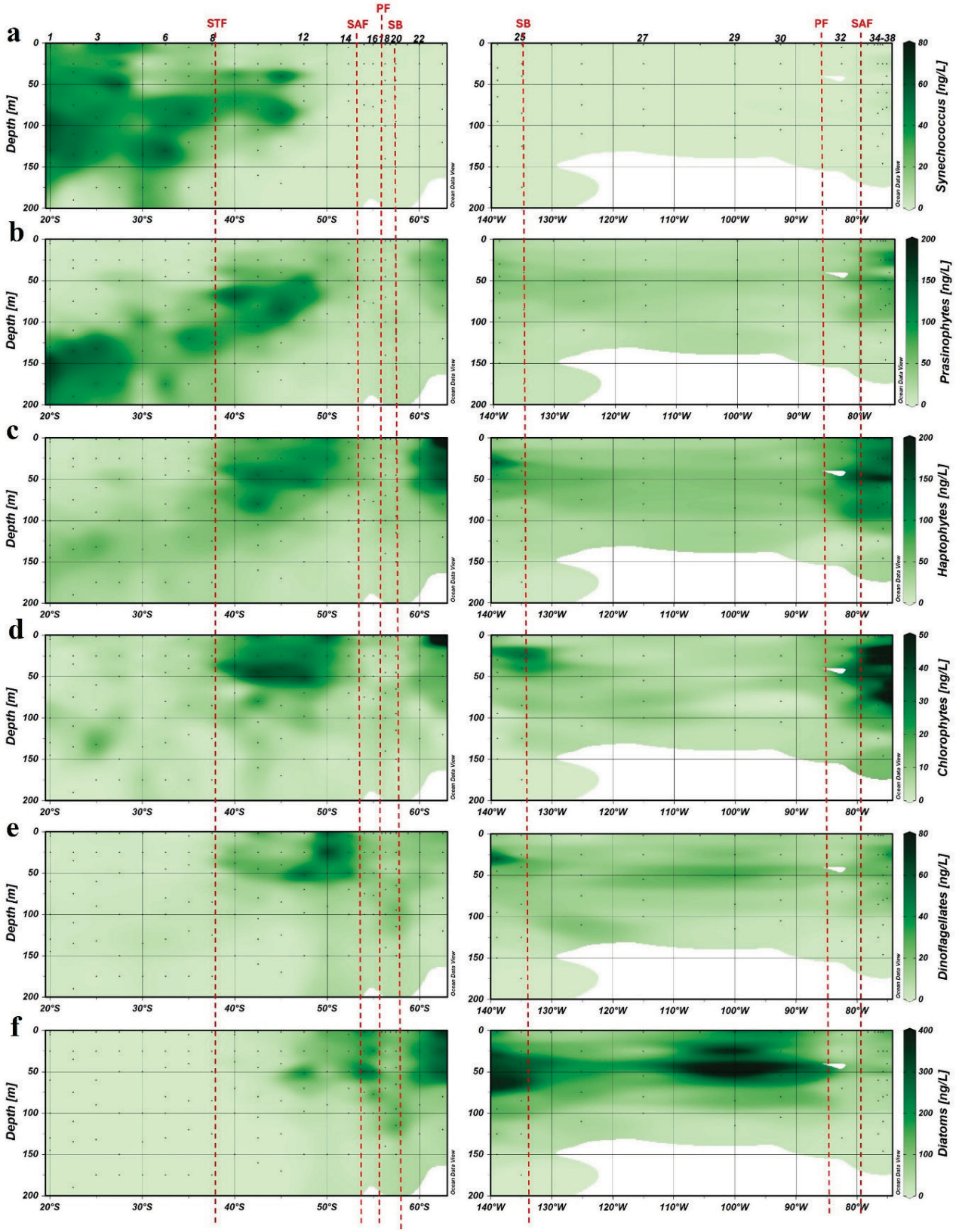

Figure 23. Predicted phytoplankton community composition based on pigment concentrations and Chl a biomass using Phytoclass (Hayward et al., 2023). Select stations are labeled above the top panels which indicate stations

Figure 23 continued. where vertical profiles of total dissolved sulfide were also obtained for the top 1000 m. Red dashed lines indicate major fronts encountered on the GP17-OCE transect: the Sub-tropical Front (STF), the Sub-Antarctic Front (SAF), Polar Front (PF), and Southern Boundary (SB).

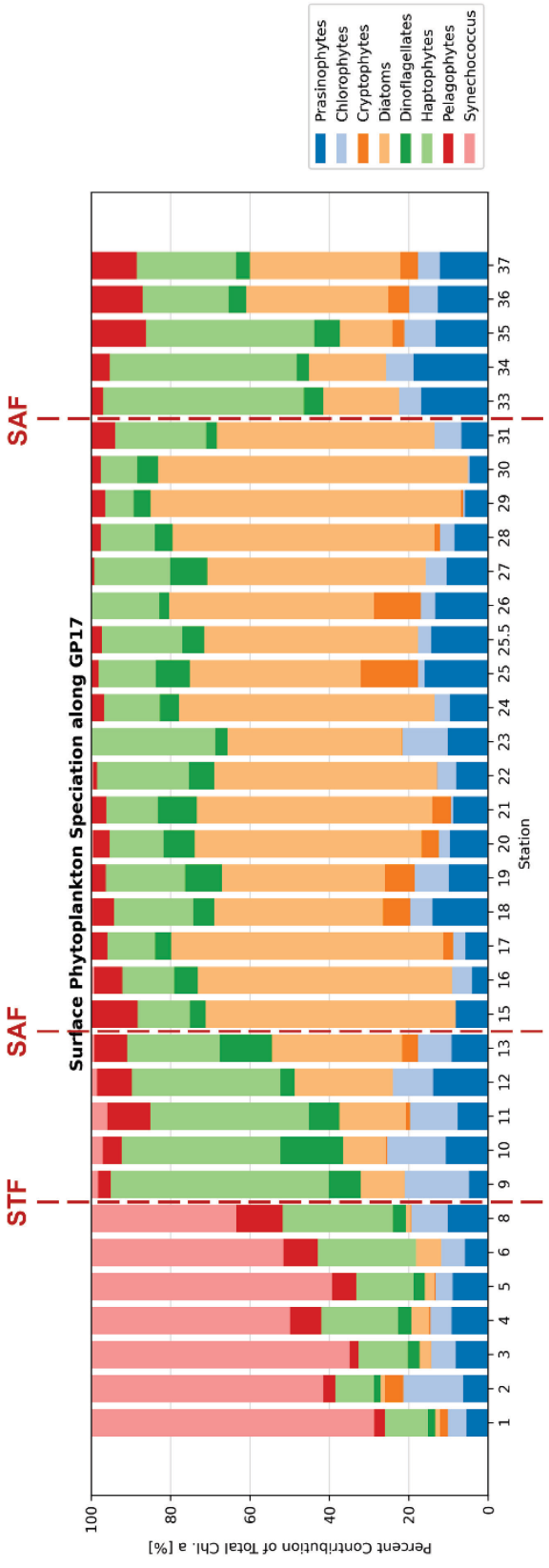

Figure 24. Percentage of Total Chl a in surface towfish samples for 8 classes of phytoplankton as estimated by Phytoclass. Red dashed lines indicate the Sub-tropical Front (STF) and the Sub-Antarctic Front (SAF) where large shifts in speciation were noticed.

in this region as well – likely due to not only a shift in the phytoplankton community from cyanophytes, but also due to colder temperatures leading to a reduction in OCS hydrolysis. Further south within the sub-zero Antarctic Intermediate Water (AAIW), TDS was typically below detection limits in the surface and rarely exceeded 10 pmol L^{-1} in the upper 50 m (Figure 21e and 25a). Interestingly, particulate acid volatile sulfide (pAVS) concentrations were the largest in this region (Figure 25b) – more than 20 times higher than typical open ocean profiles (Cutter & Radford-Knoery, 1991; Chapters 2 and 3). Notably, this ocean region is also where diatoms are the leading influence on Chl a concentrations. Of the 4 oceanic species evaluated in the culture study (Walsh et al., 1994), diatoms produced the smallest amount of total sulfide, but 35% of that was attributed towards pAVS rather than TDS – the largest portion of pAVS for any species. Therefore, it might stand to reason that for the same reason TDS is below detection in the Southern Ocean, elevated pAVS concentrations are primarily due to the shift in phytoplankton speciation. It is worth mentioning that Walsh et al. (1994) measured the sulfide production under both low and high nutrient conditions for *Synechococcus* (cyanophyte), *Emilania huxleyi* (haptophyte), and *Thalassiosira oceanica* (diatom) and under all high nutrient conditions, the ratio of pAVS-to-TDS grew. While the elevated pAVS and reduced TDS concentrations could still be the result of species specific production, others (Narender Reddy & Prasad, 1990) have previously suggested that these elevated pAVS concentrations could be associated with phytochelatins and used to improve the metal-binding capacity in algae or due to precipitation of metal-sulfides within cells under high nutrient conditions (Walsh et al., 1994). Notably, in addition to high nutrients, this region is likely iron limited which might support the role of phytochelatins as a response to metal stress (Kawakami et al., 2006).

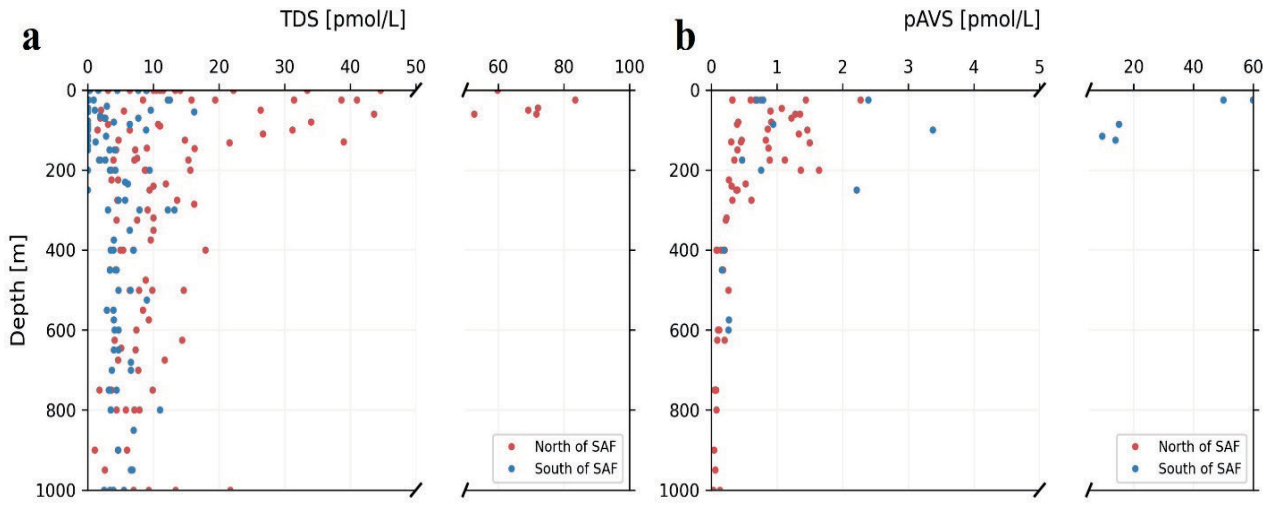

Figure 25. Total dissolved sulfide (TDS; panel a) and particulate acid volatile sulfide (pAVS; panel b) are shown for the top 1000 m along the GP17-OCE transect. Dots in red indicate samples that were collected North of the Sub-Antarctic Front (SAF) which includes Stations 1-14 and 34-38. Dots in blue indicate samples that were collected South of the SAF which includes Stations 16-32.

4.4 Conclusions

Overall, the sulfide concentrations presented here alongside available temperature and pigment data were used to assess the variability in sulfide production across several extreme temperature and nutrient gradients in the South Pacific and Southern Ocean. In the sub-tropics, TDS reached near surface maxima up to 80 pmol L^{-1} (Figure 21e and 25a) in the top 100 m, despite the DCM existing below 100 m, and likely being dominated by *Synechococcus* and prasinophytes (Figure 23a, b). However, *Synechococcus* was also abundant within the upper 100 m and is likely responsible for a large portion of the TDS observed in those surface waters north of the SAF, as results from this study (Chapter 3; Figure 16) and previous work suggested (Walsh et al., 1994). These larger TDS concentrations are presumably also supported by the warmer surface waters yielding increased production via the hydrolysis of OCS and greater biological production by other cyanophytes North of the STF. In the Subantarctic (between STF and SAF), we see a notable shift

in the phytoplankton community away from cyanophytes and towards haptophytes and chlorophytes – which is likely responsible for reduced levels of TDS observed, and the TDS maxima shoaling into the upper 50 m, where those species are most abundant (Figures 22e and 23c, d). However, south of the SB, high silicate concentrations support the abundance of diatoms as the dominant phytoplankton assemblage. We speculate that this is the probable cause of the barely detectable levels of TDS, and potentially the reason for the highly elevated pAVS concentrations. Interestingly, the pAVS concentrations were only elevated between Stations 20 and 25 suggesting that there might be species-specific pAVS production, even though diatoms were the largest predicted contributor to Chl a biomass south of SAF (between Stations 16 and 32). Once north of the SAF, we suspect that the increased haptophyte and chlorophyte abundance (Figures 23c, d and 25) are responsible for the again detectable levels of TDS closer to the Chilean margin (Figure 21e).

We propose that while the colder water temperature is likely contributing to the diminished production of TDS at higher latitudes, the largest influence on TDS (and potentially pAVS) production is due to a shift in phytoplankton community from cyanophytes in the subtropics towards diatoms in the Antarctic. While cyanophytes have demonstrated their ability to produce the most TDS, some species of diatoms, like *Nitzschia sp.*, have produced similar amounts of TDS (Table 2) whereas others species, like *Thalassiosira oceanica*, produced much less TDS (Walsh et al., 1994; Zhang, 1999). It should be noted the exact composition is only an estimate based on the ratio of pigment-to-Chl a, restricting the model to only species that produce Chl a and ignoring the likelihood that other species like *Prochlorococcus* contribute to phytoplankton community biomass, especially in the sub-tropics.

With the limited data currently available, a mass balance could only be attempted for several surface samples along the GP17-OCE transect to assess sulfide production more quantitatively by phytoplankton. In the surface subtropical South Pacific, it is estimated that OCS hydrolysis produces 1.7 pmol L^{-1} hr^{-1} of dissolved sulfide, whereas oxidation removes 1.4 pmol L^{-1} hr^{-1} (Table 12). Loss by particle sinking was not quantified here due to the lack of ^{234}Th data at the time of writing – however, previous removal fluxes in the open ocean were minimal, and did not exceed 0.18 pmol L^{-1} hr^{-1} (Radford-Knoery & Cutter, 1994). Assuming negligible removal through sinking particles, it is calculated that dissolved sulfide production by phytoplankton was not required (Table 12) to close the budget which is comparable to rates calculated from other stations in the subtropical Pacific (Chapter 3). Yet the errors in the budget suggest that estimated rates of TDS production by *Synechococcus* (Walsh et al., 1994; Zhang, 1999; Table 2) alone would sufficient to match the sulfide source needed to close the budget. However, it is expected that the mass balance in the Antarctic will differ, due to the large shift in phytoplankton species and the barely detectable TDS in the surface waters. Despite the elevated OCS concentrations, production by OCS hydrolysis is diminished due to the sub-zero temperatures (0.6 pmol L^{-1} hr^{-1}; Table 13). Furthermore, losses by oxidation to sulfate are also reduced, regardless of the higher oxygen and iodate concentrations encountered in the Southern Ocean, to 0 and 0.02 pmol L^{-1} hr^{-1}, respectively. Assuming that particle export is negligible, there is actually a surplus (0.6 ± 0.2 pmol L^{-1} hr^{-1}) of TDS in the surface where hydrolysis of OCS alone produced enough dissolved sulfide to account for all dissolved losses (0.02 pmol L^{-1} hr^{-1}; Table 13). While the large concentrations of pAVS encountered in the Southern Ocean might suggest sinking particles plays a larger role than assumed and therefore close the gap between sources and sinks, it is plausible that the pAVS present was produced by phytoplankton, rather than via precipitation of dissolved sulfide produced by

phytoplankton or OCS hydrolysis, since diatoms have been shown to produce more pAVS than TDS – especially at high nutrient concentrations (Walsh et al., 1994; Table 2). Taken together, the preliminary results presented here demonstrate the large role that phytoplankton may have in the production and speciation of hydrogen sulfide in surface waters, and consequently the biogeochemical cycle of hydrogen sulfide in the South Pacific and Southern Oceans.

Table 12. Sources and sinks of TDS in the surface subtropical South Pacific Ocean.

	Ranges of species concentration	Surface sulfide fluxes (pmol L^{-1} hr^{-1})
Station		1
Coordinates		20°S, 152°W
Sources:		
Atmospheric Input		0.03
OCS hydrolysis	10 - 26 pmol/L OCS	1.70
	Total Sources:	1.73 ± 0.36
Sinks:		
Sulfide Oxidation	200 µmol/L O_2	0.50
	0.25 µmol/L IO_3^-	0.86
Particle Sinking	pAVS	unknown
	Total Sinks:	1.36 ± 0.23
Budget Balance:		
Phytoplankton production		***-0.37 ± 0.59***

Table 13. Sources and sinks of TDS in surface Antarctic waters.

	Ranges of species concentration	Surface sulfide fluxes (pmol L^{-1} hr^{-1})
Station		25
Coordinates		67°S, 135°W
Sources:		
Atmospheric Input		0.03
OCS hydrolysis	40 - 147 pmol/L OCS	0.60
	Total Sources:	0.63 ± 0.15
Sinks:		
Sulfide Oxidation	315 - 360 µmol/L O_2	0.00
	0.40 - 0.415 µmol/L IO_3^-	0.02
Particle Sinking	pAVS	unknown
	Total Sinks:	0.02 ± 0.02
Budget Balance:		
Phytoplankton production		***-0.61 ± 0.17***

CHAPTER 5

CONCLUSIONS AND FUTURE RESEARCH DIRECTIONS

Previously, our understanding of the biogeochemical cycling of hydrogen sulfide in the open ocean was largely been based on limited profiles obtained in the North Atlantic and Pacific (e.g., Cutter et al., 1999; Cutter & Krahforst, 1988; Radford-Knoery & Cutter, 1994; Zhang, 1999). Although open ocean profiles of hydrogen sulfide are limited, the processes controlling its phase and speciation remain unchanged throughout this study. However, the relative importance of each process is likely to vary substantially throughout the several regimes covered by the more than 15,000 km of the two US GEOTRACES transects: GP15 and GP17-OCE. This study provided further insight as to whether metal-sulfide precipitates could explain the apparent dissolved metal deficits observed in low oxygen regions (Janssen et al., 2014; Janssen & Cullen, 2015; Chapter 2), the rate of sulfide production and removal along with the predicted speciation of dissolved sulfide in the surface waters throughout the North Pacific (Chapter 3), and the variability of sulfide production in the Pacific sector of the Southern Ocean (Chapter 4).

Throughout the North and South Pacific, near surface TDS concentrations were generally less than 50 pmol L^{-1} and decreased with depth in the open ocean. However, elevated concentrations were found on the Alaskan shelf (up to 240 pmol L^{-1}) and within the plume from the Loihi seamount (Chapter 2; reaching nearly 350 pmol L^{-1}). Similar to other studies (Cutter & Radford-Knoery, 1991; Radford-Knoery & Cutter, 1994), pAVS also displayed near surface maxima that rarely exceeded 5 pmol L^{-1} and decreased with depth. Carbonyl sulfide, on the other hand, was less variable than TDS but followed a clear pattern with elevated concentrations at

higher latitudes. In contrast, TDS was generally below detection in the Southern Ocean, whereas pAVS concentrations up to 60 pmol L^{-1} were observed south of the Southern Boundary in the Antarctic. Alone, these sulfide measurements give us some insight into the distribution, but combined with dissolved metal concentrations and coincidental biological data, several conclusions could be made to further our understanding of hydrogen sulfide biogeochemistry and its influence on trace metal cycling.

First of all, in the low oxygen North Pacific, observed concentrations of TDS and pAVS suggest that precipitation of CdS and ZnS are insufficient to explain the apparent nanomolar dissolved cadmium deficits, even when considering removing by sinking particles. Yet, up to 100% of the dissolved Cd and Zn deficits observed in the more intense, low oxygen eastern tropical South Pacific could be supported by sinking metal-sulfide particles. However, the low oxygen concentrations in this particular OMZ appear in the shallow, euphotic zone. Therefore, we proposed that both dissimilatory (by heterotrophs) and assimilatory (by phytoplankton) sulfate reduction producing the sulfide could explain some or all of the dissolved Cd and Zn losses observed in the ETSP OMZ. While these results do not support dissolved metal losses observed by Janssen and co-authors (2014; 2015) in the North Pacific, I suggest that similar to the ETSP, assimilatory sulfate reduction by phytoplankton could explain a portion of the largest dissolved Cd deficits observed in the euphotic zone. The coincidence of these dissolved metal deficits alongside the pAVS and fluorescence maxima suggest that the formation and stability of these metal-sulfide precipitates likely plays a larger role in the removal of dissolved metal in the oxygenated surface waters than in the low oxygen regions where originally proposed. Therefore, I recommend that future studies collect the leachate from pAVS analyses to quantify the metals released during this treatment. This will help determine the stoichiometry of Cd and Zn relative to

pAVS to assess whether sinking CdS and ZnS particles explain the dissolved metal deficits encountered in the oxygenated surface ocean.

While the existence of sulfide in low oxygen environments cannot be disputed (e.g., Bianchi et al., 2018), the input of dissolved sulfide into the oxygenated surface ocean needs to be better constrained (Radford-Knoery & Cutter, 1994; Zhang, 1999). Although one of these inputs is largely due to the species-dependent nature of production by phytoplankton, only limited studies have quantified those rates (Walsh et al., 1994; Zhang, 1999; Table 2). Since sulfide production by OCS hydrolysis and the removal by oxidation are better-constrained (along with the minimal losses through particle sinking), the estimated production by phytoplankton was adequate to balance the budget of TDS in the surface approx. 150 m of the oligotrophic gyre in the North Pacific and the equatorial Pacific (Chapter 3). However, on the Alaskan slope, the rates of production estimated based on the predicted composition of the phytoplankton community could account for between 20-100% of the production necessary to balance the budget, depending on the rate constant utilized when calculating the sulfide losses of oxidation by iodate. Nonetheless, these estimated rates calculated are likely underestimates, since only the production by 4 different classes of phytoplankton were considered, due to limited culture studies (Walsh et al., 1994). Future work would benefit from establishing production rates by several other key phytoplankton species at nutrient concentrations relevant to the coastal subArctic and subtropical regimes in addition to other biological data (e.g., abundance for several classes: diatoms, cyanobacteria, etc.), that would yield a better insight into the composition of the phytoplankton community and their sulfide production.

Throughout the North Pacific, TDS was complexed by metals at all stations. Among the dissolved metal and competing organic ligands incorporated, the chemical equilibrium model

predicts that TDS is primarily composed of aqueous zinc-sulfide, cadmium-sulfide, and lead-sulfide complexes, rather than any metal-bisulfide complexes as might be expected given that bisulfide is the dominant sulfide species at seawater pH. Sulfide in Alaskan slope waters is dominated by CdS and ZnS complexes, with the fraction of PbS increasing further offshore and in the surface waters. Yet, as many studies have suggested previously, this speciation is only one of many possibilities, due to the wide range of published stability constants. The value of the conditional stability constant is the most important factor in predicting the speciation of dissolved sulfide in the surface ocean. For this reason, future studies would profit from more accurate stability constants determined under relevant seawater conditions. Another major consideration in predicting sulfide-metal speciation is the inclusion of competing organic ligands and the purposeful exclusion of interactions between copper and sulfide. Several studies suggest that TDS is predominantly copper-complexed, and while that might be true, the large disagreement in stability constants, and the absence of dissolved copper-sulfide complexes quantified in our current analytical method makes this impossible to constrain. Thus, in addition to more accurate stability constants, improved analytical measurements that include copper and mercury complexes would shed more light on the role that certain metal-sulfide complexes like those of copper have in sulfur cycling.

To investigate variations in sulfide production across large temperature and nutrient gradients in the South Pacific and Southern Ocean, qualitative comparisons were made between predicted phytoplankton assemblages and observed dissolved and particulate sulfide concentrations. Like previous studies, it appears that TDS and pAVS production in the South Pacific and Southern Ocean are primarily controlled by assimilatory sulfate reduction by phytoplankton and partially by the hydrolysis of OCS. In the warm subtropics, the abundance of

cyanophytes support the elevated rates of dissolved sulfide input into surface water through both OCS hydrolysis (Radford-Knoery & Cutter, 1994) and the production by *Synechococcus* (Walsh et al., 1994). In contrast, the frigid, diatom-dominated waters of the Southern Ocean may explain the diminished production by phytoplankton and by OCS hydrolysis, even with elevated OCS concentrations. While some preliminary surface budgets suggest that little (1.2 pmol L^{-1} hr^{-1}) production by phytoplankton is necessary to balance the sulfide budget in the subtropical South Pacific, no production was necessary to close the budget in the Southern Ocean. Although it should be noted that while the rate of TDS production by *Synechococcus* as calculated by Zhang (1999) from Walsh et al. (1994) cultures is nearly identical to that reported in Table 2 (unpublished), the production by diatoms varied greatly. Therefore, there is likely less confidence in phytoplankton production estimates calculated in the diatom dominated Antarctic region. Also, the Phytoclass program appears to yield accurate estimates when compared to images from the flow cytobot, but the program relies on the ratio of pigment-to-Chl a and consequently, overlooks species like *Prochlorococcus* which could contribute to elevated levels of sulfide encountered in the subtropical North and South Pacific. The sulfide production rates by several other algal classes, such as dinoflagellates and prasinophytes, which have not previously been measured, or additional species of diatoms, haptophytes, or cyanophytes such as *Phaeocystis* or *Prochlorococcus*, relevant to these regimes, need to be measured to verify the fluxes estimated in the mass balance and constrain biological sulfide input into surface waters – which should be considered in the future as more data becomes available.

Once the uncertainties associated with phytoplankton production have been addressed, we can quantify the contribution by phytoplankton with more accuracy to help close the gap between the production and removal of TDS in the upper water column. Arguably, the most significant

contribution would be a method that quantifies the unknown, copper and mercury sulfide complexes – possibly having a larger influence on copper cycling than originally believed. Interestingly, a recent study suggests that more than 90% of dissolved copper in the open Pacific ocean is chemically inert and might explain the high dissolved Cu concentrations found in surface waters (Moriyasu, John, et al., 2023). While known TDS concentrations from this study are much lower, an improved method for quantifying TDS might show that dissolved Cu-sulfide complexes dominate the composition of TDS as several studies have suggested previously, and/or regulating the production by phytoplankton to control metal toxicity (Brand et al., 1986; Walsh et al., 1994). Only then will we understand the fate of hydrogen sulfide and the processes that govern its concentration, phase, and chemical speciation throughout the global ocean.

REFERENCES

Al-Farawati, R., & van den Berg, C. M. G. (1999). Metal–sulfide complexation in seawater. *Marine Chemistry*, *63*(3), 331–352. https://doi.org/10.1016/S0304-4203(98)00056-5

Anderson, R. (2020). GEOTRACES: Accelerating Research on the Marine Biogeochemical Cycles of Trace Elements and Their Isotopes. *Annual Review of Marine Science*, *12*(1), 49–85. https://doi.org/10.1146/annurev-marine-010318-095123

Anderson, R., Mawji, E., Cutter, G., Measures, C., & Jeandel, C. (2014). GEOTRACES: Changing the Way We Explore Ocean Chemistry. *Oceanography*, *27*(1), 50–61. https://doi.org/10.5670/oceanog.2014.07

Andreae, M. O. (1990). Ocean-atmosphere interactions in the global biogeochemical sulfur cycle. *Marine Chemistry*, *30*, 1–29. https://doi.org/10.1016/0304-4203(90)90059-L

Andreae, T. W., Cutter, G. A., Hussain, N., Radford-Knoery, J., & Andreae, M. O. (1991). Hydrogen sulfide and radon in and over the western North Atlantic Ocean. *Journal of Geophysical Research: Atmospheres*, *96*, 18753–18760. https://doi.org/10.1029/91JD01628

Baars, O., Abouchami, W., Galer, S. J. G., Boye, M., & Croot, P. L. (2014). Dissolved cadmium in the Southern Ocean: Distribution, speciation, and relation to phosphate. *Limnology and Oceanography*, *59*(2), 385–399. https://doi.org/10.4319/lo.2014.59.2.0385

Bianchi, D., Weber, T. S., Kiko, R., & Deutsch, C. (2018). Global niche of marine anaerobic metabolisms expanded by particle microenvironments. *Nature Geoscience*, *11*(4), Article 4. https://doi.org/10.1038/s41561-018-0081-0

Bidigare, R., Schofield, O., & Prezelin, B. (1989). Influence of zeaxanthin on quantum yield of photosynthesis of Synechococcus clone WH7803 (DC2). *Marine Ecology Progress Series*, *56*, 177–188. https://doi.org/10.3354/meps056177

Bishop, J. K. B., Lam, P. J., & Wood, T. J. (2012). Getting good particles: Accurate sampling of particles by large volume in-situ filtration. *Limnology and Oceanography: Methods*, *10*(9), 681–710. https://doi.org/10.4319/lom.2012.10.681

Black, E. E., Buesseler, K. O., Pike, S. M., & Lam, P. J. (2018). 234Th as a tracer of particulate export and remineralization in the southeastern tropical Pacific. *Marine Chemistry*, *201*, 35–50. https://doi.org/10.1016/j.marchem.2017.06.009

Black, E. E., Lam, P. J., Lee, J.-M., & Buesseler, K. O. (2019). Insights From the 238U-234Th Method Into the Coupling of Biological Export and the Cycling of Cadmium, Cobalt, and Manganese in the Southeast Pacific Ocean. *Global Biogeochemical Cycles*, *33*(1), 15–36. https://doi.org/10.1029/2018GB005985

Boiteau, R. M., Till, C. P., Ruacho, A., Bundy, R. M., Hawco, N. J., McKenna, A. M., Barbeau, K. A., Bruland, K. W., Saito, M. A., & Repeta, D. J. (2016). Structural Characterization of Natural Nickel and Copper Binding Ligands along the US GEOTRACES Eastern Pacific Zonal Transect. *Frontiers in Marine Science*, *3*. https://www.frontiersin.org/articles/10.3389/fmars.2016.00243

Bonnet, S., Guieu, C., Bruyant, F., Prášil, O., Van Wambeke, F., Raimbault, P., Moutin, T., Grob, C., Gorbunov, M. Y., Zehr, J. P., Masquelier, S. M., Garczarek, L., & Claustre, H. (2008). Nutrient limitation of primary productivity in the Southeast Pacific (BIOSOPE cruise). *Biogeosciences*, *5*(1), 215–225. https://doi.org/10.5194/bg-5-215-2008

Boyle, E. A., Sclater, F., & Edmond, J. M. (1976). On the marine geochemistry of cadmium. *Nature*, *263*(5572), 42–44. https://doi.org/10.1038/263042a0

Brand, L. E., Sunda, W. G., & Guillard, R. R. L. (1986). Reduction of marine phytoplankton reproduction rates by copper and cadmium. *Journal of Experimental Marine Biology and Ecology*, *96*(3), 225–250. https://doi.org/10.1016/0022-0981(86)90205-4

Bruland, K. W. (1989). Complexation of zinc by natural organic ligands in the central North Pacific. *Limnology and Oceanography*, *34*(2), 269–285. https://doi.org/10.4319/lo.1989.34.2.0269

Bruland, K. W. (1992). Complexation of cadmium by natural organic ligands in the central North Pacific. *Limnology and Oceanography*, *37*(5), 1008–1017. https://doi.org/10.4319/lo.1992.37.5.1008

Bruland, K. W., Knauer, G. A., & Martin, J. H. (1978). Zinc in north-east Pacific water. *Nature*, *271*(5647), 741–743. https://doi.org/10.1038/271741a0

Bruland, K. W., & Lohan, M. C. (2006). Controls of Trace Metals in Seawater. In *Treatise on Geochemistry* (1st ed., Vol. 6, pp. 23–47). Elsevier.

Buck, K. N., Moffett, J., Barbeau, K. A., Bundy, R. M., Kondo, Y., & Wu, J. (2012). The organic complexation of iron and copper: An intercomparison of competitive ligand exchange-adsorptive cathodic stripping voltammetry (CLE-ACSV) techniques. *Limnology and Oceanography: Methods*, *10*(7), 496–515. https://doi.org/10.4319/lom.2012.10.496

Buesseler, K. O., Bacon, M. P., Kirk Cochran, J., & Livingston, H. D. (1992). Carbon and nitrogen export during the JGOFS North Atlantic Bloom experiment estimated from 234Th: 238U disequilibria. *Deep Sea Research Part A. Oceanographic Research Papers*, *39*(7), 1115–1137. https://doi.org/10.1016/0198-0149(92)90060-7

Buesseler, K. O., Benitez-Nelson, C. R., Moran, S. B., Burd, A., Charette, M., Cochran, J. K., Coppola, L., Fisher, N. S., Fowler, S. W., Gardner, W. D., Guo, L. D., Gustafsson, Ö., Lamborg, C., Masque, P., Miquel, J. C., Passow, U., Santschi, P. H., Savoye, N., Stewart, G., & Trull, T. (2006). An assessment of particulate organic carbon to thorium-234 ratios in the ocean and their impact on the application of 234Th as a POC flux proxy. *Marine Chemistry*, *100*(3), 213–233. https://doi.org/10.1016/j.marchem.2005.10.013

Buesseler, K. O., Benitez-Nelson, C., Rutgers van der Loeff, M., Andrews, J., Ball, L., Crossin, G., & Charette, M. A. (2001). An intercomparison of small- and large-volume techniques for thorium-234 in seawater. *Marine Chemistry*, *74*(1), 15–28. https://doi.org/10.1016/S0304-4203(00)00092-X

Buesseler, K. O., Trull, T. W., Steinberg, D. K., Silver, M. W., Siegel, D. A., Saitoh, S.-I., Lamborg, C. H., Lam, P. J., Karl, D. M., Jiao, N. Z., Honda, M. C., Elskens, M., Dehairs, F., Brown, S. L., Boyd, P. W., Bishop, J. K. B., & Bidigare, R. R. (2008). VERTIGO (VERtical Transport In the Global Ocean): A study of particle sources and flux attenuation in the North Pacific. *Deep Sea Research Part II: Topical Studies in Oceanography*, *55*(14), 1522–1539. https://doi.org/10.1016/j.dsr2.2008.04.024

Callbeck, C. M., Canfield, D. E., Kuypers, M. M. M., Yilmaz, P., Lavik, G., Thamdrup, B., Schubert, C. J., & Bristow, L. A. (2021). Sulfur cycling in oceanic oxygen minimum zones. *Limnology and Oceanography*, *66*(6), 2360–2392. https://doi.org/10.1002/lno.11759

Canfield, D. E., Stewart, F. J., Thamdrup, B., De Brabandere, L., Dalsgaard, T., Delong, E. F., Revsbech, N. P., & Ulloa, O. (2010). A Cryptic Sulfur Cycle in Oxygen-Minimum–Zone

Waters off the Chilean Coast. *Science*, *330*(6009), 1375–1378. https://doi.org/10.1126/science.1196889

Capodaglio, G., Coale, K. H., & Bruland, K. W. (1990). Lead speciation in surface waters of the eastern North Pacific. *Marine Chemistry*, *29*, 221–233. https://doi.org/10.1016/0304-4203(90)90015-5

Carter, B. R., Radich, J. A., Doyle, H. L., & Dickson, A. G. (2013). An automated system for spectrophotometric seawater pH measurements: Automated spectrophotometric pH measurement. *Limnology and Oceanography: Methods*, *11*(1), 16–27. https://doi.org/10.4319/lom.2013.11.16

Chavez, F. P., Bertrand, A., Guevara-Carrasco, R., Soler, P., & Csirke, J. (2008). The northern Humboldt Current System: Brief history, present status and a view towards the future. *Progress in Oceanography*, *79*(2), 95–105. https://doi.org/10.1016/j.pocean.2008.10.012

Chmiel, R., Lanning, N., Laubach, A., Lee, J.-M., Fitzsimmons, J., Hatta, M., Jenkins, W., Lam, P., McIlvin, M., Tagliabue, A., & Saito, M. (2022). Major processes of the dissolved cobalt cycle in the North and equatorial Pacific Ocean. *Biogeosciences*, *19*(9), 2365–2395. https://doi.org/10.5194/bg-19-2365-2022

Clayton, T. D., & Byrne, R. H. (1993). Spectrophotometric seawater pH measurements: Total hydrogen ion concentration scale calibration of m-cresol purple and at-sea results. *Deep Sea Research Part I: Oceanographic Research Papers*, *40*(10), 2115–2129. https://doi.org/10.1016/0967-0637(93)90048-8

Clevenger, S. J., Benitez-Nelson, C. R., Drysdale, J., Pike, S., Puigcorbé, V., & Buesseler, K. O. (2021). Review of the analysis of 234Th in small volume (2–4 L) seawater samples:

Improvements and recommendations. *Journal of Radioanalytical and Nuclear Chemistry*, *329*(1), 1–13. https://doi.org/10.1007/s10967-021-07772-2

Coale, K. H., & Bruland, K. W. (1985). 234Th:238U disequilibria within the California Current. *Limnology and Oceanography*, *30*(1), 22–33. https://doi.org/10.4319/lo.1985.30.1.0022

Coale, K. H., & Bruland, K. W. (1990). Spatial and temporal variability in copper complexation in the North Pacific. *Deep Sea Research Part A. Oceanographic Research Papers*, *37*(2), 317–336. https://doi.org/10.1016/0198-0149(90)90130-N

Conway, T. M., & John, S. G. (2014). The biogeochemical cycling of zinc and zinc isotopes in the North Atlantic Ocean. *Global Biogeochemical Cycles*, *28*(10), 1111–1128. https://doi.org/10.1002/2014GB004862

Conway, T. M., & John, S. G. (2015a). Biogeochemical cycling of cadmium isotopes along a high-resolution section through the North Atlantic Ocean. *Geochimica et Cosmochimica Acta*, *148*, 269–283. https://doi.org/10.1016/j.gca.2014.09.032

Conway, T. M., & John, S. G. (2015b). The cycling of iron, zinc and cadmium in the North East Pacific Ocean – Insights from stable isotopes. *Geochimica et Cosmochimica Acta*, *164*, 262–283. https://doi.org/10.1016/j.gca.2015.05.023

Conway, T. M., Rosenberg, A. D., Adkins, J. F., & John, S. G. (2013). A new method for precise determination of iron, zinc and cadmium stable isotope ratios in seawater by double-spike mass spectrometry. *Analytica Chimica Acta*, *793*, 44–52. https://doi.org/10.1016/j.aca.2013.07.025

Craig, H. (1969). Abyssal carbon and radiocarbon in the Pacific. *Journal of Geophysical Research (1896-1977)*, *74*(23), 5491–5506. https://doi.org/10.1029/JC074i023p05491

Cutter, G. A. (1991). Dissolved arsenic and antimony in the Black Sea. *Deep Sea Research Part A. Oceanographic Research Papers*, *38*, S825–S843. https://doi.org/10.1016/S0198-0149(10)80011-1

Cutter, G. A., & Bruland, K. W. (2012). Rapid and noncontaminating sampling system for trace elements in global ocean surveys. *Limnology and Oceanography: Methods*, *10*(6), 425–436. https://doi.org/10.4319/lom.2012.10.425

Cutter, G. A., Casciotti, K., Croot, P., Geibert, W., Heimbürger, L.-E., Lohan, M., Planquette, H., & van de Flierdt, T. (2017). *Sampling and Sample-handling Protocols for GEOTRACES Cruises. Version 3, August 2017.* [Report]. GEOTRACES International Project Office. https://repository.oceanbestpractices.org/handle/11329/409

Cutter, G. A., Casciotti, K., & Lam, P. J. (2018). *US GEOTRACES Pacific Meridional Transect—GP15 Cruise Report*. https://datadocs.bco-dmo.org/docs/geotraces/GEOTRACES_PMT/casciotti/data_docs/GP15_Cruise_Report_with_ODF_Report.pdf

Cutter, G. A., & Kluckhohn, R. S. (1999). The cycling of particulate carbon, nitrogen, sulfur, and sulfur species (iron monosulfide, greigite, pyrite, and organic sulfur) in the water columns of Framvaren Fjord and the Black Sea. *Marine Chemistry*, *67*(3), 149–160. https://doi.org/10.1016/S0304-4203(99)00056-0

Cutter, G. A., & Krahforst, C. F. (1988). Sulfide in surface waters of the western Atlantic Ocean. *Geophysical Research Letters*, *15*, 1393–1396. https://doi.org/10.1029/GL015i012p01393

Cutter, G. A., Moffett, J., Nielsdóttir, M. C., & Sanial, V. (2018). Multiple oxidation state trace elements in suboxic waters off Peru: In situ redox processes and advective/diffusive

horizontal transport. *Marine Chemistry*, *201*, 77–89. https://doi.org/10.1016/j.marchem.2018.01.003

Cutter, G. A., & Radford-Knoery, J. (1991). Determination of Carbon, Nitrogen, Sulfur, and Inorganic Sulfur Species in Marine Particles. In *Marine Particles: Analysis and Characterization* (pp. 57–63). American Geophysical Union (AGU). https://doi.org/10.1029/GM063p0057

Cutter, G. A., S. Walsh, R., & Silva de Echols, C. (1999). Production and speciation of hydrogen sulfide in surface waters of the high latitude North Atlantic Ocean. *Deep Sea Research Part II: Topical Studies in Oceanography*, *46*(5), 991–1010. https://doi.org/10.1016/S0967-0645(99)00013-2

Daskalakis, K. D., & Helz, G. R. (1993). The solubility of sphalerite (ZnS) in sulfidic solutions at 25°C and 1 atm pressure. *Geochimica et Cosmochimica Acta*, *57*(20), 4923–4931. https://doi.org/10.1016/0016-7037(93)90129-K

de Souza, G. F., Vance, D., Sieber, M., Conway, T. M., & Little, S. H. (2022). Re-assessing the influence of particle-hosted sulphide precipitation on the marine cadmium cycle. *Geochimica et Cosmochimica Acta*, *322*, 274–296. https://doi.org/10.1016/j.gca.2022.02.009

DiTullio, G. R., Geesey, M. E., Jones, D. R., Daly, K. L., Campbell, L., & Smith, W. O. (2003). Phytoplankton assemblage structure and primary productivity along 170° W in the South Pacific Ocean. *Marine Ecology Progress Series*, *255*, 55–80.

Dyrssen, D. (1985). Metal complex formation in sulphidic seawater. *Marine Chemistry*, *15*(4), 285–293. https://doi.org/10.1016/0304-4203(85)90039-8

Dyrssen, D. (1988a). Sulfide complexation in surface seawater. *Marine Chemistry*, *24*(2), 143–153. https://doi.org/10.1016/0304-4203(88)90045-X

Dyrssen, D. (1988b). The state of dissolved copper in sulfidic seawater. *Marine Chemistry*, *23*(3), 457–459. https://doi.org/10.1016/0304-4203(88)90111-9

Dyrssen, D., & Wedborg, M. (1989). The state of dissolved trace sulphide in seawater. *Marine Chemistry*, *26*(3), 289–293. https://doi.org/10.1016/0304-4203(89)90009-1

Elliott, S. (1988). Linear free energy techniques for estimation of metal sulfide complexation constants. *Marine Chemistry*, *24*(3–4), 203–213. https://doi.org/10.1016/0304-4203(88)90032-1

Elliott, S., Lu, E., & Rowland, F. S. (1987). Carbonyl sulfide hydrolysis as a source of hydrogen sulfide in open ocean seawater. *Geophysical Research Letters*, *14*(2), 131–134. https://doi.org/10.1029/GL014i002p00131

Elliott, S., Lu, E., & Rowland, F. S. (1989). Rates and mechanisms for the hydrolysis of carbonyl sulfide in natural waters. *Environmental Science & Technology*, *23*(4), 458–461. https://doi.org/10.1021/es00181a011

Elliott, S., & Rowland, F. S. (1990). The effect of metal complexation on hydrogen sulfide transport across the sea-air interface. *Journal of Atmospheric Chemistry*, *10*(3), 315–327. https://doi.org/10.1007/BF00053866

Ellwood, M. J., & van den Berg, C. M. G. (2001). Determination of organic complexation of cobalt in seawater by cathodic stripping voltammetry. *Marine Chemistry*, *75*(1), 33–47. https://doi.org/10.1016/S0304-4203(01)00024-X

Ferek, R. J., & Andreae, M. O. (1984). Photochemical production of carbonyl sulphide in marine surface waters. *Nature*, *307*(5947), 148–150. https://doi.org/10.1038/307148a0

Goates, J. R., Gordon, M. B., & Faux, N. (1952). Calculated Values for the Solubility Product Constants of the Metallic Sulfides. *Journal of the American Chemical Society*, *74*(3), 835–836.

Goericke, R., Olson, R. J., & Shalapyonok, A. (2000). A novel niche for Prochlorococcus sp. In low-light suboxic environments in the Arabian Sea and the Eastern Tropical North Pacific. *Deep Sea Research Part I: Oceanographic Research Papers*, *47*(7), 1183–1205. https://doi.org/10.1016/S0967-0637(99)00108-9

Guinoiseau, D., Galer, S. J. G., & Abouchami, W. (2018). Effect of cadmium sulphide precipitation on the partitioning of Cd isotopes: Implications for the oceanic Cd cycle. *Earth and Planetary Science Letters*, *498*, 300–308. https://doi.org/10.1016/j.epsl.2018.06.039

Guinoiseau, D., Galer, S. J. G., Abouchami, W., Frank, M., Achterberg, E. P., & Haug, G. H. (2019). Importance of Cadmium Sulfides for Biogeochemical Cycling of Cd and Its Isotopes in Oxygen Deficient Zones—A Case Study of the Angola Basin. *Global Biogeochemical Cycles*, *33*(12), 1746–1763. https://doi.org/10.1029/2019GB006323

Hayes, C. T., Black, E. E., Anderson, R. F., Baskaran, M., Buesseler, K. O., Charette, M. A., Cheng, H., Cochran, J. K., Edwards, R. L., Fitzgerald, P., Lam, P. J., Lu, Y., Morris, S. O., Ohnemus, D. C., Pavia, F. J., Stewart, G., & Tang, Y. (2018). Flux of Particulate Elements in the North Atlantic Ocean Constrained by Multiple Radionuclides. *Global Biogeochemical Cycles*, *32*(12), 1738–1758. https://doi.org/10.1029/2018GB005994

Hayward, A., Pinkerton, M. H., & Gutierrez-Rodriguez, A. (2023). phytoclass: A pigment-based chemotaxonomic method to determine the biomass of phytoplankton classes. *Limnology and Oceanography: Methods*, *21*(4), 220–241. https://doi.org/10.1002/lom3.10541

Janssen, D. J., Abouchami, W., Galer, S. J. G., Purdon, K. B., & Cullen, J. T. (2019). Particulate cadmium stable isotopes in the subarctic northeast Pacific reveal dynamic Cd cycling and a new isotopically light Cd sink. *Earth and Planetary Science Letters*, *515*, 67–78. https://doi.org/10.1016/j.epsl.2019.03.006

Janssen, D. J., Conway, T. M., John, S. G., Christian, J. R., Kramer, D. I., Pedersen, T. F., & Cullen, J. T. (2014). Undocumented water column sink for cadmium in open ocean oxygen-deficient zones. *Proceedings of the National Academy of Sciences*, *111*(19), 6888–6893. https://doi.org/10.1073/pnas.1402388111

Janssen, D. J., & Cullen, J. T. (2015). Decoupling of zinc and silicic acid in the subarctic northeast Pacific interior. *Marine Chemistry*, *177*, 124–133. https://doi.org/10.1016/j.marchem.2015.03.014

Jensen, L. T., Wyatt, N. J., Landing, W. M., & Fitzsimmons, J. N. (2020). Assessment of the stability, sorption, and exchangeability of marine dissolved and colloidal metals. *Marine Chemistry*, *220*, 103754. https://doi.org/10.1016/j.marchem.2020.103754

Jia-Zhong, Z., & Whitfield, M. (1986). Kinetics of inorganic redox reactions in seawater: I. The reduction of iodate by bisulphide. *Marine Chemistry*, *19*(2), 121–137. https://doi.org/10.1016/0304-4203(86)90044-7

John, S. G., Helgoe, J., & Townsend, E. (2018). Biogeochemical cycling of Zn and Cd and their stable isotopes in the Eastern Tropical South Pacific. *Marine Chemistry*, *201*, 256–262. https://doi.org/10.1016/j.marchem.2017.06.001

Kadko, D. (2017). Upwelling and primary production during the U.S. GEOTRACES East Pacific Zonal Transect. *Global Biogeochemical Cycles*, *31*(2), 218–232. https://doi.org/10.1002/2016GB005554

Kawakami, S. K., Gledhill, M., & Achterberg, E. P. (2006). Production of Phytochelatins and Glutathione by Marine Phytoplankton in Response to Metal Stress1. *Journal of Phycology*, *42*(5), 975–989. https://doi.org/10.1111/j.1529-8817.2006.00265.x

Kuwabara, J. S., & Luther, G. W. (1993). Dissolved sulfides in the oxic water column of San Francisco Bay, California | SpringerLink. *Estuaries*, *16*, 567–573.

Lam, P. J., Lee, J.-M., Heller, M. I., Mehic, S., Xiang, Y., & Bates, N. R. (2018). Size-fractionated distributions of suspended particle concentration and major phase composition from the U.S. GEOTRACES Eastern Pacific Zonal Transect (GP16). *Marine Chemistry*, *201*, 90–107. https://doi.org/10.1016/j.marchem.2017.08.013

Lavin, P., González, B., Santibáñez, J. F., Scanlan, D. J., & Ulloa, O. (2010). Novel lineages of Prochlorococcus thrive within the oxygen minimum zone of the eastern tropical South Pacific. *Environmental Microbiology Reports*, *2*(6), 728–738. https://doi.org/10.1111/j.1758-2229.2010.00167.x

Lee, J.-M., Heller, M. I., & Lam, P. J. (2018). Size distribution of particulate trace elements in the U.S. GEOTRACES Eastern Pacific Zonal Transect (GP16). *Marine Chemistry*, *201*, 108–123. https://doi.org/10.1016/j.marchem.2017.09.006

Lennartz, S. T., Marandino, C. A., von Hobe, M., Andreae, M. O., Aranami, K., Atlas, E., Berkelhammer, M., Bingemer, H., Booge, D., Cutter, G., Cortes, P., Kremser, S., Law, C. S., Marriner, A., Simó, R., Quack, B., Uher, G., Xie, H., & Xu, X. (2020). Marine carbonyl sulfide (OCS) and carbon disulfide (CS_2): A compilation of measurements in seawater and the marine boundary layer. *Earth System Science Data*, *12*(1), 591–609. https://doi.org/10.5194/essd-12-591-2020

Liu, T., Krisch, S., Xie, R. C., Hopwood, M. J., Dengler, M., & Achterberg, E. P. (2022). Sediment Release in the Benguela Upwelling System Dominates Trace Metal Input to the Shelf and Eastern South Atlantic Ocean. *Global Biogeochemical Cycles*, *36*(9), e2022GB007466. https://doi.org/10.1029/2022GB007466

Luther, G. W., Church, T. M., & Powell, D. (1991). Sulfur speciation and sulfide oxidation in the water column of the Black Sea. *Deep Sea Research Part A. Oceanographic Research Papers*, *38*, S1121–S1137. https://doi.org/10.1016/S0198-0149(10)80027-5

Luther, G. W., Rickard, D. T., Theberge, S., & Olroyd, A. (1996). Determination of Metal (Bi)Sulfide Stability Constants of Mn2+, Fe2+, Co2+, Ni2+, Cu2+, and Zn2+ by Voltammetric Methods. *Environmental Science & Technology*, *30*(2), 671–679. https://doi.org/10.1021/es950417i

Luther, G. W., Theberge, S. M., & Rickard, D. T. (1999). Evidence for aqueous clusters as intermediates during zinc sulfide formation. *Geochimica et Cosmochimica Acta*, *63*(19–20), 3159–3169. https://doi.org/10.1016/S0016-7037(99)00243-4

Luther, G. W., & Tsamakis, E. (1989). Concentration and form of dissolved sulfide in the oxic water column of the ocean. *Marine Chemistry*, *27*(3), 165–177. https://doi.org/10.1016/0304-4203(89)90046-7

Mackey, M., Mackey, D., Higgins, H., & Wright, S. (1996). CHEMTAX - a program for estimating class abundances from chemical markers:application to HPLC measurements of phytoplankton. *Marine Ecology Progress Series*, *144*, 265–283. https://doi.org/10.3354/meps144265

Mantoura, R. F. C., & Llewellyn, C. A. (1983). The rapid determination of algal chlorophyll and carotenoid pigments and their breakdown products in natural waters by reverse-phase

high-performance liquid chromatography. *Analytica Chimica Acta*, *151*, 297–314. https://doi.org/10.1016/S0003-2670(00)80092-6

Martin, J. H., Knauer, G. A., Karl, D. M., & Broenkow, W. W. (1987). VERTEX: Carbon cycling in the northeast Pacific. *Deep Sea Research Part A. Oceanographic Research Papers*, *34*(2), 267–285. https://doi.org/10.1016/0198-0149(87)90086-0

Middag, R., Baar, H. J. W., & Bruland, K. W. (2019). The Relationships Between Dissolved Zinc and Major Nutrients Phosphate and Silicate Along the GEOTRACES GA02 Transect in the West Atlantic Ocean. *Global Biogeochemical Cycles*, *33*(1), 63–84. https://doi.org/10.1029/2018GB006034

Middag, R., van Heuven, S. M. A. C., Bruland, K. W., & de Baar, H. J. W. (2018). The relationship between cadmium and phosphate in the Atlantic Ocean unravelled. *Earth and Planetary Science Letters*, *492*, 79–88. https://doi.org/10.1016/j.epsl.2018.03.046

Millero, F. J. (1986). The thermodynamics and kinetics of the hydrogen sulfide system in natural waters. *Marine Chemistry*, *18*(2–4), 121–147. https://doi.org/10.1016/0304-4203(86)90003-4

Millero, F. J. (1996). *Chemical Oceanography* (Second). CRC Press.

Millero, F. J., Hubinger, Scott., Fernandez, Marino., & Garnett, Stephen. (1987). Oxidation of H2S in seawater as a function of temperature, pH, and ionic strength. *Environmental Science & Technology*, *21*(5), 439–443. https://doi.org/10.1021/es00159a003

Millero, F. J., LeFerriere, A., Fernandez, M., Hubinger, S., & Hershey, J. P. (1989). Oxidation of hydrogen sulfide with hydrogen peroxide in natural waters. *Environmental Science & Technology*, *23*(2), 209–213. https://doi.org/10.1021/es00179a012

Moore, L. E., Heller, M. I., Barbeau, K. A., Moffett, J. W., & Bundy, R. M. (2021). Organic complexation of iron by strong ligands and siderophores in the eastern tropical North Pacific oxygen deficient zone. *Marine Chemistry*, *236*, 104021. https://doi.org/10.1016/j.marchem.2021.104021

Morel, F. M. M., Milligan, A. J., & Saito, M. A. (2003). Marine Bioinorganic Chemistry: The Role of Trace Metals in the Oceanic Cycles of Major Nutrients. In *Treatise on Geochemistry* (1st ed., Vol. 6, pp. 113–143). Elsevier.

Morel, F. M. M., & Price, N. M. (2003). The Biogeochemical Cycles of Trace Metals in the Oceans. *Science*, *300*(5621), 944–947.

Moriyasu, R., Bolster, K. M., Hardisty, D. S., Kadko, D. C., Stephens, M. P., & Moffett, J. W. (2023). Meridional Survey of the Central Pacific Reveals Iodide Accumulation in Equatorial Surface Waters and Benthic Sources in the Abyssal Plain. *Global Biogeochemical Cycles*, *37*(3), e2021GB007300. https://doi.org/10.1029/2021GB007300

Morse, J. W., & Luther, G. W. (1999). Chemical influences on trace metal-sulfide interactions in anoxic sediments. *Geochimica et Cosmochimica Acta*, *63*(19), 3373–3378. https://doi.org/10.1016/S0016-7037(99)00258-6

Narender Reddy, G., & Prasad, M. N. V. (1990). Heavy metal-binding proteins/peptides: Occurrence, structure, synthesis and functions. A review. *Environmental and Experimental Botany*, *30*(3), 251–264. https://doi.org/10.1016/0098-8472(90)90037-5

Ohnemus, D. C., Rauschenberg, S., Cutter, G. A., Fitzsimmons, J. N., Sherrell, R. M., & Twining, B. S. (2016). Elevated trace metal content of prokaryotic communities associated with marine oxygen deficient zones. *Limnology and Oceanography*, *62*(1), 3–25. https://doi.org/10.1002/lno.10363

Orsi, A. H., Whitworth, T., & Nowlin, W. D. (1995). On the meridional extent and fronts of the Antarctic Circumpolar Current. *Deep Sea Research Part I: Oceanographic Research Papers*, *42*(5), 641–673. https://doi.org/10.1016/0967-0637(95)00021-W

Owens, S. A., Buesseler, K. O., & Sims, K. W. W. (2011). Re-evaluating the 238U-salinity relationship in seawater: Implications for the 238U–234Th disequilibrium method. *Marine Chemistry*, *127*(1), 31–39. https://doi.org/10.1016/j.marchem.2011.07.005

Pearson, R. G. (1963). Hard and Soft Acids and Bases. *Journal of the American Chemical Society*, *85*(22), 3533–3539. https://doi.org/10.1021/ja00905a001

Plass, A., Schlosser, C., Sommer, S., Dale, A. W., Achterberg, E. P., & Scholz, F. (2020). The control of hydrogen sulfide on benthic iron and cadmium fluxes in the oxygen minimum zone off Peru. *Biogeosciences*, *17*(13), 3685–3704. https://doi.org/10.5194/bg-17-3685-2020

Pos, W. H., Milne, P. J., Riemer, D. D., & Zika, R. G. (1997). Photoinduced oxidation of H2S species: A sink for sulfide in seawater. *Journal of Geophysical Research: Atmospheres*, *102*(D11), 12831–12837. https://doi.org/10.1029/96JD03817

Radford-Knoery, J. (1993). *THE BIOGEOCHEMISTRY OF HYDROGEN SULFIDE IN THE OPEN OCEAN*. Old Dominion University.

Radford-Knoery, J., & Cutter, G. A. (1993). Determination of carbonyl sulfide and hydrogen sulfide species in natural waters using specialized collection procedures and gas chromatography with flame photometric detection. *Analytical Chemistry*, *65*(8), 976–982. https://doi.org/10.1021/ac00056a005

Radford-Knoery, J., & Cutter, G. A. (1994). Biogeochemistry of dissolved hydrogen sulfide species and carbonyl sulfide in the western North Atlantic Ocean. *Geochimica et Cosmochimica Acta*, *58*(24), 5421–5431. https://doi.org/10.1016/0016-7037(94)90239-9

Rennenberg, H. (1984). The Fate of Excess Sulfur in Higher Plants. *Annual Review of Plant Biology*, *35*, 121–153. https://doi.org/10.1146/annurev.pp.35.060184.001005

Rennenberg, H. (1989). Synthesis and emission of hydrogen sulfide by higher plants. In *Biogenic Sulfur in the Environment* (pp. 44–57). ACS.

Rennenberg, H. (1991). The Significance of Higher Plants in the Emission of Sulfur Compounds from Terrestrial Ecosystems. In T. D. Sharkey, E. A. Holland, & H. A. Mooney (Eds.), *Trace Gas Emissions by Plants* (pp. 217–260). Academic Press. https://doi.org/10.1016/B978-0-12-639010-0.50015-7

Rickard, D., & Luther, G. W., III. (2006). Metal Sulfide Complexes and Clusters. *Reviews in Mineralogy and Geochemistry*, *61*(1), 421–504. https://doi.org/10.2138/rmg.2006.61.8

Roshan, S., & DeVries, T. (2021). Global Contrasts Between Oceanic Cycling of Cadmium and Phosphate. *Global Biogeochemical Cycles*, *35*(6). https://agupubs.onlinelibrary.wiley.com/doi/10.1029/2021GB006952

Rozan, T. F., Luther, G. W., Ridge, D., & Robinson, S. (2003). Determination of Pb Complexation in Oxic and Sulfidic Waters Using Pseudovoltammetry. *Environmental Science & Technology*, *37*(17), 3845–3852. https://doi.org/10.1021/es034014r

Rue, E. L., & Bruland, K. W. (1995). Complexation of iron(III) by natural organic ligands in the Central North Pacific as determined by a new competitive ligand equilibration/adsorptive cathodic stripping voltammetric method. *Marine Chemistry*, *50*(1), 117–138. https://doi.org/10.1016/0304-4203(95)00031-L

Schlosser, C., Streu, P., Frank, M., Lavik, G., Croot, P. L., Dengler, M., & Achterberg, E. P. (2018). H2S events in the Peruvian oxygen minimum zone facilitate enhanced dissolved Fe concentrations. *Scientific Reports*, *8*(1), Article 1. https://doi.org/10.1038/s41598-018-30580-w

Schmitt, A.-D., Galer, S. J. G., & Abouchami, W. (2009). Mass-dependent cadmium isotopic variations in nature with emphasis on the marine environment. *Earth and Planetary Science Letters*, *277*(1), 262–272. https://doi.org/10.1016/j.epsl.2008.10.025

Sieber, M., Conway, T. M., de Souza, G. F., Obata, H., Takano, S., Sohrin, Y., & Vance, D. (2019). Physical and biogeochemical controls on the distribution of dissolved cadmium and its isotopes in the Southwest Pacific Ocean. *Chemical Geology*, *511*, 494–509. https://doi.org/10.1016/j.chemgeo.2018.07.021

Sieber, M., Lanning, N. T., Bian, X., Yang, S.-C., Takano, S., Sohrin, Y., Weber, T. S., Fitzsimmons, J. N., John, S. G., & Conway, T. M. (2023). The Importance of Reversible Scavenging for the Marine Zn Cycle Evidenced by the Distribution of Zinc and Its Isotopes in the Pacific Ocean. *Journal of Geophysical Research: Oceans*, *128*(4), e2022JC019419. https://doi.org/10.1029/2022JC019419

Sieber, M., Lanning, N. T., Bunnell, Z. B., Bian, X., Yang, S.-C., Marsay, C. M., Landing, W. M., Buck, C. S., Fitzsimmons, J. N., John, S. G., & Conway, T. M. (2023). Biological, Physical, and Atmospheric Controls on the Distribution of Cadmium and Its Isotopes in the Pacific Ocean. *Global Biogeochemical Cycles*, *37*(2), e2022GB007441. https://doi.org/10.1029/2022GB007441

Ste-Marie, J., Torma, A. E., & Gübeli, A. O. (1964). THE STABILITY OF THIOCOMPLEXES AND SOLUBILITY PRODUCTS OF METAL SULPHIDES: I. CADMIUM

SULPHIDE. *Canadian Journal of Chemistry*, *42*(3), 662–668. https://doi.org/10.1139/v64-097

Ştreangă, I.-M., Repeta, D. J., Blusztajn, J. S., & Horner, T. J. (2024). Speciation and cycling of iodine in the subtropical North Pacific Ocean. *Frontiers in Marine Science*, *10*. https://www.frontiersin.org/articles/10.3389/fmars.2023.1272968

Stumm, W., & Morgan, J. J. (1981). *Aquatic Chemistry: An Introduction Emphasizing Chemical Equilibria in Natural Waters*. Wiley.

Theberge, S. M., Luther, G. W., & Farrenkopf, A. M. (1997). On the existence of free and metal complexed sulfide in the Arabian Sea and its oxygen minimum zone. *Deep Sea Research Part II: Topical Studies in Oceanography*, *44*(6), 1381–1390. https://doi.org/10.1016/S0967-0645(97)00012-X

Tsang, J. J., Rozan, T. F., Hsu-Kim, H., Mullaugh, K. M., & Luther, G. W. (2006). Pseudopolarographic Determination of Cd^{2+} Complexation in Freshwater. *Environmental Science & Technology*, *40*(17), 5388–5394. https://doi.org/10.1021/es0525509

Ulloa, O., Henríquez-Castillo, C., Ramírez-Flandes, S., Plominsky, A. M., Murillo, A. A., Morgan-Lang, C., Hallam, S. J., & Stepanauskas, R. (2021). The cyanobacterium Prochlorococcus has divergent light-harvesting antennae and may have evolved in a low-oxygen ocean. *Proceedings of the National Academy of Sciences*, *118*(11), e2025638118. https://doi.org/10.1073/pnas.2025638118

Van Den Berg, C. M. G., & Nimmo, M. (1987). Determination of interactions of nickel with dissolved organic material in seawater using cathodic stripping voltammetry. *Science of The Total Environment*, *60*, 185–195. https://doi.org/10.1016/0048-9697(87)90415-3

Vance, D., de Souza, G. F., Zhao, Y., Cullen, J. T., & Lohan, M. C. (2019). The relationship between zinc, its isotopes, and the major nutrients in the North-East Pacific. *Earth and Planetary Science Letters*, *525*, 115748. https://doi.org/10.1016/j.epsl.2019.115748

Vance, D., Little, S. H., de Souza, G. F., Khatiwala, S., Lohan, M. C., & Middag, R. (2017). Silicon and zinc biogeochemical cycles coupled through the Southern Ocean. *Nature Geoscience*, *10*(3), 202–206. https://doi.org/10.1038/ngeo2890

Vazquez, F. G., Zhang, J., & Millero, F. J. (1989). Effect of metals on the rate of the oxidation of H2S in seawater. *Geophysical Research Letters*, *16*(12), 1363–1366. https://doi.org/10.1029/GL016i012p01363

Walsh, R. S., Cutter, G. A., Dunstan, W. M., Radford-Knoery, J., & Elder, J. T. (1994). The biogeochemistry of hydrogen sulfide: Phytoplankton production in the surface ocean. *Limnology and Oceanography*, *39*(4), 941–948. https://doi.org/10.4319/lo.1994.39.4.0941

Wang, F., & Tessier, A. (1999). Cadmium Complexation with Bisulfide. *Environmental Science & Technology*, *33*(23), 4270–4277. https://doi.org/10.1021/es990283z

Weber, T., John, S., Tagliabue, A., & DeVries, T. (2018). Biological uptake and reversible scavenging of zinc in the global ocean. *Science*, *361*, 72–76.

Xie, R. C., Galer, S. J. G., Abouchami, W., & Frank, M. (2019). Limited impact of eolian and riverine sources on the biogeochemical cycling of Cd in the tropical Atlantic. *Chemical Geology*, *511*, 371–379.

Xie, R. C., Le Moigne, F. A. C., Rapp, I., Lüdke, J., Gasser, B., Dengler, M., Liebetrau, V., & Achterberg, E. P. (2020). Effects of ^{238}U variability and physical transport on water

column ^{234}Th downward fluxes in the coastal upwelling system off Peru. *Biogeosciences*, *17*(19), 4919–4936. https://doi.org/10.5194/bg-17-4919-2020

Xie, R. C., Rehkämper, M., Grasse, P., van de Flierdt, T., Frank, M., & Xue, Z. (2019). Isotopic evidence for complex biogeochemical cycling of Cd in the eastern tropical South Pacific. *Earth and Planetary Science Letters*, *512*, 134–146. https://doi.org/10.1016/j.epsl.2019.02.001

Yang, J., Li, Y., Liu, S., Tian, H., Chen, C., Liu, J., & Shi, Y. (2015). Theoretical calculations of Cd isotope fractionation in hydrothermal fluids. *Chemical Geology*, *391*, 74–82. https://doi.org/10.1016/j.chemgeo.2014.10.029

Yuan, J., & Shiller, A. M. (2004). Hydrogen peroxide in deep waters of the North Pacific Ocean. *Geophysical Research Letters*, *31*(1). https://doi.org/10.1029/2003GL018439

Zhang, J.-Z., & Millero, F. J. (1994). Investigation of metal sulfide complexes in sea water using cathodic stripping square wave voltammetry. *Analytica Chimica Acta*, *284*(3), 497–504. https://doi.org/10.1016/0003-2670(94)85056-9

Zhang, J.-Z., & Whitfield, M. (1986). Kinetics of inorganic redox reactions in seawater: I. The reduction of iodate by bisulphide. *Marine Chemistry*, *19*(2), 121–137. https://doi.org/10.1016/0304-4203(86)90044-7

Zhang, L. (1999). *THE EFFECTS OF METAL COMPLEXATION ON THE OXIDATION OF HYDROGEN SULFIDE IN SULFIDE BY IODATE IN SEAWATER.* Old Dominion University.

APPENDIX A

DISSOLVED SULFIDE AND CARBONYL SULFIDE CONCENTRATIONS FROM THE GP15 CRUISE

Station #	Lat. [+N, -S]	Long. [+E, -W]	Sample #	Depth [m]	TDS [pmol/L]	SD [pmol/L]	OCS [pmol/L]	SD [pmol/L]
1	56.1	-157.0	12430	0	145.0	21.0	53.5	1.8
1	56.1	-157.0	12442	20	144.3	nd	64.4	nd
1	56.1	-157.0	12440	30	90.8	nd	57.2	nd
1	56.1	-157.0	12438	40	134.7	nd	68.4	nd
1	56.1	-157.0	12436	50	150.4	nd	60.5	nd
1	56.1	-157.0	12434	70	123.0	nd	49.7	nd
1	56.1	-157.0	12432	85	152.9	nd	105.8	nd
2	55.7	-156.0	12455	0	198.9	88.3	47.8	7.1
2	55.6	-156.0	12470	45	179.5	nd	36.1	nd
2	55.6	-156.0	12468	66	138.8	nd	49.6	nd
2	55.6	-156.0	12466	101	169.8	nd	43.0	nd
2	55.6	-156.0	12464	151	187.0	nd	51.4	nd
2	55.6	-156.0	12462	191	220.1	nd	33.1	nd
2	55.6	-156.0	12460	225	234.5	nd	49.7	nd
2	55.6	-156.0	12458	250	235.7	nd	47.4	nd
3	55.1	-155.7	12556	0	138.6	nd	55.1	nd
3	55.1	-155.7	12509	35	119.6	5.3	63.4	4.8
3	55.1	-155.7	12507	62	66.7	nd	36.5	nd
3	55.1	-155.7	12505	101	85.7	nd	46.3	nd
3	55.1	-155.7	12503	176	144.2	nd	28.5	nd
3	55.1	-155.7	12501	301	158.0	nd	28.9	nd
3	55.1	-155.7	12499	502	154.5	nd	25.2	nd
3	55.1	-155.7	12497	702	173.4	nd	23.5	nd
3	55.1	-155.7	12495	801	162.9	nd	26.3	nd
3	55.1	-155.7	12493	1102	180.4	nd	31.5	nd
3	55.1	-155.7	12491	1402	186.1	nd	32.1	nd
3	55.1	-155.7	12489	1563	182.8	33.4	35.4	5.7
3	55.1	-155.7	12487	1597	150.1	23.7	32.0	6.6
4	55.7	-155.2	12558	0	136.0	nd	45.5	nd
4	54.7	-155.2	12583	21	75.2	nd	63.0	nd
4	54.7	-155.2	12581	31	71.9	nd	50.0	nd
4	54.7	-155.2	12579	39	83.3	nd	47.9	nd
4	54.7	-155.2	12577	50	32.1	nd	38.1	nd
4	54.7	-155.2	12575	62	44.9	nd	29.9	nd
4	54.7	-155.2	12573	70	39.1	nd	25.1	nd

Station #	Lat. [+N, -S]	Long. [+E, -W]	Sample #	Depth [m]	TDS [pmol/L]	SD [pmol/L]	OCS [pmol/L]	SD [pmol/L]
4	54.7	-155.2	12571	100	62.5	nd	34.0	nd
4	54.7	-155.2	12569	146	96.9	8.5	25.0	0.7
4	54.7	-155.2	12567	201	119.5	nd	26.3	nd
4	54.7	-155.2	12565	252	98.4	nd	24.6	nd
4	54.7	-155.2	12563	302	126.0	nd	35.7	nd
4	54.7	-155.2	12561	402	121.2	nd	32.4	nd
5	53.7	-153.8	12347	25	167.0	nd	92.9	nd
5	53.7	-153.8	12345	41	151.4	nd	46.1	nd
5	53.7	-153.8	12343	55	87.3	nd	43.3	nd
5	53.7	-153.8	12341	70	87.3	nd	43.3	nd
5	53.7	-153.8	12339	92	126.1	nd	44.6	nd
5	53.7	-153.8	12337	123	87.3	nd	42.0	nd
5	53.7	-153.8	12335	142	210.1	nd	42.0	nd
5	53.7	-153.8	12333	304	188.3	nd	32.9	nd
5	53.7	-153.8	12331	455	229.9	nd	35.2	nd
5	53.7	-153.8	12329	608	187.0	nd	27.9	nd
5	53.7	-153.8	12327	810	195.4	nd	30.6	nd
5	53.7	-153.8	12325	1015	224.0	nd	30.9	nd
6	52.0	-152.0	12714	0	36.5	nd	58.7	nd
6	52.0	-152.0	12751	25	71.4	nd	77.5	nd
6	52.0	-152.0	12747	41	20.4	nd	49.4	nd
6	52.0	-152.0	12749	60	66.8	nd	68.9	nd
6	52.0	-152.0	12745	91	18.0	nd	45.0	nd
6	52.0	-152.0	12743	121	51.6	nd	37.9	nd
6	52.0	-152.0	12741	151	42.7	nd	35.8	nd
6	52.0	-152.0	12739	251	73.1	nd	37.5	nd
6	52.0	-152.0	12737	351	47.9	nd	32.9	nd
6	52.0	-152.0	12735	441	55.4	nd	42.3	nd
6	52.0	-152.0	12733	551	30.1	nd	33.8	nd
6	52.0	-152.0	12731	758	48.5	nd	53.2	nd
6	52.0	-152.0	12729	1012	42.3	nd	46.4	nd
8	47.2	-152.0	12905	0	61.2	11.1	54.6	8.9
8	47.0	-152.0	12904	28	16.5	7.6	55.8	12.1
8	47.0	-152.0	12901	45	0.0	0.0	56.9	5.1
8	47.0	-152.0	12898	66	0.0	nd	54.4	nd
8	47.0	-152.0	12895	90	0.0	nd	57.3	nd
8	47.0	-152.0	12892	115	11.7	nd	48.9	nd
8	47.0	-152.0	12889	151	11.8	nd	41.6	nd
8	47.0	-152.0	12886	199	0.0	nd	53.7	nd
8	47.0	-152.0	13019	303	27.7	9.9	41.1	12.5

Station #	Lat. [+N, -S]	Long. [+E, -W]	Sample #	Depth [m]	TDS [pmol/L]	SD [pmol/L]	OCS [pmol/L]	SD [pmol/L]
8	47.0	-152.0	12883	399	8.6	nd	35.8	nd
8	47.0	-152.0	13016	499	15.1	nd	46.2	nd
8	47.0	-152.0	13013	600	11.3	nd	47.4	nd
8	47.0	-152.0	13010	700	20.2	nd	31.2	nd
8	47.0	-152.0	13007	801	19.0	7.8	36.2	4.2
8	47.0	-152.0	13004	900	24.0	nd	34.5	nd
8	47.0	-152.0	13001	1002	26.8	nd	29.1	nd
9	44.8	-152.0	13033	0	49.0	nd	49.5	nd
10	42.2	-152.0	13076	0	23.3	nd	46.5	nd
10	42.0	-152.0	13101	26	33.7	10.8	49.6	1.4
10	42.0	-152.0	13099	40	29.3	nd	51.5	nd
10	42.0	-152.0	13097	60	17.6	nd	46.6	nd
10	42.0	-152.0	13095	81	11.3	nd	43.0	nd
10	42.0	-152.0	13093	101	11.3	nd	40.8	nd
10	42.0	-152.0	13091	150	11.2	nd	39.7	nd
10	42.0	-152.0	13089	226	17.0	nd	35.9	nd
10	42.0	-152.0	13087	299	15.4	nd	40.0	nd
10	42.0	-152.0	13085	402	19.5	7.8	40.2	3.4
10	42.0	-152.0	13083	602	11.6	nd	42.6	nd
10	42.0	-152.0	13081	802	20.7	nd	34.1	nd
10	42.0	-152.0	13079	1002	17.1	nd	38.8	nd
11	39.7	-152.0	13187	0	27.7	nd	50.0	nd
12	37.2	-152.0	13236	0	30.7	3.0	42.3	5.0
12	37.0	-152.0	13190	25	30.2	nd	47.7	nd
12	37.0	-152.0	13212	41	40.9	nd	54.9	nd
12	37.0	-152.0	13210	61	26.8	nd	45.8	nd
12	37.0	-152.0	13208	75	26.2	nd	55.9	nd
12	37.0	-152.0	13206	86	20.7	nd	36.4	nd
12	37.0	-152.0	13204	95	15.8	nd	39.3	nd
12	37.0	-152.0	13202	105	9.3	nd	30.7	nd
12	37.0	-152.0	13200	140	23.6	nd	41.6	nd
12	37.0	-152.0	13198	180	27.9	nd	31.9	nd
12	37.0	-152.0	13196	250	24.7	nd	39.3	nd
12	37.0	-152.0	13194	326	13.0	nd	27.1	nd
12	37.0	-152.0	13336	426	19.7	7.9	37.1	4.6
12	37.0	-152.0	13333	500	17.4	nd	22.5	nd
12	37.0	-152.0	13331	601	21.1	nd	21.8	nd
12	37.0	-152.0	13329	700	18.5	nd	26.7	nd
12	37.0	-152.0	13327	801	18.5	nd	27.1	nd
12	37.0	-152.0	13325	901	9.5	nd	28.1	nd

Station #	Lat. [+N, -S]	Long. [+E, -W]	Sample #	Depth [m]	TDS [pmol/L]	SD [pmol/L]	OCS [pmol/L]	SD [pmol/L]
12	37.0	-152.0	13323	1101	15.8	nd	17.8	nd
12	37.0	-152.0	13321	1301	14.5	nd	22.7	nd
13	34.6	-152.0	13374	0	26.4	nd	34.7	nd
14	32.2	-152.0	13414	0	48.3	5.6	28.6	4.7
14	32.0	-152.0	13439	25	17.5	nd	49.9	nd
14	32.0	-152.0	13436	46	21.9	nd	51.1	nd
14	32.0	-152.0	13433	76	13.5	2.5	42.4	6.4
14	32.0	-152.0	13430	101	9.4	nd	52.5	nd
14	32.0	-152.0	13427	125	9.9	nd	43.1	nd
14	32.0	-152.0	13424	150	16.1	nd	40.8	nd
14	32.0	-152.0	13421	201	11.9	nd	28.0	nd
14	32.0	-152.0	13418	301	10.6	nd	26.1	nd
14	32.0	-152.0	13530	401	16.6	nd	30.1	nd
14	32.0	-152.0	13527	500	0.0	nd	34.8	nd
14	32.0	-152.0	13524	601	14.1	nd	23.6	nd
14	32.0	-152.0	13521	701	0.0	nd	31.5	nd
14	32.0	-152.0	13518	800	7.4	nd	20.0	nd
14	32.0	-152.0	13515	901	0.0	nd	29.1	nd
14	32.0	-152.0	13512	1001	7.0	nd	17.9	nd
14	32.0	-152.0	13509	1101	0.0	nd	22.8	nd
14	32.0	-152.0	13571	1201	7.5	nd	15.0	nd
14	32.0	-152.0	13568	1301	2.5	nd	17.8	nd
14	32.0	-152.0	13565	1502	9.3	nd	19.2	nd
14	32.0	-152.0	13562	1702	4.9	nd	23.2	nd
14	32.0	-152.0	13559	1900	6.7	nd	16.7	nd
14	32.0	-152.0	13556	2101	3.2	nd	26.2	nd
14	32.0	-152.0	13553	2302	0.0	nd	13.9	nd
14	32.0	-152.0	13550	2500	0.0	nd	18.2	nd
15	29.7	-152.0	13609	0	17.9	nd	53.9	4.1
16	27.3	-152.0	13620	0	50.0	nd	37.4	nd
16	27.0	-152.0	13635	31	15.0	nd	46.0	nd
16	27.0	-152.0	13657	65	17.0	nd	40.2	nd
16	27.0	-152.0	13655	111	0.0	nd	35.7	nd
16	27.0	-152.0	13653	126	7.6	nd	36.8	nd
16	27.0	-152.0	13651	151	9.0	nd	37.4	nd
16	27.0	-152.0	13649	201	9.5	nd	29.9	nd
16	27.0	-152.0	13647	300	11.0	nd	24.9	nd
16	27.0	-152.0	13645	400	10.0	nd	20.8	nd
16	27.0	-152.0	13643	527	20.7	nd	23.3	nd
16	27.0	-152.0	13641	602	10.6	nd	27.1	nd

Station #	Lat. [+N, -S]	Long. [+E, -W]	Sample #	Depth [m]	TDS [pmol/L]	SD [pmol/L]	OCS [pmol/L]	SD [pmol/L]
16	27.0	-152.0	13639	700	8.6	nd	27.6	nd
16	27.0	-152.0	13637	851	6.9	nd	24.4	nd
16	27.0	-152.0	13694	850	5.7	0.7	23.5	0.6
16	27.0	-152.0	13692	1001	26.5	nd	20.4	nd
16	27.0	-152.0	13690	1251	3.8	nd	19.9	nd
16	27.0	-152.0	13688	1747	16.1	nd	23.5	nd
16	27.0	-152.0	13686	2251	1.4	nd	20.7	nd
16	27.0	-152.0	13684	2501	6.4	nd	21.1	nd
16	27.0	-152.0	13682	3001	2.7	nd	15.9	nd
18	22.2	-152.0	13782	0	50.0	nd	17.1	nd
18	22.0	-152.0	13807	40	12.9	nd	41.2	nd
18	22.0	-152.0	13805	80	21.2	nd	23.8	nd
18	22.0	-152.0	13503	111	6.9	nd	31.8	nd
18	22.0	-152.0	13801	130	13.7	nd	42.7	nd
18	22.0	-152.0	13799	151	14.0	nd	59.8	nd
18	22.0	-152.0	13797	200	19.7	nd	29.1	nd
18	22.0	-152.0	13795	301	19.5	nd	23.0	nd
18	22.0	-152.0	13793	451	17.9	nd	22.7	nd
18	22.0	-152.0	13791	600	19.5	nd	15.1	nd
18	22.0	-152.0	13789	701	13.1	nd	24.2	nd
18	22.0	-152.0	13787	851	5.0	nd	20.4	nd
18	22.0	-152.0	13785	1002	7.9	nd	16.9	nd
18	22.0	-152.0	13842	1101	6.9	nd	10.8	nd
18	22.0	-152.0	13840	1252	13.8	nd	15.2	nd
18	22.0	-152.0	13838	1752	13.4	nd	19.1	nd
18	22.0	-152.0	13836	2252	8.8	nd	13.7	nd
18	22.0	-152.0	13834	2750	12.0	nd	19.7	nd
18.3	19.7	-154.5	13916	26	7.3	2.8	61.3	4.9
18.3	19.7	-154.5	13914	101	7.1	nd	39.6	nd
18.3	19.7	-154.5	13912	301	7.3	nd	21.2	nd
18.3	19.7	-154.5	13910	501	12.1	nd	23.0	nd
18.3	19.7	-154.5	13908	800	6.4	nd	18.0	nd
18.3	19.7	-154.5	13906	1101	6.2	nd	16.5	nd
18.3	19.7	-154.5	13904	1301	8.9	nd	17.9	nd
18.3	19.7	-154.5	13902	1601	10.4	nd	15.8	nd
18.3	19.7	-154.5	13900	1921	8.4	nd	16.7	nd
18.3	19.7	-154.5	13898	2041	8.2	nd	17.4	nd
18.3	19.7	-154.5	13896	2101	20.8	nd	18.8	nd
18.3	19.7	-154.5	13894	2131	11.6	nd	33.0	nd
18.6	18.9	-155.3	13932	101	10.2	nd	54.2	nd

Station #	Lat. [+N, -S]	Long. [+E, -W]	Sample #	Depth [m]	TDS [pmol/L]	SD [pmol/L]	OCS [pmol/L]	SD [pmol/L]
18.6	18.9	-155.3	13930	631	0.0	nd	19.1	nd
18.6	18.9	-155.3	13928	850	12.6	nd	19.6	nd
18.6	18.9	-155.3	13926	1001	0.0	nd	21.3	nd
18.6	18.9	-155.3	13924	1100	33.4	nd	21.9	nd
18.6	18.9	-155.3	13922	1201	46.0	nd	26.3	nd
18.6	18.9	-155.3	13920	1252	218.4	nd	21.0	nd
18.6	18.9	-155.3	13918	1291	347.3	86.3	46.4	nd
19	17.6	-152.3	13963	0	9.8	nd	28.1	nd
19	17.5	-152.0	13988	26	35.7	nd	68.4	nd
19	17.5	-152.0	13986	56	34.0	nd	86.3	nd
19	17.5	-152.0	13984	81	9.1	nd	77.2	nd
19	17.5	-152.0	13982	111	15.5	nd	60.5	nd
19	17.5	-152.0	13980	121	8.7	nd	65.9	nd
19	17.5	-152.0	13978	161	2.3	nd	28.4	nd
19	17.5	-152.0	13976	210	0.0	nd	46.1	nd
19	17.5	-152.0	13974	261	11.3	nd	38.0	nd
19	17.5	-152.0	13972	302	4.5	nd	47.8	nd
19	17.5	-152.0	13970	351	14.1	nd	44.3	nd
19	17.5	-152.0	13968	401	0.0	nd	42.6	nd
19	17.5	-152.0	13966	552	7.2	nd	47.3	nd
19	17.5	-152.0	14086	551	0.0	nd	22.5	nd
19	17.5	-152.0	14084	652	8.9	nd	29.6	nd
19	17.5	-152.0	14082	802	5.7	nd	33.1	nd
19	17.5	-152.0	14080	901	12.5	nd	31.1	nd
19	17.5	-152.0	14078	1000	6.0	nd	35.2	nd
19	17.5	-152.0	14076	1076	6.9	nd	38.8	nd
19	17.5	-152.0	14074	1147	4.4	nd	39.4	nd
19	17.5	-152.0	14072	1202	11.2	nd	43.1	nd
19	17.5	-152.0	14070	1301	11.4	nd	33.5	nd
19	17.5	-152.0	14068	1501	11.1	nd	44.3	nd
19	17.5	-152.0	14066	1701	0.0	nd	27.6	nd
19	17.5	-152.0	14064	1900	11.3	nd	43.0	nd
19	17.5	-152.0	14046	1902	0.0	nd	25.4	nd
19	17.5	-152.0	14044	2101	9.3	nd	29.6	nd
19	17.5	-152.0	14042	2302	0.0	nd	32.2	nd
19	17.5	-152.0	14040	2501	9.1	nd	34.5	nd
19	17.5	-152.0	14038	2701	9.1	nd	34.5	nd
19	17.5	-152.0	14036	3001	0.0	nd	28.4	nd
20	14.5	-152.0	14101	0	31.0	5.1	43.6	5.9
21	11.1	-152.0	14137	0	17.9	nd	34.0	nd

Station #	Lat. [+N, -S]	Long. [+E, -W]	Sample #	Depth [m]	TDS [pmol/L]	SD [pmol/L]	OCS [pmol/L]	SD [pmol/L]
21	11.0	-152.0	14162	21	30.5	nd	88.8	nd
21	11.0	-152.0	14160	46	29.4	nd	48.2	nd
21	11.0	-152.0	14158	61	11.0	nd	48.4	nd
21	11.0	-152.0	14156	81	11.1	nd	42.2	nd
21	11.0	-152.0	14154	101	2.9	nd	51.4	nd
21	11.0	-152.0	14152	126	11.9	nd	40.5	nd
21	11.0	-152.0	14150	152	10.8	nd	42.3	nd
21	11.0	-152.0	14148	176	17.2	nd	40.1	nd
21	11.0	-152.0	14146	201	19.5	nd	31.6	nd
21	11.0	-152.0	14144	252	20.7	nd	53.6	nd
21	11.0	-152.0	14142	301	16.0	nd	46.6	nd
21	11.0	-152.0	14140	401	24.4	nd	42.5	nd
22	9.4	-152.0	14275	0	21.5	nd	52.7	nd
23	7.7	-152.0	14322	0	29.5	nd	54.5	nd
23	7.5	-152.0	14359	25	14.2	nd	64.0	nd
23	7.5	-152.0	14356	61	22.7	nd	45.3	nd
23	7.5	-152.0	14353	81	17.6	nd	121.5	nd
23	7.5	-152.0	14350	101	18.5	nd	56.5	nd
23	7.5	-152.0	14347	130	24.7	nd	44.0	nd
23	7.5	-152.0	14344	160	8.2	nd	38.1	nd
23	7.5	-152.0	14341	200	19.4	nd	35.8	nd
23	7.5	-152.0	14338	202	24.6	nd	41.5	nd
23	7.5	-152.0	14474	499	16.4	nd	28.0	nd
23	7.5	-152.0	14471	601	12.1	nd	46.6	nd
23	7.5	-152.0	14468	801	14.5	2.9	38.9	4.3
23	7.5	-152.0	14465	1001	21.5	nd	36.5	nd
23	7.5	-152.0	14462	1251	9.8	nd	32.1	nd
23	7.5	-152.0	14459	1501	17.8	nd	31.1	nd
23	7.5	-152.0	14456	1749	8.9	nd	38.9	nd
23	7.5	-152.0	14453	2001	20.2	nd	40.1	nd
25	5.1	-152.0	14537	0	18.3	2.7	36.1	2.2
25	5.0	-152.0	14536	26	21.7	nd	63.0	nd
25	5.0	-152.0	14534	51	41.8	nd	52.8	nd
25	5.0	-152.0	14532	80	23.8	7.1	48.0	5.5
25	5.0	-152.0	14530	100	34.1	nd	40.5	nd
25	5.0	-152.0	14528	125	0.0	nd	38.6	nd
25	5.0	-152.0	14526	151	19.9	nd	36.6	nd
25	5.0	-152.0	14524	201	0.0	nd	31.2	nd
25	5.0	-152.0	14522	251	19.7	nd	33.4	nd
25	5.0	-152.0	14520	301	10.3	nd	31.7	nd

Station #	Lat. [+N, -S]	Long. [+E, -W]	Sample #	Depth [m]	TDS [pmol/L]	SD [pmol/L]	OCS [pmol/L]	SD [pmol/L]
25	5.0	-152.0	14518	351	10.3	nd	31.7	nd
25	5.0	-152.0	14516	401	4.9	nd	35.6	nd
25	5.0	-152.0	14514	452	20.0	0.0	36.9	5.9
27	2.7	-152.0	14639	0	54.2	7.2	57.4	5.5
27	2.5	-152.0	14664	25	35.2	nd	45.5	nd
27	2.5	-152.0	14662	46	39.1	nd	57.6	nd
27	2.5	-152.0	14660	61	17.2	nd	48.2	nd
27	2.5	-152.0	14658	81	19.8	nd	53.0	nd
27	2.5	-152.0	14656	101	0.0	nd	85.8	nd
27	2.5	-152.0	14654	121	0.0	nd	61.7	nd
27	2.5	-152.0	14652	161	0.0	nd	40.6	nd
27	2.5	-152.0	14650	202	13.7	nd	40.8	nd
27	2.5	-152.0	14648	251	10.3	nd	35.6	nd
27	2.5	-152.0	14646	301	16.1	nd	45.8	nd
27	2.5	-152.0	14644	351	0.0	nd	37.6	nd
27	2.5	-152.0	14642	401	18.3	nd	49.4	nd
29	0.1	-152.0	14786	0	26.5	1.9	66.8	5.6
29	0.0	-152.0	14832	26	0.0	nd	47.6	nd
29	0.0	-152.0	14829	51	4.3	nd	53.3	nd
29	0.0	-152.0	14826	75	0.0	nd	58.8	nd
29	0.0	-152.0	14823	90	0.0	nd	77.3	nd
29	0.0	-152.0	14820	116	0.0	nd	49.0	nd
29	0.0	-152.0	14817	132	0.0	nd	56.6	nd
29	0.0	-152.0	14814	154	19.1	nd	52.0	nd
29	0.0	-152.0	14811	174	26.3	nd	36.5	nd
29	0.0	-152.0	14959	201	13.1	nd	35.3	nd
29	0.0	-152.0	14956	250	11.3	nd	33.4	nd
29	0.0	-152.0	14953	301	5.6	nd	33.2	nd
29	0.0	-152.0	14950	351	14.2	nd	39.2	nd
29	0.0	-152.0	14947	401	10.4	nd	36.9	nd
29	0.0	-152.0	14944	500	4.1	nd	40.9	nd
29	0.0	-152.0	14941	601	9.6	nd	48.6	nd
29	0.0	-152.0	14938	701	6.1	nd	nd	nd
31	-2.4	-152.0	14975	0	24.5	nd	65.1	nd
31	-2.5	-152.0	15000	31	28.7	13.1	50.3	8.3
31	-2.5	-152.0	14998	66	29.6	nd	54.2	nd
31	-2.5	-152.0	14996	86	19.4	nd	54.7	nd
31	-2.5	-152.0	14994	106	22.7	nd	52.7	nd
31	-2.5	-152.0	14992	131	0.0	nd	45.5	nd
31	-2.5	-152.0	14990	151	7.2	nd	47.1	nd

Station #	Lat. [+N, -S]	Long. [+E, -W]	Sample #	Depth [m]	TDS [pmol/L]	SD [pmol/L]	OCS [pmol/L]	SD [pmol/L]
31	-2.5	-152.0	14988	181	0.0	nd	38.6	nd
31	-2.5	-152.0	14986	210	12.8	nd	39.7	nd
31	-2.5	-152.0	14984	261	3.0	nd	36.9	nd
31	-2.5	-152.0	14982	301	9.6	nd	54.4	nd
31	-2.5	-152.0	14980	341	2.3	nd	48.2	nd
31	-2.5	-152.0	15094	401	14.5	nd	54.2	nd
31	-2.5	-152.0	15092	451	5.8	nd	31.0	nd
31	-2.5	-152.0	15090	500	5.6	nd	33.0	nd
31	-2.5	-152.0	15088	600	5.5	nd	42.5	nd
31	-2.5	-152.0	15086	700	3.5	nd	40.3	nd
31	-2.5	-152.0	15084	800	7.8	nd	38.9	nd
33	-4.8	-152.0	15108	0	11.8	nd	54.0	nd
33	-5.0	-152.0	15154	26	68.0	32.5	56.7	nd
33	-5.0	-152.0	15152	66	35.4	nd	49.5	9.1
33	-5.0	-152.0	15150	81	24.2	nd	47.9	nd
33	-5.0	-152.0	15498	101	22.1	nd	57.3	nd
33	-5.0	-152.0	15146	126	4.7	nd	69.3	nd
33	-5.0	-152.0	15144	150	0.0	nd	50.4	nd
33	-5.0	-152.0	15142	176	10.9	nd	50.5	nd
33	-5.0	-152.0	15140	201	6.3	nd	49.7	nd
33	-5.0	-152.0	15138	250	11.0	nd	38.0	nd
33	-5.0	-152.0	15136	301	15.3	nd	48.9	nd
33	-5.0	-152.0	15134	350	17.8	nd	44.6	nd
33	-5.0	-152.0	15240	401	13.0	nd	28.0	nd
33	-5.0	-152.0	15238	451	15.2	nd	28.9	nd
33	-5.0	-152.0	15236	500	12.6	nd	34.9	nd
33	-5.0	-152.0	15234	601	11.9	nd	39.8	nd
33	-5.0	-152.0	15232	702	11.0	nd	45.7	nd
33	-5.0	-152.0	15230	801	10.6	nd	48.2	nd
34	-7.3	-152.0	15267	0	20.9	7.0	76.9	3.5
35	-10.2	-152.0	15319	0	43.1	nd	78.2	nd
35	-10.5	-152.0	15344	25	29.8	nd	50.3	nd
35	-10.5	-152.0	15341	50	29.1	nd	53.0	nd
35	-10.5	-152.0	15338	75	15.5	6.5	45.6	3.3
35	-10.5	-152.0	15335	101	0.0	nd	77.1	nd
35	-10.5	-152.0	15332	125	0.0	nd	43.9	nd
35	-10.5	-152.0	15329	150	9.8	nd	64.1	nd
35	-10.5	-152.0	15326	226	7.9	nd	58.0	nd
35	-10.5	-152.0	15323	301	19.7	nd	72.5	nd
35	-8.4	-152.0	15459	351	6.1	nd	25.7	nd

Station #	Lat. [+N, -S]	Long. [+E, -W]	Sample #	Depth [m]	TDS [pmol/L]	SD [pmol/L]	OCS [pmol/L]	SD [pmol/L]
35	-8.4	-152.0	15456	451	12.3	nd	33.2	nd
35	-8.4	-152.0	15453	550	10.8	nd	34.5	nd
35	-8.4	-152.0	15450	801	10.6	nd	45.5	nd
36	-12.6	-152.0	15473	0	35.6	nd	61.6	nd
37	-14.8	-152.0	15544	0	16.0	nd	69.4	nd
37	-15.0	-152.0	15543	26	14.7	nd	48.3	nd
37	-15.0	-152.0	15541	60	28.9	nd	50.6	nd
37	-15.0	-152.0	15539	101	9.9	nd	42.3	nd
37	-15.0	-152.0	15537	136	15.1	nd	50.5	nd
37	-15.0	-152.0	15535	150	0.0	nd	55.9	nd
37	-15.0	-152.0	15533	181	9.2	nd	48.0	nd
37	-15.0	-152.0	15531	200	11.6	nd	41.5	nd
37	-15.0	-152.0	15529	251	21.9	nd	43.4	nd
37	-15.0	-152.0	15527	300	17.8	nd	47.9	nd
37	-15.0	-152.0	15525	350	19.1	nd	45.7	nd
37	-15.0	-152.0	15523	401	11.9	nd	49.9	nd
37	-15.0	-152.0	15639	451	7.7	nd	36.8	nd
37	-15.0	-152.0	15637	501	9.0	nd	34.5	nd
37	-15.0	-152.0	15635	576	7.0	nd	35.9	nd
37	-15.0	-152.0	15633	651	9.0	nd	39.0	nd
37	-15.0	-152.0	15631	726	9.4	nd	35.1	nd
37	-15.0	-152.0	15629	801	6.1	nd	38.9	nd
38	-17.4	-152.0	15657	0	11.8	nd	63.1	nd
39	-19.9	-152.0	15705	0	21.0	nd	68.9	nd
39	-20.0	-152.0	15742	25	20.4	nd	43.4	nd
39	-20.0	-152.0	15740	45	23.5	nd	42.2	nd
39	-20.0	-152.0	15738	91	9.4	nd	43.0	nd
39	-20.0	-152.0	15736	121	17.3	nd	51.4	nd
39	-20.0	-152.0	15734	151	0.0	nd	41.8	nd
39	-20.0	-152.0	15732	201	16.7	nd	36.3	nd
39	-20.0	-152.0	15730	250	13.6	nd	34.7	nd
39	-20.0	-152.0	15728	301	13.8	nd	43.7	nd
39	-20.0	-152.0	15726	350	13.3	nd	35.9	nd
39	-20.0	-152.0	15724	400	16.2	nd	48.6	nd
39	-20.0	-152.0	15722	451	6.4	nd	50.6	nd
39	-20.0	-152.0	15720	501	15.0	nd	58.0	nd

APPENDIX B

SMALL SIZE PARTICULATE CHROMIUM REDUCIBLE SULFIDE AND ACID-VOLATILE SULFIDE CONCENTRATIONS FROM THE GP15 CRUISE

Station #	Lat. [+N, -S]	Long. [+E, -W]	Sample #	Depth [m]	pCRS [pmol/L]	pAVS [pmol/L]
1	56.1	-157.0	12451	18	85.65	32.43
1	56.1	-157.0	12452	37	37.72	8.45
1	56.1	-157.0	12453	65	50.24	2.39
1	56.1	-157.0	12454	78	61.04	3.62
3	55.1	-156.0	12523	45	9.02	3.51
3	55.1	-156.0	12524	112	3.89	2.36
3	55.1	-156.0	12525	314	3.46	1.11
3	55.1	-156.0	12526	515	2.03	0.58
3	55.1	-156.0	12527	813	3.67	0.48
3	55.1	-156.0	12527	1107	5.60	0.46
3	55.1	-156.0	12529	1398	4.72	0.28
3	55.1	-156.0	12530	1559	6.12	0.44
4	54.7	-155.0	12597	34	13.56	6.93
4	54.7	-155.0	12598	74	10.45	3.31
4	54.7	-155.0	12599	104	4.93	4.34
4	54.7	-155.0	12600	204	4.29	3.28
4	54.7	-155.0	12601	405	2.69	nd
4	54.7	-155.0	12602	806	3.27	nd
4	54.7	-155.0	12603	1205	3.12	0.43
4	54.7	-155.0	12604	1607	4.11	0.45
5	53.7	-154.0	12361	28	14.74	3.27
5	53.7	-154.0	12362	43	12.84	2.65
5	53.7	-154.0	12363	73	5.27	3.32
5	53.7	-154.0	12364	93	3.19	2.21
5	53.7	-154.0	12365	143	nd	3.09
5	53.7	-154.0	12366	303	4.54	1.19
5	53.7	-154.0	12367	453	6.05	0.30
5	53.7	-154.0	12368	803	6.28	0.23
5	53.7	-154.0	12407	984	5.32	0.23
5	53.7	-154.0	12408	1491	4.49	0.13
5	53.7	-154.0	12409	2502	2.91	0.16
5	53.7	-154.0	12410	3517	1.88	0.17
5	53.7	-154.0	12411	4171	2.51	0.13
5	53.7	-154.0	12413	4519	5.33	0.22
5	53.7	-154.0	12414	4595	12.26	0.32

Station #	Lat. [+N, -S]	Long. [+E, -W]	Sample #	Depth [m]	pCRS [pmol/L]	pAVS [pmol/L]
6	52.0	-152.0	12706	38	20.30	3.44
6	52.0	-152.0	12707	58	10.06	1.21
6	52.0	-152.0	12709	248	6.66	1.52
6	52.0	-152.0	12710	348	5.52	1.25
6	52.0	-152.0	12711	549	4.72	0.19
6	52.0	-152.0	12712	747	3.63	0.36
6	52.0	-152.0	12713	nd	4.35	0.28
8	47.0	-152.0	12873	25	12.37	2.45
8	47.0	-152.0	12874	41	14.06	3.49
8	47.0	-152.0	12875	61	4.94	2.49
8	47.0	-152.0	12876	86	5.24	2.92
8	47.0	-152.0	12877	145	5.13	2.00
8	47.0	-152.0	12878	195	4.68	1.67
8	47.0	-152.0	12879	297	2.98	1.49
8	47.0	-152.0	12880	398	4.37	1.42
8	47.0	-152.0	12939	401	4.84	1.32
10	42.0	-152.0	13115	40	4.49	1.18
10	42.0	-152.0	13116	60	8.30	1.19
10	42.0	-152.0	13117	80	4.51	2.66
10	42.0	-152.0	13118	150	3.89	1.32
10	42.0	-152.0	13119	225	3.55	1.18
10	42.0	-152.0	13120	399	6.55	0.92
10	42.0	-152.0	13121	599	5.43	0.49
10	42.0	-152.0	13122	998	5.08	0.25
12	37.0	-152.0	13227	22	3.43	1.62
12	37.0	-152.0	13228	57	22.43	0.89
12	37.0	-152.0	13229	82	4.54	nd
12	37.0	-152.0	13230	102	4.92	3.76
12	37.0	-152.0	13231	177	3.19	1.16
12	37.0	-152.0	13232	421	3.65	0.76
12	37.0	-152.0	13233	696	4.18	0.24
12	37.0	-152.0	13234	1094	2.73	0.16
12	37.0	-152.0	13305	43	3.56	2.29
14	32.0	-152.0	13393	21	9.80	3.51
14	32.0	-152.0	13394	41	11.98	2.87
14	32.0	-152.0	13395	71	9.09	1.86
14	32.0	-152.0	13396	96	8.36	1.66
14	32.0	-152.0	13397	121	11.95	1.10
14	32.0	-152.0	13398	145	9.06	2.54
14	32.0	-152.0	13399	296	6.07	nd

Station #	Lat. [+N, -S]	Long. [+E, -W]	Sample #	Depth [m]	pCRS [pmol/L]	pAVS [pmol/L]
14	32.0	-152.0	13400	499	6.41	0.31
14	32.0	-152.0	13478	500	3.81	0.35
14	32.0	-152.0	13479	599	5.59	0.42
14	32.0	-152.0	13480	799	7.67	0.09
14	32.0	-152.0	13481	1001	9.09	0.07
14	32.0	-152.0	13482	1199	6.36	0.13
14	32.0	-152.0	13483	1499	4.58	0.13
14	32.0	-152.0	13484	1700	4.09	0.02
14	32.0	-152.0	13485	1904	4.19	0.08
14	32.0	-152.0	13499	1894	3.29	0.12
14	32.0	-152.0	13500	2296	7.03	0.07
14	32.0	-152.0	13501	2746	3.86	0.08
14	32.0	-152.0	13502	3496	2.68	0.08
14	32.0	-152.0	13503	4496	4.39	0.05
14	32.0	-152.0	13504	5082	3.95	0.06
14	32.0	-152.0	13505	5166	10.04	0.07
14	32.0	-152.0	13506	5205	9.43	0.05
16	27.0	-152.0	13611	27	3.37	3.17
16	27.0	-152.0	13612	60	2.13	nd
16	27.0	-152.0	13614	147	1.75	nd
16	27.0	-152.0	13615	195	1.70	1.38
16	27.0	-152.0	13616	294	1.34	0.69
16	27.0	-152.0	13617	519	1.81	0.32
16	27.0	-152.0	13618	849	1.30	0.17
16	27.0	-152.0	13696	98	3.37	2.17
18	22.0	-152.0	13761	37	4.87	4.45
18	22.0	-152.0	13762	76	2.90	5.49
18	22.0	-152.0	13763	107	2.01	4.38
18	22.0	-152.0	13764	146	1.36	2.59
18	22.0	-152.0	13765	296	1.48	0.47
18	22.0	-152.0	13766	445	2.28	0.27
18	22.0	-152.0	13767	696	3.04	0.16
18	22.0	-152.0	13768	1001	2.70	0.12
18.3	19.7	-152.0	13885	497	nd	0.26
18.3	19.7	-152.0	13886	1098	4.89	0.08
18.3	19.7	-152.0	13887	1297	3.54	0.14
18.3	19.7	-152.0	13889	1917	2.68	0.10
18.3	19.7	-152.0	13890	2040	4.54	0.24
18.3	19.7	-152.0	13891	2101	3.98	0.18
18.3	19.7	-152.0	13892	2132	4.27	0.06

Station #	Lat. [+N, -S]	Long. [+E, -W]	Sample #	Depth [m]	pCRS [pmol/L]	pAVS [pmol/L]
19	17.5	-152.0	13943	22	7.33	1.96
19	17.5	-152.0	13944	52	6.89	1.42
19	17.5	-152.0	13945	106	2.86	5.43
19	17.5	-152.0	13946	260	2.71	1.01
19	17.5	-152.0	13947	398	2.38	0.48
19	17.5	-152.0	13948	547	5.87	0.25
19	17.5	-152.0	13949	795	3.47	0.23
19	17.5	-152.0	13950	1078	3.04	0.11
21	11.0	-152.0	14129	17	5.58	0.53
21	11.0	-152.0	14130	41	8.30	0.85
21	11.0	-152.0	14131	96	4.19	3.39
21	11.0	-152.0	14132	145	6.13	3.05
21	11.0	-152.0	14133	245	5.47	0.41
21	11.0	-152.0	14134	395	5.11	0.32
21	11.0	-152.0	14135	592	5.05	0.23
21	11.0	-152.0	14136	900	2.16	0.20
23	7.5	-152.0	14314	23	1.19	1.03
23	7.5	-152.0	14315	78	2.51	0.87
23	7.5	-152.0	14316	98	1.91	1.68
23	7.5	-152.0	14317	158	2.10	1.81
23	7.5	-152.0	14318	198	2.11	0.56
23	7.5	-152.0	14319	298	3.27	0.76
23	7.5	-152.0	14320	498	2.92	0.41
23	7.5	-152.0	14321	798	2.95	0.40
23	7.5	-152.0	14398	792	nd	0.35
23	7.5	-152.0	14399	1241	4.36	0.06
23	7.5	-152.0	14400	1739	1.37	0.19
23	7.5	-152.0	14401	2137	2.63	0.17
23	7.5	-152.0	14402	2287	2.00	0.18
23	7.5	-152.0	14403	2434	1.69	0.18
23	7.5	-152.0	14404	2587	0.79	0.14
23	7.5	-152.0	14405	2741	2.03	0.17
23	7.5	-152.0	14443	2919	1.69	0.08
23	7.5	-152.0	14444	3117	1.91	0.06
23	7.5	-152.0	14445	3315	0.64	0.10
23	7.5	-152.0	14446	3509	nd	0.09
23	7.5	-152.0	14447	4002	1.51	0.01
23	7.5	-152.0	14448	4501	2.42	0.01
23	7.5	-152.0	14449	4748	3.30	0.01
23	7.5	-152.0	14450	5055	1.60	0.01

Station #	Lat. [+N, -S]	Long. [+E, -W]	Sample #	Depth [m]	pCRS [pmol/L]	pAVS [pmol/L]
25	5.0	-152.0	14505	25	1.64	1.13
25	5.0	-152.0	14506	78	2.64	1.04
25	5.0	-152.0	14507	123	2.32	1.49
25	5.0	-152.0	14508	196	3.85	1.11
25	5.0	-152.0	14509	490	3.78	0.37
25	5.0	-152.0	14510	784	3.83	0.26
25	5.0	-152.0	14511	1569	2.19	0.14
25	5.0	-152.0	14512	1961	1.85	0.10
27	2.5	-152.0	14678	25	4.19	0.94
27	2.5	-152.0	14679	60	5.20	0.69
27	2.5	-152.0	14680	99	3.84	0.93
27	2.5	-152.0	14681	159	4.68	2.64
27	2.5	-152.0	14682	248	4.98	nd
27	2.5	-152.0	14683	496	4.00	0.20
27	2.5	-152.0	14684	794	3.50	0.22
27	2.5	-152.0	14685	1390	3.20	0.09
29	0.0	-152.0	14789	24	3.72	1.42
29	0.0	-152.0	14790	73	2.94	1.42
29	0.0	-152.0	14791	112	3.80	3.99
29	0.0	-152.0	14792	127	3.92	3.07
29	0.0	-152.0	14793	151	3.08	3.64
29	0.0	-152.0	14794	195	2.21	0.98
29	0.0	-152.0	14795	244	2.69	0.68
29	0.0	-152.0	14796	342	7.07	0.80
29	0.0	-152.0	14883	399	7.87	1.33
29	0.0	-152.0	14884	498	5.78	0.47
29	0.0	-152.0	14885	598	5.47	0.61
29	0.0	-152.0	14886	698	3.69	0.35
29	0.0	-152.0	14887	797	3.24	0.24
29	0.0	-152.0	14888	997	3.77	0.28
29	0.0	-152.0	14889	1196	3.75	0.11
29	0.0	-152.0	14890	1395	5.27	0.11
29	0.0	-152.0	14916	1796	3.53	0.15
29	0.0	-152.0	14917	2195	7.38	0.08
29	0.0	-152.0	14918	2793	3.14	0.10
29	0.0	-152.0	14919	3591	3.22	0.08
29	0.0	-152.0	14920	3990	2.72	0.09
29	0.0	-152.0	14921	4205	4.28	0.13
29	0.0	-152.0	14922	4285	3.72	0.07
29	0.0	-152.0	14923	4324	3.52	0.09

Station #	Lat. [+N, -S]	Long. [+E, -W]	Sample #	Depth [m]	pCRS [pmol/L]	pAVS [pmol/L]
31	-2.5	-152.0	14967	30	2.51	0.61
31	-2.5	-152.0	14968	84	1.56	0.72
31	-2.5	-152.0	14969	149	1.98	2.77
31	-2.5	-152.0	14970	258	1.21	0.95
31	-2.5	-152.0	14971	397	0.84	0.56
31	-2.5	-152.0	14972	596	1.90	nd
31	-2.5	-152.0	14973	894	1.57	0.29
31	-2.5	-152.0	14974	1390	3.12	0.13
33	-5.0	-152.0	15123	25	3.49	nd
33	-5.0	-152.0	15124	80	2.15	0.78
33	-5.0	-152.0	15125	124	1.65	1.25
33	-5.0	-152.0	15126	174	1.71	2.29
33	-5.0	-152.0	15127	249	2.00	0.32
33	-5.0	-152.0	15128	398	3.27	0.34
33	-5.0	-152.0	15129	597	3.82	0.39
33	-5.0	-152.0	15130	896	nd	0.16
35	-10.5	-152.0	15293	25	5.10	1.02
35	-10.5	-152.0	15924	75	5.90	0.93
35	-10.5	-152.0	15295	99	6.50	1.14
35	-10.5	-152.0	15296	149	5.84	2.45
35	-10.5	-152.0	15297	224	7.49	1.30
35	-10.5	-152.0	15298	348	6.21	0.43
35	-10.5	-152.0	15299	547	10.31	0.53
35	-10.5	-152.0	15300	795	7.95	0.22
35	-10.5	-152.0	15346	799	3.37	0.24
35	-10.5	-152.0	15347	1398	0.89	0.15
35	-10.5	-152.0	15348	1997	3.36	0.12
35	-10.5	-152.0	15349	2197	7.24	0.09
35	-10.5	-152.0	15350	2397	1.05	0.11
35	-10.5	-152.0	15351	2596	0.61	0.12
35	-10.5	-152.0	15352	2796	0.64	0.07
35	-10.5	-152.0	15353	2996	2.19	0.07
35	-10.5	-152.0	15404	3200	4.20	0.09
35	-10.5	-152.0	15405	3600	1.00	0.09
35	-10.5	-152.0	15406	4000	1.27	0.08
35	-10.5	-152.0	15407	4500	6.59	0.17
35	-10.5	-152.0	15408	4750	0.76	0.06
35	-10.5	-152.0	15409	4970	0.84	0.12
35	-10.5	-152.0	15410	5050	0.60	0.05
35	-10.5	-152.0	15411	5090	4.09	nd

Station #	Lat. [+N, -S]	Long. [+E, -W]	Sample #	Depth [m]	pCRS [pmol/L]	pAVS [pmol/L]
37	-15.0	-152.0	15512	25	2.15	2.89
37	-15.0	-152.0	15513	60	2.38	2.97
37	-15.0	-152.0	15514	135	1.13	1.19
37	-15.0	-152.0	15515	250	1.11	0.76
37	-15.0	-152.0	15516	449	1.42	0.35
37	-15.0	-152.0	15517	798	1.68	0.24
37	-15.0	-152.0	15518	1198	0.99	0.17
37	-15.0	-152.0	15519	1796	2.01	0.14
39	-20.0	-152.0	15696	25	6.47	2.07
39	-20.0	-152.0	15697	45	6.95	3.55
39	-20.0	-152.0	15698	119	2.18	2.56
39	-20.0	-152.0	15699	149	3.74	2.78
39	-20.0	-152.0	15700	198	1.72	2.00
39	-20.0	-152.0	15701	297	2.59	0.55
39	-20.0	-152.0	15702	396	1.39	0.83
39	-20.0	-152.0	15703	495	0.36	0.30
39	-20.0	-152.0	15744	500	nd	0.33
39	-20.0	-152.0	15745	599	2.33	0.24
39	-20.0	-152.0	15746	798	1.45	0.21
39	-20.0	-152.0	15747	998	0.53	0.14
39	-20.0	-152.0	15748	1197	0.96	0.07
39	-20.0	-152.0	15749	1397	1.49	0.08
39	-20.0	-152.0	15750	1597	2.12	0.09
39	-20.0	-152.0	15751	1796	1.37	0.08
39	-20.0	-152.0	15802	1600	4.41	0.07

APPENDIX C

DISSOLVED SULFIDE AND CARBONYL SULFIDE CONCENTRATIONS FROM THE GP17 CRUISE

Station #	Lat. [+N, -S]	Long. [+E, -W]	Sample #	Depth [m]	TDS [pmol/L]	SD [pmol/L]	OCS [pmol/L]	SD [pmol/L]
1	-20.0	-152.0	15907	0	11.0	6.6	21.1	4.9
1	-20.0	-152.0	15933	25	41.0	37.9	nd	nd
1	-20.0	-152.0	15934	60	43.6	5.1	nd	nd
1	-20.0	-152.0	15935	100	6.4	1.2	nd	nd
1	-20.0	-152.0	15936	130	39.0	0.8	59.2	0.1
1	-20.0	-152.0	15937	145	9.0	0.6	nd	nd
1	-20.0	-152.0	15938	200	15.6	0.4	nd	nd
1	-20.0	-152.0	15939	285	16.2	1.7	nd	nd
1	-20.0	-152.0	15940	400	5.0	0.1	nd	nd
1	-20.0	-152.0	15941	500	9.8	0.2	nd	nd
1	-20.0	-152.0	15942	625	4.1	0.4	nd	nd
1	-20.0	-152.0	15943	700	7.7	0.2	nd	nd
1	-20.0	-152.0	15944	800	4.4	0.1	nd	nd
1	-20.0	-152.0	16007	1000	9.3	5.9	nd	nd
1	-20.0	-152.0	16008	1200	6.7	0.8	30.5	1.1
1	-20.0	-152.0	16009	1550	3.9	0.3	20.8	2.1
2	-22.5	-151.6	16021	0	3.1	1.3	25.7	7.2
3	-25.0	-151.3	16061	0	11.5	2.8	11.7	5.6
3	-25.0	-151.3	16115	25	19.4	0.5	nd	nd
3	-25.0	-151.3	16116	60	71.6	0.6	47.8	3.2
3	-25.0	-151.3	16117	90	11.0	2.2	34.7	1.3
3	-25.0	-151.3	16118	132	21.6	0.2	35.9	0.7
3	-25.0	-151.3	16119	170	7.5	0.0	nd	nd
3	-25.0	-151.3	16120	200	8.7	0.1	nd	nd
3	-25.0	-151.3	16121	235	11.9	0.3	nd	nd
3	-25.0	-151.3	16122	300	9.1	0.5	nd	nd
3	-25.0	-151.3	16123	400	17.9	0.2	nd	nd
3	-25.0	-151.3	16124	500	6.4	0.4	nd	nd
3	-25.0	-151.3	16125	600	7.4	0.6	nd	nd
3	-25.0	-151.3	16126	750	1.8	0.2	nd	nd
3	-25.0	-151.3	16170	900	1.1	0.4	0.8	0.2
3	-25.0	-151.3	16171	1100	3.2	0.6	24.0	1.7
3	-25.0	-151.3	16172	1300	3.3	1.7	6.5	8.0
3	-25.0	-151.3	16173	1500	4.0	0.7	nd	nd
4	-27.4	-150.9	16253	0	22.2	2.5	10.1	2.2

Station #	Lat. [+N, -S]	Long. [+E, -W]	Sample #	Depth [m]	TDS [pmol/L]	SD [pmol/L]	OCS [pmol/L]	SD [pmol/L]
5	-29.8	-150.5	16293	0	13.3	3.7	14.4	7.8
6	-32.5	-150.0	16380	45	72.1	10.2	41.1	10.1
6	-32.5	-150.0	16382	100	31.2	3.8	21.4	0.2
6	-32.5	-150.0	16384	175	15.3	0.8	22.6	0.1
6	-32.5	-150.0	16386	320	10.0	0.4	33.2	1.1
6	-32.5	-150.0	16388	645	5.1	0.7	21.9	1.5
6	-32.5	-150.0	16390	1250	3.9	0.1	33.4	0.5
8	-37.5	-149.3	16507	0	6.4	1.3	15.5	0.5
8	-37.5	-149.3	16566	25	15.8	2.5	nd	nd
8	-37.5	-149.3	16567	50	69.2	25.8	16.4	3.0
8	-37.5	-149.3	16568	85	10.7	0.3	20.1	1.3
8	-37.5	-149.3	16569	125	4.7	0.3	12.0	1.2
8	-37.5	-149.3	16570	175	3.9	0.6	26.1	1.8
8	-37.5	-149.3	16571	225	4.6	0.3	27.8	1.1
8	-37.5	-149.3	16572	325	4.4	0.4	17.2	0.3
8	-37.5	-149.3	16573	550	8.4	0.5	27.5	3.2
8	-37.5	-149.3	16574	750	3.6	0.4	24.1	3.0
8	-37.5	-149.3	16575	950	2.6	0.1	14.7	2.1
8	-37.5	-149.3	16576	1200	2.3	0.3	16.2	0.8
8	-37.5	-149.3	16577	1500	2.2	0.1	25.6	0.3
9	-39.8	-148.9	16641	0	33.4	4.0	28.1	1.0
12	-47.5	-147.5	16840	0	10.5	1.4	22.0	1.3
12	-47.5	-147.5	16884	25	83.5	18.0	nd	nd
12	-47.5	-147.5	16885	52	5.5	2.7	25.0	0.6
12	-47.5	-147.5	16886	70	2.5	0.2	57.9	7.9
12	-47.5	-147.5	16887	98	0.0	0.0	16.2	0.1
12	-47.5	-147.5	16888	150	4.3	0.3	nd	nd
12	-47.5	-147.5	16889	200	8.8	3.5	55.5	0.6
12	-47.5	-147.5	16890	240	10.0	0.9	43.9	0.1
12	-47.5	-147.5	16891	350	10.0	1.8	18.9	0.1
12	-47.5	-147.5	16892	500	14.6	0.3	42.7	3.3
12	-47.5	-147.5	16893	750	9.9	0.0	19.3	3.2
12	-47.5	-147.5	16894	1000	13.4	1.2	31.6	1.7
12	-47.5	-147.5	16895	1250	7.8	0.1	15.6	2.0
13	-49.9	-147.0	16960	0	44.6	5.8	29.4	5.5
14	-52.3	-146.4	17185	0	0.0	0.0	47.5	0.5
14	-52.3	-146.4	17026	25	31.4	1.0	nd	nd
14	-52.3	-146.4	17027	50	2.0	0.1	67.8	1.0
14	-52.3	-146.4	17028	70	1.9	0.2	30.5	7.3
14	-52.3	-146.4	17029	100	1.5	0.3	19.3	0.1

Station #	Lat. [+N, -S]	Long. [+E, -W]	Sample #	Depth [m]	TDS [pmol/L]	SD [pmol/L]	OCS [pmol/L]	SD [pmol/L]
14	-52.3	-146.4	17030	150	7.2	1.6	44.4	1.7
14	-52.3	-146.4	17031	250	9.4	0.8	19.1	1.3
14	-52.3	-146.4	17032	325	7.5	0.3	39.9	6.5
14	-52.3	-146.4	17033	400	5.4	0.4	19.1	0.0
14	-52.3	-146.4	17034	500	7.8	0.2	42.0	3.2
14	-52.3	-146.4	17035	650	7.3	0.3	17.0	3.5
14	-52.3	-146.4	17036	800	7.1	1.2	21.3	1.1
14	-52.3	-146.4	17037	1000	7.0	0.6	13.1	1.5
14	-52.3	-146.4	17147	1100	2.1	0.6	23.8	14.2
14	-52.3	-146.4	17147	1100	2.6	1.3	nd	nd
14	-52.3	-146.4	17148	1200	1.6	0.5	11.1	5.6
14	-52.3	-146.4	17149	1300	1.0	0.0	12.2	0.4
14	-52.3	-146.4	17150	1450	6.3	1.2	21.8	2.4
15	-53.8	-146.0	17187	0	0.0	0.0	40.1	3.5
16	-55.0	-145.7	17270	25	0.9	1.6	25.5	44.1
16	-55.0	-145.7	17271	50	1.1	1.6	28.7	40.6
16	-55.0	-145.7	17272	77	0.0	0.0	58.5	1.7
16	-55.0	-145.7	17273	100	0.0	0.0	18.0	2.0
16	-55.0	-145.7	17274	150	3.3	0.6	34.4	2.7
16	-55.0	-145.7	17275	200	3.4	0.0	26.4	0.2
16	-55.0	-145.7	17276	300	3.1	0.5	31.7	0.9
16	-55.0	-145.7	17277	450	4.2	1.6	19.9	2.2
16	-55.0	-145.7	17278	600	4.1	0.8	23.7	1.3
16	-55.0	-145.7	17279	750	4.4	0.5	24.2	3.3
16	-55.0	-145.7	17280	900	4.6	0.1	22.8	2.5
16	-55.0	-145.7	17281	1100	3.5	0.1	10.4	0.9
16	-55.0	-145.7	17342	1300	3.7	0.1	30.0	17.1
16	-55.0	-145.7	17341	1500	8.8	1.3	41.6	0.2
18	-56.3	-145.3	17345	0	0.0	0.0	54.9	2.9
18	-56.3	-145.3	17440	25	0.0	0.0	105.6	12.6
18	-56.3	-145.3	17441	45	0.0	0.0	52.2	11.6
18	-56.3	-145.3	17442	70	2.7	0.2	91.1	0.2
18	-56.3	-145.3	17443	100	0.0	0.0	43.0	0.6
18	-56.3	-145.3	17444	140	0.0	0.0	41.8	1.7
18	-56.3	-145.3	17445	230	5.7	2.1	71.7	1.4
18	-56.3	-145.3	17446	300	7.9	1.0	29.4	2.5
18	-56.3	-145.3	17447	450	4.4	0.1	20.8	0.0
18	-56.3	-145.3	17448	600	4.7	2.1	34.4	4.5
18	-56.3	-145.3	17449	800	3.5	0.2	19.0	3.6
18	-56.3	-145.3	17450	1000	3.9	1.0	30.4	9.3

Station #	Lat. [+N, -S]	Long. [+E, -W]	Sample #	Depth [m]	TDS [pmol/L]	SD [pmol/L]	OCS [pmol/L]	SD [pmol/L]
18	-56.3	-145.3	17451	1200	9.8	0.5	18.4	1.1
20	-57.6	-144.9	17459	0	0.0	0.0	60.2	5.9
20	-57.6	-144.9	17484	25	0.0	0.0	94.7	2.4
20	-57.6	-144.9	17485	45	0.0	0.0	62.4	7.4
20	-57.6	-144.9	17486	65	1.9	0.1	75.3	0.4
20	-57.6	-144.9	17487	95	0.0	0.0	38.4	2.1
20	-57.6	-144.9	17488	115	0.0	0.0	120.0	49.8
20	-57.6	-144.9	17489	150	0.0	0.0	61.7	1.5
20	-57.6	-144.9	17490	200	0.0	0.0	43.2	0.2
20	-57.6	-144.9	17491	250	0.0	0.0	45.1	1.1
20	-57.6	-144.9	17492	350	6.4	0.8	41.8	4.2
20	-57.6	-144.9	17493	450	3.4	2.1	20.3	2.2
20	-57.6	-144.9	17494	550	3.9	0.4	36.4	4.9
20	-57.6	-144.9	17495	650	4.7	0.9	31.3	1.2
20	-57.6	-144.9	17564	650	4.0	0.3	57.8	10.1
20	-57.6	-144.9	17565	800	11.0	0.0	51.3	3.2
20	-57.6	-144.9	17556	1000	3.4	0.2	43.7	0.9
20	-57.6	-144.9	17567	1200	2.9	0.1	46.6	2.9
20	-57.6	-144.9	17568	1400	4.6	0.3	45.0	8.1
22	-60.0	-144.0	17644	25	0.0	0.0	71.7	24.4
22	-60.0	-144.0	17645	55	0.0	0.0	95.0	11.7
22	-60.0	-144.0	17646	90	0.0	0.0	39.5	0.3
22	-60.0	-144.0	17647	125	0.0	0.0	39.7	3.2
22	-60.0	-144.0	17648	200	4.2	1.3	64.8	0.6
22	-60.0	-144.0	17649	300	12.2	4.3	nd	nd
22	-60.0	-144.0	17650	400	3.9	0.4	21.7	0.3
22	-60.0	-144.0	17651	550	2.9	3.6	114.3	8.2
22	-60.0	-144.0	17652	700	3.7	0.1	23.4	0.8
22	-60.0	-144.0	17653	850	7.0	0.1	37.0	4.6
22	-60.0	-144.0	17654	1000	2.5	0.0	14.5	1.9
22	-60.0	-144.0	17655	1200	7.0	2.7	37.2	15.6
23	-62.5	-143.0	17728	0	0.3	0.4	56.0	1.3
24	-65.0	-139.0	17772	0	0.2	0.3	63.4	9.6
25	-67.0	-135.0	17772	0	0.2	0.1	69.8	0.6
25	-67.0	-135.0	17841	25	12.5	3.7	42.0	6.4
25	-67.0	-135.0	17842	40	2.9	0.5	33.7	1.6
25	-67.0	-135.0	17843	85	0.0	0.0	25.1	0.9
25	-67.0	-135.0	17844	125	0.0	0.0	30.2	2.5
25	-67.0	-135.0	17845	175	1.9	0.3	22.5	3.1
25	-67.0	-135.0	17846	275	5.7	0.0	103.4	2.3

Station #	Lat. [+N, -S]	Long. [+E, -W]	Sample #	Depth [m]	TDS [pmol/L]	SD [pmol/L]	OCS [pmol/L]	SD [pmol/L]
25	-67.0	-135.0	17847	375	4.0	0.9	20.3	2.3
25	-67.0	-135.0	17848	500	4.7	0.2	75.5	3.3
25	-67.0	-135.0	17849	750	3.2	0.4	22.4	0.4
25	-67.0	-135.0	17850	950	6.6	1.0	31.6	9.9
25	-67.0	-135.0	17851	1250	3.7	0.1	22.0	1.8
25	-67.0	-135.0	17852	1500	8.0	0.9	45.2	1.5
26	-67.0	-125.0	17927	0	4.5	2.1	146.4	23.0
27	-67.0	-115.0	17966	0	7.7	3.2	70.5	15.0
27	-67.0	-115.0	17996	25	12.2	7.6	98.1	3.3
27	-67.0	-115.0	17997	55	16.2	3.1	64.9	22.4
27	-67.0	-115.0	17998	80	4.0	0.8	33.6	11.0
27	-67.0	-115.0	17999	100	8.9	4.3	94.4	5.0
27	-67.0	-115.0	18000	150	4.1	0.1	32.5	9.7
27	-67.0	-115.0	18001	200	9.4	2.0	nd	nd
27	-67.0	-115.0	18002	300	13.2	3.2	19.9	5.8
27	-67.0	-115.0	18003	400	6.9	1.6	45.4	1.0
27	-67.0	-115.0	18004	500	6.5	1.4	26.0	0.1
27	-67.0	-115.0	18005	700	6.6	3.7	34.5	0.6
27	-67.0	-115.0	18006	900	4.6	0.4	21.4	1.4
27	-67.0	-115.0	18007	1100	6.1	0.3	46.7	2.7
27	-67.0	-115.0	18055	1100	2.4	0.8	19.3	8.0
27	-67.0	-115.0	18056	1250	3.8	0.7	22.6	10.3
27	-67.0	-115.0	18057	1400	2.2	0.2	21.8	1.9
27	-67.0	-115.0	18058	1600	11.7	1.4	57.9	0.5
29	-67.0	-100.0	18120	0	0.0	0.0	39.6	3.0
29	-67.0	-100.0	18146	25	0.0	nd	51.6	9.6
29	-67.0	-100.0	18147	50	9.6	6.0	55.7	11.2
29	-67.0	-100.0	18148	85	6.4	0.6	29.6	3.2
29	-67.0	-100.0	18149	115	2.8	0.0	37.0	1.0
29	-67.0	-100.0	18150	175	1.7	0.3	29.8	0.8
29	-67.0	-100.0	18151	235	6.1	0.7	nd	nd
29	-67.0	-100.0	18152	400	3.5	0.4	20.5	0.7
29	-67.0	-100.0	18153	575	4.0	0.8	22.1	3.4
29	-67.0	-100.0	18154	750	3.3	0.4	16.3	1.8
29	-67.0	-100.0	18155	1000	5.5	nd	17.7	nd
29	-67.0	-100.0	18156	1250	2.6	0.0	10.8	0.5
29	-67.0	-100.0	18157	1500	7.8	0.1	25.6	0.2
30	-65.0	-92.5	18217	0	1.6	0.6	51.7	4.6
32	-60.0	-82.5	18258	0	8.9	0.6	58.8	7.4
32	-60.0	-82.5	18283	25	0.1	0.2	44.1	6.2

Station #	Lat. [+N, -S]	Long. [+E, -W]	Sample #	Depth [m]	TDS [pmol/L]	SD [pmol/L]	OCS [pmol/L]	SD [pmol/L]
32	-60.0	-82.5	18284	70	7.7	4.7	67.7	10.7
32	-60.0	-82.5	18285	130	1.2	2.1	22.6	6.7
32	-60.0	-82.5	18286	175	2.7	0.5	27.3	0.1
32	-60.0	-82.5	18287	275	4.7	0.8	19.7	2.7
32	-60.0	-82.5	18288	400	7.0	0.4	26.2	6.6
32	-60.0	-82.5	18289	525	9.0	0.2	28.7	4.0
32	-60.0	-82.5	18290	680	6.6	0.6	22.4	0.5
32	-60.0	-82.5	18291	950	6.8	3.2	18.9	1.8
32	-60.0	-82.5	18292	1250	6.4	0.4	13.9	1.8
32	-60.0	-82.5	18293	1500	5.0	0.2	16.8	3.9
32	-60.0	-82.5	18294	1800	11.2	0.9	23.1	3.6
34	-55.0	-77.0	18379	0	9.0	3.3	43.4	3.4
35	-54.4	-76.6	18426	0	59.8	6.5	81.7	6.2
35	-54.4	-76.6	18454	25	8.4	4.4	47.5	8.5
35	-54.4	-76.6	18455	60	52.7	2.3	62.5	3.0
35	-54.4	-76.6	18456	85	3.1	0.2	34.1	0.1
35	-54.4	-76.6	18457	125	14.8	0.4	107.8	1.2
35	-54.4	-76.6	18458	200	3.6	0.5	22.4	0.6
35	-54.4	-76.6	18459	275	13.6	0.7	33.6	1.1
35	-54.4	-76.6	18460	450	3.4	0.2	20.0	1.4
35	-54.4	-76.6	18461	625	14.4	4.8	39.8	1.6
35	-54.4	-76.6	18462	800	5.8	1.3	42.9	4.0
35	-54.4	-76.6	18463	1000	21.7	5.4	44.6	0.7
35	-54.4	-76.6	18464	1250	3.5	0.2	24.5	5.7
35	-54.4	-76.6	18465	1500	16.6	1.2	42.4	2.5
37	-53.5	-75.8	18615	0	14.1	2.0	141.1	9.8
37	-53.5	-75.8	18655	25	38.6	0.0	94.6	9.4
37	-53.5	-75.8	18656	50	26.3	29.2	61.0	69.0
37	-53.5	-75.8	18657	80	34.0	0.2	50.0	2.3
37	-53.5	-75.8	18658	110	26.7	23.1	36.4	31.6
37	-53.5	-75.8	18659	146	16.3	1.5	49.3	nd
37	-53.5	-75.8	18660	175	7.1	0.7	23.9	1.2
37	-53.5	-75.8	18661	225	3.6	0.7	14.9	1.8
37	-53.5	-75.8	18662	275	4.5	1.0	31.6	4.9
37	-53.5	-75.8	18663	375	9.6	7.1	39.0	3.8
37	-53.5	-75.8	18664	475	8.8	0.4	34.9	2.5
37	-53.5	-75.8	18665	575	9.3	0.9	28.0	2.3
37	-53.5	-75.8	18666	675	11.7	1.1	21.8	1.6
37	-53.5	-75.8	18728	675	4.6	nd	9.8	nd
37	-53.5	-75.8	18729	800	7.9	3.5	27.0	1.2

Station #	Lat. [+N, -S]	Long. [+E, -W]	Sample #	Depth [m]	TDS [pmol/L]	SD [pmol/L]	OCS [pmol/L]	SD [pmol/L]
37	-53.5	-75.8	18730	900	6.0	nd	18.1	4.8
37	-53.5	-75.8	18731	1100	3.8	0.4	11.1	1.7
37	-53.5	-75.8	18733	1500	1.3	nd	14.9	nd
38	-52.7	-75.0	18752	0	10.0	0.3	407.5	18.1

APPENDIX D

SMALL SIZE PARTICULATE ACID-VOLATILE SULFIDE CONCENTRATIONS FROM THE GP17 CRUISE

Station #	Lat. [+N, -S]	Long. [+E, -W]	Sample #	Depth [m]	pAVS [pmol/L]	SD [pmol/L]
1	-20.0	-152.0	15953	25	nd	nd
1	-20.0	-152.0	15952	60	1.28	0.11
1	-20.0	-152.0	15951	100	1.46	0.04
1	-20.0	-152.0	16006	145	0.87	0.01
1	-20.0	-152.0	15949	200	1.36	0.32
1	-20.0	-152.0	15948	400	0.08	0.02
1	-20.0	-152.0	15947	625	0.09	0.01
1	-20.0	-152.0	15946	800	0.08	0.02
1	-20.0	-152.0	16005	1000	0.03	0
1	-20.0	-152.0	16004	1550	0.03	0
1	-20.0	-152.0	16003	2400	0	0
1	-20.0	-152.0	16002	3400	0.02	0.01
1	-20.0	-152.0	16001	3800	0	0
1	-20.0	-152.0	16000	4140	0.03	0.01
1	-20.0	-152.0	15999	4180	0.11	0.06
3	-26.2	-152.0	16063	25	0.75	0.05
3	-26.2	-152.0	16064	60	1.35	0.01
3	-26.2	-152.0	16065	132	1.5	0.13
3	-26.2	-152.0	16066	200	1.64	0.31
3	-26.2	-152.0	16067	235	0.52	0.02
3	-26.2	-152.0	16068	400	0.09	0.03
3	-26.2	-152.0	16069	600	0.1	0.02
3	-26.2	-152.0	16070	750	0.07	0.02
3	-26.2	-152.0	16088	400	0.15	0
3	-26.2	-152.0	16087	750	0.05	0
3	-26.2	-152.0	16085	1100	0.09	0
3	-26.2	-152.0	16084	1500	0.09	0.03
3	-26.2	-152.0	16082	2175	0.04	0
3	-26.2	-152.0	16081	2400	0.02	0
3	-26.2	-152.0	16079	2400	0.03	0
3	-26.2	-152.0	16078	2800	0.06	0.01
3	-26.2	-152.0	16077	3300	0.25	0.03
3	-26.2	-152.0	16075	4200	0.06	0.01
3	-26.2	-152.0	16074	4400	0.07	0.01
3	-26.2	-152.0	16073	4540	0.05	0

Station #	Lat. [+N, -S]	Long. [+E, -W]	Sample #	Depth [m]	pAVS [pmol/L]	SD [pmol/L]
3	-26.2	-152.0	16072	4590	0.13	0
6	-32.5	-150.0	16335	25	0.32	0.01
6	-32.5	-150.0	16336	80	0.41	0.08
6	-32.5	-150.0	16337	130	0.3	0.04
6	-32.5	-150.0	16338	175	0.35	0.02
6	-32.5	-150.0	16339	250	0.4	0.01
6	-32.5	-150.0	16340	320	0.23	0.02
6	-32.5	-150.0	16341	450	0.18	0.05
6	-32.5	-150.0	16342	950	0.06	0
8	-37.5	-149.3	16547	25	0.32	0.01
8	-37.5	-149.3	16548	85	0.39	0.01
8	-37.5	-149.3	16549	125	0.46	0.05
8	-37.5	-149.3	16550	175	0.89	0.05
8	-37.5	-149.3	16551	225	0.27	0.01
8	-37.5	-149.3	16552	325	0.22	0.02
8	-37.5	-149.3	16553	750	0.07	0
8	-37.5	-149.3	16554	1200	0.08	0.01
8	-37.5	-149.3	16556	1750	0.05	0
8	-37.5	-149.3	16557	2300	0.04	0
8	-37.5	-149.3	16558	3000	0.04	0
8	-37.5	-149.3	16559	4000	0.04	0.04
8	-37.5	-149.3	16560	4500	0.04	0
8	-37.5	-149.3	16562	5576	0.03	0
8	-37.5	-149.3	16563	5595	0.07	0.01
10	-42.5	-148.5	16712	25	0.67	0.11
10	-42.5	-148.5	16713	46	1.07	0.01
10	-42.5	-148.5	16714	80	0.91	0.01
10	-42.5	-148.5	16715	130	0.45	0.03
10	-42.5	-148.5	16716	250	0.38	0.02
10	-42.5	-148.5	16717	400	0.2	0
10	-42.5	-148.5	16718	600	0.12	0.02
10	-42.5	-148.5	16719	900	0.04	0
12	-47.5	-147.5	16842	25	0.6	0.08
12	-47.5	-147.5	16843	52	0.9	0.05
12	-47.5	-147.5	16844	70	1.22	0.17
12	-47.5	-147.5	16845	98	0.86	0
12	-47.5	-147.5	16846	150	0.4	0.03
12	-47.5	-147.5	16847	240	0.31	0.02
12	-47.5	-147.5	16848	500	0.26	0.04
12	-47.5	-147.5	16849	1000	0.13	0.02

Station #	Lat. [+N, -S]	Long. [+E, -W]	Sample #	Depth [m]	pAVS [pmol/L]	SD [pmol/L]
12	-47.5	-147.5	16851	1500	0.15	0.01
12	-47.5	-147.5	16852	2100	0.12	0
12	-47.5	-147.5	16853	2800	0.14	0.04
12	-47.5	-147.5	16854	3600	0.48	0.02
12	-47.5	-147.5	16855	4000	0.17	0.04
12	-47.5	-147.5	16856	4500	0.08	0.01
12	-47.5	-147.5	16857	4980	0.12	0.02
12	-47.5	-147.5	16858	5020	0.29	0.06
14	-52.3	-146.4	17018	1600	0.31	nd
14	-52.3	-146.4	17019	2100	0.15	nd
14	-52.3	-146.4	17020	2700	0.15	nd
14	-52.3	-146.4	17021	3300	0.09	nd
14	-52.3	-146.4	17022	3500	0.06	nd
14	-52.3	-146.4	17023	3740	0.1	nd
14	-52.3	-146.4	17024	3820	0.14	nd
14	-52.3	-146.4	17025	3860	0.03	nd
18	-56.3	-145.3	17415	600	0.26	0.07
20	-57.6	-144.9	17500	25	50.03	11.78
20	-57.6	-144.9	17497	115	9.41	3.02
20	-57.6	-144.9	17498	250	2.21	0.11
20	-57.6	-144.9	17499	450	0.16	0.03
20	-57.6	-144.9	17504	2000	0.43	0.09
20	-57.6	-144.9	17509	3075	0.05	0.01
22	-60.0	-144.0	17663	25	2.39	0.2
22	-60.0	-144.0	17664	125	13.82	1.32
25	-67.0	-135.0	17813	25	59.85	10.26
25	-67.0	-135.0	17814	85	15.02	2.13
25	-67.0	-135.0	17815	175	0.47	0.09
25	-67.0	-135.0	17906	4550	0.1	0.01
27	-67.0	-115.0	17992	25	0.79	0.12
27	-67.0	-115.0	17993	100	3.37	2.24
27	-67.0	-115.0	17994	200	0.76	0.07
27	-67.0	-115.0	18047	400	0.19	0.01
27	-67.0	-115.0	18054	2000	0.02	0.02
27	-67.0	-115.0	18100	4710	0.11	0.08
29	-67.0	-100.0	18160	25	0.69	0.12
29	-67.0	-100.0	18161	85	0.94	0.34
29	-67.0	-100.0	18163	575	0.27	0.09
34	-55.0	-77.0	18421	2300	0.09	0.02
34	-55.0	-77.0	18422	2600	0.13	0

Station #	Lat. [+N, -S]	Long. [+E, -W]	Sample #	Depth [m]	pAVS [pmol/L]	SD [pmol/L]
34	-55.0	-77.0	18424	3250	0.05	0.01
35	-54.4	-76.6	18468	25	1.44	0.05
35	-54.4	-76.6	18470	125	0.83	0.01
35	-54.4	-76.6	18473	275	0.61	0.03
35	-54.4	-76.6	18477	625	0.2	0.03
35	-54.4	-76.6	18525	2750	0.07	0.01
35	-54.4	-76.6	18528	3839	0.06	0
35	-54.4	-76.6	18529	3919	0.14	0.02
35	-54.4	-76.6	18530	3984	0.06	0.06
36	-53.7	-76.0	18573	2300	0.04	0.02
36	-53.7	-76.0	18574	2500	0.06	0.01
36	-53.7	-76.0	18576	2900	0.06	0
36	-53.7	-76.0	18578	3300	0.04	0
37	-53.5	-75.8	18602	25	2.27	0.11
37	-53.5	-75.8	18603	110	1.33	0.11
37	-53.5	-75.8	18604	175	1.12	0.01
37	-53.5	-75.8	18605	275	0.32	0.05
37	-53.5	-75.8	18595	2800	0.08	0
37	-53.5	-75.8	18598	3190	0.17	0.06
37	-53.5	-75.8	18599	3270	0.23	0.01
37	-53.5	-75.8	18600	3310	0.15	0.02

VITA

Nicole R. Buckley
Dept. of Ocean and Earth Sciences
Old Dominion University
Norfolk, VA 23529

EDUCATION

PhD, Oceanography, Old Dominion University, Expected 2024
MS, Ocean and Earth Science, Old Dominion University, 2021
BS, Chemistry, University of Wisconsin – Milwaukee, 2018

PUBLICATIONS

Buckley, **N.R.**, Black, E.E., Kenyon, J.A., Lanning, N.T., Sieber, M., Conway, T.M., Fitzsimmons, J.N., and G.A. Cutter. Re-evaluating hydrogen sulfide as a sink for cadmium and zinc in the oxic to suboxic upper water column of the Pacific Ocean. *Global Biogeochemical Cycles*. 2024.

Jenkins, W.J., Hatta, M., Fitzsimmons, J.N., Schlitzer, R., Lanning, N.T., Shiller, A., **Buckley**, **N.R.**, German, C.R., Lott III, D.E., Weiss, G., Whitmore, L., Casciotti, K., Lam, P.J., Cutter, G.A., and K.L. Cahill. An intermediate-depth source of hydrothermal ^{3}He and dissolved iron in the North Pacific. *Earth and Planetary Science Letters*. 2020.

PRESENTATIONS

Buckley, N., and G. Cutter. Biogeochemical cycling of hydrogen sulfide in the Surface South Pacific and Southern Ocean. *Oral presentation* at Ocean Sciences Meeting, New Orleans, LA. February 2024.

Buckley, N., and G. Cutter. Biogeochemical cycling of hydrogen sulfide in the South Pacific and Southern Ocean. *Poster presentation* at the Chemical Oceanography Gordon Research Conference, Manchester, NH. July 2023.

Buckley, N., and G. Cutter. Biogeochemical cycling of hydrogen sulfide in the upper water column along the Pacific Meridional transect – GP15. *Oral presentation* at Ocean Sciences Meeting, online. February 2022.

Buckley, N., and G. Cutter. Biogeochemical cycling of hydrogen sulfide in the oxic Pacific Ocean. *Oral presentation* at Ocean Sciences Meeting, San Diego, CA. February 2020.

Buckley, N. Can hydrogen sulfide in oxygen-deficient zones affect metal cycling? *Poster presentation* at Goldschmidt Conference, Barcelona, Spain. August 2019.